NAVAL POSTGRADUATE SCHOOL

MONTEREY, CALIFORNIA

THESIS

UNDERSTANDING THE IMPORTANCE OF OCEANIC FORCING ON SEA ICE VARIABILITY

by

Joanne E. Haynes

December 2010

Thesis Advisor:	Wieslaw Maslowski
Second Reader:	William Shaw

Approved for public release; distribution is unlimited

THIS PAGE INTENTIONALLY LEFT BLANK

REPORT DOCUMENTATION PAGE			*Form Approved OMB No. 0704-0188*
Public reporting burden for this collection of information is estimated to average 1 hour per response, including the time for reviewing instruction, searching existing data sources, gathering and maintaining the data needed, and completing and reviewing the collection of information. Send comments regarding this burden estimate or any other aspect of this collection of information, including suggestions for reducing this burden, to Washington headquarters Services, Directorate for Information Operations and Reports, 1215 Jefferson Davis Highway, Suite 1204, Arlington, VA 22202-4302, and to the Office of Management and Budget, Paperwork Reduction Project (0704-0188) Washington DC 20503.			
1. AGENCY USE ONLY ***(Leave blank)***	**2. REPORT DATE** December 2010	**3. REPORT TYPE AND DATES COVERED** Master's Thesis	
4. TITLE AND SUBTITLE Understanding the Importance of Oceanic Forcing on Sea Ice Variability		**5. FUNDING NUMBERS**	
6. AUTHOR(S) Haynes, Joanne E.			
7. PERFORMING ORGANIZATION NAME(S) AND ADDRESS(ES) Naval Postgraduate School Monterey, CA 93943-5000		**8. PERFORMING ORGANIZATION REPORT NUMBER**	
9. SPONSORING /MONITORING AGENCY NAME(S) AND ADDRESS(ES) N/A		**10. SPONSORING/MONITORING AGENCY REPORT NUMBER**	
11. SUPPLEMENTARY NOTES The views expressed in this thesis are those of the author and do not reflect the official policy or position of the Department of Defense or the U.S. Government. IRB Protocol number _____.			
12a. DISTRIBUTION / AVAILABILITY STATEMENT Approved for public release; distribution is unlimited		**12b. DISTRIBUTION CODE**	

13. ABSTRACT (maximum 200 words)

The rapid decline in Arctic sea ice over the past few decades has prompted scientists to better understand the factors driving sea ice variability. Analyses and syntheses of numerical model results and available observational data are presented in order to advance the understanding of critical processes and feedbacks affecting the oceanic forcing of sea ice in the western Arctic Ocean, where melt has been particularly pronounced. Results from the eddy permitting (~9km) NPS coupled ice-ocean model are analyzed for the large-scale and long-term context and compared to results from the eddy resolving (~2.3km) model over the western Arctic. Observational data from ice-tethered profilers (ITPs) and co-located ice mass-balance buoys (IMBs) are analyzed over the same region, with a focus on the entrainment of heat into the mixed layer. Results indicate that entrainment events may be a significant contributor to sea ice melt and a limiting factor for ice growth, particularly in winter. Qualitative comparisons are made to oceanic processes occurring in the Southern Ocean to determine any similarities, especially if the current trajectory of Arctic sea ice decline continues towards a similar regime as that of its southern counterpart, where sea ice is largely seasonal and where ice melt is increasingly driven by oceanic processes.

14. SUBJECT TERMS Arctic Ocean, Southern Ocean, Sea Ice Variability, Coupled Ice-Ocean Model, Ice-Tethered Profiler, Ice Mass-Balance Buoy, Oceanic Forcing, Eddies and Mesoscale Processes			**15. NUMBER OF PAGES** 180
			16. PRICE CODE
17. SECURITY CLASSIFICATION OF REPORT Unclassified	**18. SECURITY CLASSIFICATION OF THIS PAGE** Unclassified	**19. SECURITY CLASSIFICATION OF ABSTRACT** Unclassified	**20. LIMITATION OF ABSTRACT** UU

NSN 7540-01-280-5500

Standard Form 298 (Rev. 2-89)
Prescribed by ANSI Std. 239-18

THIS PAGE INTENTIONALLY LEFT BLANK

Approved for public release; distribution is unlimited

UNDERSTANDING THE IMPORTANCE OF OCEANIC FORCING ON SEA ICE VARIABILITY

Joanne E. Haynes
Lieutenant, Royal Australian Navy
BSc(Hons), University of New South Wales, 2001
GradDip(Met), Bureau of Meteorology, 2005

Submitted in partial fulfillment of the
requirements for the degree of

MASTER OF SCIENCE IN PHYSICAL OCEANOGRAPHY

from the

NAVAL POSTGRADUATE SCHOOL
December 2010

Author: Joanne Haynes

Approved by: Wieslaw Maslowski
Thesis Advisor

William Shaw
Second Reader

Jeffrey Paduan
Chairman, Department of Oceanography

THIS PAGE INTENTIONALLY LEFT BLANK

ABSTRACT

The rapid decline in Arctic sea ice over the past few decades has prompted scientists to better understand the factors driving sea ice variability. Analyses and syntheses of numerical model results and available observational data are presented in order to advance the understanding of critical processes and feedbacks affecting the oceanic forcing of sea ice in the western Arctic Ocean, where melt has been particularly pronounced. Results from the eddy permitting (~9km) NPS coupled ice-ocean model are analyzed for the large-scale and long-term context and compared to results from the eddy resolving (~2.3km) model over the western Arctic. Observational data from ice-tethered profilers (ITPs) and co-located ice mass-balance buoys (IMBs) are analyzed over the same region, with a focus on the entrainment of heat into the mixed layer. Results indicate that entrainment events may be a significant contributor to sea ice melt, especially in regions frequently populated by mesoscale eddies, and a limiting factor for ice growth, particularly in winter. Qualitative comparisons are made to oceanic processes occurring in the Southern Ocean to determine any similarities, especially if the current trajectory of Arctic sea ice decline continues towards a similar regime as that of its southern counterpart, where sea ice is largely seasonal and where ice melt is increasingly driven by oceanic processes.

THIS PAGE INTENTIONALLY LEFT BLANK

TABLE OF CONTENTS

LIST OF FIGURES

THIS PAGE INTENTIONALLY LEFT BLANK

LIST OF TABLES

THIS PAGE INTENTIONALLY LEFT BLANK

LIST OF ACRONYMS AND ABBREVIATIONS

AABW	Antarctic Bottom Water
AAD	Australian Antarctic Division
AAO	Antarctic Oscillation
ACC	Alaskan Coastal Current
ACC	Antarctic Circumpolar Current
ACW	Antarctic Circumpolar Wave
AFMA	Australian Fisheries Management Authority
AMAP	Arctic Monitoring and Assessment Programme
ANARE	Australian National Antarctic Research Expedition
ANZFLUX	Antarctic Zone Flux
AOFB	Autonomous Ocean Flux Buoy
AR4	Fourth Assessment Report
ASPeCt	Antarctic Sea Ice Processes and Climate
AO	Arctic Oscillation
CAA	Canadian Arctic Archipelago
CHL	Cold Halocline Layer
CO_2	Carbon Dioxide
CRREL	Cold Regions Research and Engineering Laboratory
CTD	Conductivity Temperature Depth
DGST	Deployable Geospatial Survey Team
ECMWF	European Center for Medium-range Weather Forecasts
EEZ	Exclusive Economic Zone
EKE	Eddy Kinetic Energy
EM	Electromagnetic
ENSO	El Nino Southern Oscillation
FFV	Foreign Fishing Vessel
FWC	Fresh Water Content
GCM	Global Climate Model
GHG	Greenhouse Gas
GIS	Greenland Ice Sheet

GOOS	Global Ocean Observing System
GPS	Global Positioning System
HSPD	Homeland Security Presidential Directive
IBCAO	International Bathymetric Chart of the Arctic Ocean
ICESat	Ice Cloud and land Elevation Satellite
ICEX	Ice Exercise
IGY	International Geophysical Year
IHO	International Hydrographic Organization
IMB	Ice Mass-balance Buoy
IPCC	Intergovernmental Panel on Climate Change
ITP	Ice-tethered Profiler
METOC	Meteorology and Oceanography
MIZ	Marginal Ice Zone
MLD	Mixed Layer Depth
NADW	North Atlantic Deep Water
NAM	Northern Annular Mode
NAME	NPS Arctic Modeling Effort
NAO	North Atlantic Oscillation
NPS	Naval Postgraduate School
NSF	National Science Foundation
NSIDC	National Sea and Ice Data Center
NSPD	National Security Presidential Directive
NSR	Northern Sea Route
NSTM	Near Surface Temperature Maximum
NWP	Northwest Passage
PDO	Pacific Decadal Oscillation
PSW	Pacific Summer Water
RAAF	Royal Australian Air Force
RGPS	RADARSAT Geophysical Processor System
RAN	Royal Australian Navy
RN	Royal Navy
SAM	Science Accommodation Mission

SAM	Southern Annular Mode
SAR	Search and Rescue
SAT	Surface Air Temperature
SCICEX	Science Ice Exercise
SEDNA	Sea ice Experiment – Dynamic Nature of the Arctic
SHEBA	Surface Heat Budget of the Arctic Ocean
SLD	Sonic Layer Depth
SOLAS	Safety of Life at Sea
SSH	Sea Surface Height
SSHA	Sea Surface Height Anomaly
SST	Sea Surface Temperature
TFCC	Task Force Climate Change
TKE	Total Kinetic Energy
T-S	Temperature-Salinity
ULS	Upward Looking Sonar
UNCLOS	United Nations Convention on Law of the Sea
USCG	United States Coast Guard
USGS	United States Geological Survey
USMC	United States Marine Corps
USN	United States Navy
WDW	Weddell Deep Water
WHOI	Woods Hole Oceanographic Institution
WWSP	Winter Weddell Sea Project

THIS PAGE INTENTIONALLY LEFT BLANK

ACKNOWLEDGMENTS

First and foremost, thank you to Professor Wieslaw Maslowski for the many hours spent providing helpful advice, suggestions for improvement, guidance and encouragement throughout the course of this work. His enthusiasm and knowledge of polar oceanography is inspirational, and I could not have hoped for a better advisor.

I also wish to extend sincere thanks to my second reader, Dr. Bill Shaw, for his assistance, input and advice, and for sharing some of his expertise of the polar oceans.

I am very grateful to have had the assistance of Jackie Clement Kinney, especially with the model data and in particular the production of the 2km model figures. I also appreciate her help with Ferret and for solving several computing issues.

Thank you to Don Perovich and Bruce Elder at the Cold Regions Research and Engineering Laboratory for processing and providing the IMB data, and for answering my subsequent questions regarding the results.

Many thanks are due to Robert Osinski at the Institute of Oceanology of the Polish Academy of Sciences for the development and integration of the 2km model.

Thank you to Jackie Grebmeier and Lee Cooper at the Chesapeake Biological Laboratory for the unforgettable opportunity of assisting on a scientific cruise in the Arctic Ocean.

The Royal Australian Navy deserves thanks for providing the opportunity to achieve my long-term goal of an overseas posting and for enabling me to complete further tertiary education.

To the many friends that I have made in the USA, thank you for making me feel welcome and for the fantastic experiences that we have shared together over the past eighteen months.

Last, but by no means least, thank you to my wonderful family and friends in Australia for encouraging me to pursue this opportunity and for your ongoing love and support.

THIS PAGE INTENTIONALLY LEFT BLANK

I. INTRODUCTION

A. BACKGROUND AND MOTIVATION FOR SEA ICE RESEARCH

For hundreds of years, the polar regions have held mystery and intrigue for adventurers and scientists alike. Many of the most experienced early polar explorers, including Scott, Amundsen, and Shackleton, eventually lost their lives during quests to better understand and conquer some of the most challenging conditions on earth. Despite advances in modern technology, even today the polar seas remain largely untouched due to the extreme conditions that make it difficult to sustain human life for any prolonged period of time. Unfortunately, these once pristine wildernesses are not completely immune to the effects of climate change, increasing world populations, and anthropogenic influences are beginning to take their toll.

The release of the Intergovernmental Panel on Climate Change (IPCC)'s *Fourth Assessment Report (AR4)* in 2004 saw a renewed world focus on anthropogenic global warming and, in particular, its effects on ice and snow covered regions. Increased levels of greenhouse gas (GHG) emissions over the past few decades are unequivocally linked to the warming of the climate system (IPCC 2007). The effects of this warming are most pronounced in polar areas, due to 'polar amplification', whereby greater temperature increases occur in the Arctic in comparison to the earth as a whole, due to the collective effects of feedbacks and other processes (McBean et al. 2005). Sea ice can be seen as a keystone indicator of GHG induced climate change, and comparisons of observed variations in Arctic sea ice extent with atmospheric carbon dioxide (CO_2) levels indicate that in recent decades the rate of sea ice decrease mirrors the increase in CO_2 (Johannessen 2008). Since the mid 1990s, there has been a notable decrease in sea ice in the Arctic and in the summer of 2007, Arctic sea ice extent reached an all time record low since the beginning of the satellite measurements in 1979. At the end of the melt season, September 2007 sea ice was 39% below the long-term average from 1979 to 2000 (National Sea and Ice Data Center (NSIDC) 2007). Sea ice extent has continued to reach extreme summer minimums since this time, and the observed decrease in extent has been faster than predicted by most global climate models (GCMs) (Stroeve et al. 2007).

Melt has consequences for ecosystems, shipping, natural resource development and defense. If Arctic sea ice continues to decrease, shrubs and forests will extend northwards, further decreasing surface albedo. Coastal erosion will increase as ice retreats from shore, since winds have longer fetch over open water, resulting in more wave action. Many Arctic mammals, such as seals, walruses and polar bears depend on the sea ice for their habitat, and may face possible extinction if they are unable to adapt to the changing conditions. This will also impact the traditional hunting practices of indigenous cultures.

Variability in sea ice has the potential to affect the heat budget of the earth and the global circulation of the world ocean by limiting or inhibiting the formation of deep water at high latitudes. Furthermore, if the decrease in Arctic sea ice continues, significant changes to meteorological conditions are likely, including increased surface air temperatures, increased precipitation levels, changes in storm tracks and more extreme weather events. The total melt of the Greenland Ice Sheet (GIS) alone may cause a substantial (up to about 6m) rise in sea level. Vast stores of carbon previously frozen into permafrost have the potential to accelerate warming even more (Overpeck et al. 2005). Sea level rise is likely to cause human populations to retreat further inland, away from low lying coastal areas. It is probable that many of the small South Pacific islands will be completely underwater during the next hundred years or so.

In summer 2007, the fabled Northwest Passage (NWP), which extends along the northern coast of North America, was open for shipping for the first time in centuries and the view of the Arctic as a non-navigable region began to change. The route between Europe and Asia via the NWP is nearly 25% shorter than the alternative routes through the Panama Canal or around Cape Horn. There are undisputable time and money saving advantages for shipping companies using the newly accessible sea lane of the NWP, along with the Northern Sea Route (NSR). The NSR borders the Russian Arctic coast and offers a 35 to 60% saving in distance for shipping between Northern Europe and the Far East (Titley and St. John 2010). However, these newly opened sea routes present security concerns, including their potential as avenues for smuggling and terrorist

activities. Increased shipping traffic in these poorly surveyed waters has also raised questions about safety of life at sea (SOLAS) and environmental issues, such as pollution.

The Arctic is a potential gold mine of natural resources including minerals, oil, gas, fish, timber and freshwater reserves. The United States Geological Survey (USGS) estimates that the Arctic holds as much as one quarter of the world's remaining undiscovered oil and gas deposits (Borgerson 2008). The largest deposits are thought to be near Russia, although the Shell Company holds millions of dollars worth of leases in the Beaufort Sea off the coast of Alaska. It is estimated that by 2015 oil production in the Arctic region will account for 40% of the world's total, and it seems ironic that declining sea ice is likely to produce more of the commodities that precipitated its melt in the first place - fossil fuels (Borgerson 2008).

Arctic sea ice has been rapidly declining over the past few decades, with the most extreme decline seen in the summer melt season. Increasing air and sea temperatures due to global warming, coupled with cycles of natural variability, are the most likely cause of this melt. According to the NSIDC, as of September 2010, Arctic sea ice extent (which is the total area of ocean covered with at least 15% of ice) was estimated to be decreasing at the alarming rate of 11.5% per decade in summer relative to the 1979 to 2000 average. Furthermore, estimates from satellite data indicate that over the last 30 years the length of the melt season has increased by about 20 days and for the entire Arctic, the melt season has lengthened at a rate of 6.4 days per decade (Markus 2009). Recent model estimates for when we may see an ice free summer in the Arctic range from thirty years (Wang and Overland 2009) to as early as 2016 (Maslowski 2010). Paleoclimatic evidence suggests that such a 'super interglacial' state has not been witnessed for at least a million years (Overpeck et al. 2005).

The recently observed decline in sea ice area, coupled with the concern that multiyear ice is being exported at an alarming rate from the Arctic Ocean (Kwok 2007), has caused a shift in focus away from areal ice extent and towards modeling and observing three dimensional changes, which includes ice thickness and volume. A number of studies suggest that sea ice thickness and volume may be decreasing at an

even faster rate than ice extent (e.g., Maslowski et al. 2008; Rothrock et al. 2008; Kwok and Rothrock 2009; Kwok et al. 2009). Much of the research into sea ice variability in the Arctic has concentrated on the atmospheric contribution to ice melt, citing the well known ice-albedo feedback mechanism as the primary driver for sea ice decline (e.g., Francis and Hunter 2006; Francis and Hunter 2007; Perovich et al. 2008). Links have also been drawn between phases of ice melt and growth and the various modes of climate variability affecting heating and circulation in the Arctic region, such as the North Atlantic Oscillation (NAO). The NAO describes the fluctuations in mean sea level pressure between the Azores High and the Icelandic Low, which reside over the North Atlantic Ocean, affecting wind strength, wind direction and storm tracks, the consequences of which also affect conditions in the Arctic. Although both atmospheric heating and long term trends in climate variability are important, they alone do not explain the rapid decline in ice thickness observed in recent years. Research suggests that atmospheric factors typically account for approximately 20 to 60% of Arctic sea ice variability (Francis et al. 2005; Tseng 2010). The contribution of oceanic forcing and its effects on melting sea ice from below should therefore not be neglected. Relatively few past studies have concentrated primarily on observing and modeling the oceanic processes that affect sea ice variability.

The declining trend in Arctic sea ice during recent years has raised concerns that the area has already passed a ‘tipping point’, whereby the ocean-atmosphere system entered a new regime of thin ice and increased open water due to positive feedbacks (Lindsay and Zhang 2005). If the current trajectory of sea ice decline continues, the Arctic Ocean may move towards a similar regime (i.e., seasonal sea ice cover) as that of its southern counterpart, the Southern Ocean. There are obvious geographic, atmospheric and oceanic differences between the Arctic and Southern Oceans and, until recently, the sea ice characteristics and behavior of the two hemispheres were quite dissimilar. Sea ice in the Southern Ocean is largely seasonal, and about 90% of the sea ice cover melts annually, with a few relatively small areas where multiyear ice survives. Unlike the Arctic Ocean, it is widely accepted that melting of sea ice by oceanic heat from below is the primary cause of ice melt in the Southern Ocean, since air temperatures are cold year

round, inhibiting any significant melting from above. Although the primary aim is of this study is to better understand the oceanic factors affecting sea ice variability in the Arctic Ocean, a qualitative comparison of the oceanic processes affecting sea ice in the Arctic and Southern Oceans is also made, since this has not been done previously.

B. NAVY RELEVANCE

A better understanding of sea ice and the factors affecting its variability in both hemispheres is beneficial to what is becoming an increasingly 'global' Navy. Sea ice research has the potential to assist the Navy in its operations in polar regions, including the most effective use of ships, submarines and aircraft, safety of navigation, optimal sonar operation, tactics, and future vessel design. The role of the Meteorology and Oceanography (METOC) Officer in polar forecasting should not be underestimated, as the provision of accurate forecasts forms an integral part in mitigating risk and ensuring the success of Navy operations conducted in these areas of the world.

1. The Arctic Ocean

The Arctic Ocean is unlike any other world ocean because it is a semi-enclosed basin which is geographically constrained by the continents surrounding it (Figure 1). Until recently, the nations surrounding the Arctic Ocean had reasonably well defined boundaries outlined by the United Nations Convention on Law of the Sea (UNCLOS), and the ownership of islands within the region was determined through a system of treaties. In 1966 the Arctic Council was formed as a means of promoting cooperation between the Arctic states. The USA is a member of the Council, which promotes sustainable development and environmental protection in the Arctic. There are, however, currently no overarching political or legal structures that can mediate political disagreements in the region (Borgerson 2008).

Figure 1. Map of the Arctic Region showing the Arctic Ocean, adjacent seas and political boundaries. Red line shows 10°C isotherm for July (from U.S. Central Intelligence Agency 2010).

The recent rapid decline in Arctic sea ice has raised issues regarding territory and the accessibility of sea lanes and resources within the area, which have posed new national economic and security concerns. These concerns, coupled with other potential impacts of sea ice melt, are likely to ensure that the United States Navy (USN) will have

an increased role in the Arctic Ocean in the future. There has even been some speculation that disagreements between nations over the Arctic could potentially lead to another Cold War (e.g., Reid 2007; Mahr 2010).

During the Cold War era, the Arctic Ocean was seen as a valuable strategic location for the transport of ballistic missiles and Soviet submarines. Post Cold War, the value of the Arctic as an arena for military operations was somewhat diminished. USN involvement in the Arctic during the past couple of decades has mainly been limited to scientific expeditions and training exercises. During the 1990s, USN submarines deployed on a number of co-operative Science Ice Exercises (SCICEXs), which carried scientists under the ice to make observations and to conduct research. Further information and data is available at http://www.ldeo.columbia.edu/res/pi/SCICEX/. In 2000, the USN and National Science Foundation (NSF) signed a memorandum of understanding for SCICEX Phase II. This memorandum introduced Science Accommodation Missions (SAMs), where time is set aside for the collection of unclassified scientific data during otherwise classified submarine exercises (SCICEX Science Advisory Committee 2010). These missions will continue to occur until they are deemed obsolete or impractical. For a number of years the USN has also conducted biennial Ice Exercises (ICEXs), with the goals of testing submarine capabilities in the Arctic environment and conducting scientific research.

The decline in sea ice during the last decade has seen a new scramble for territory by several Arctic nations who are eager to exploit new shipping routes and potential resources. Under UNCLOS, nations who have ratified the treaty may submit claims to extend their continental shelf, giving them exclusive rights to any resources on the seabed. The main players among the Arctic nations are Russia, Canada, the USA, Denmark and Norway. Of these five nations, the USA is the only nation to have not ratified UNCLOS, which means that they cannot formally assert any rights to resources off the north coast of Alaska beyond their Exclusive Economic Zone (EEZ) (Borgerson 2008).

In 2001, Russia submitted a claim to extend their continental shelf to the North Pole, based on the premise that the Lomonosov Ridge is geologically linked to the Siberian continental shelf. Although the claim was rejected, Russia dispatched a nuclear powered icebreaker and two submarines to plant its flag on the sea floor of the North Pole. Since 2007, Russia has increased its military presence in the Arctic, by conducting strategic bomber flights over the region and by reinstating permanent patrols by its Northern Fleet. In April 2010, Russia and Norway finally reached an agreement following a 40-year dispute over their respective borders in the Barents Sea, and Russian Prime Minister Vladimir Putin stated that "geopolitically Russia's deepest interests are linked to the Arctic."

Canada has also laid claims to its sovereignty in the Arctic Ocean. In 2006, Canada claimed the NWP as part of their internal waters, even though it is considered by most nations to be an international strait whereby foreign vessels have the right of free passage for the purposes of transit. Canada has since found funding for up to eight new Arctic capable patrol ships to secure the passage. With the unveiling of the *Canada First Defence Strategy* in 2008, Prime Minister Stephen Harper announced Canada's plans to establish a deep water port and an Arctic Training Centre, to expand its military presence, and to increase satellite and aerial surveillance of the Arctic region. Canada is also involved in ongoing territorial disputes with Denmark regarding the ownership of Hans Island, situated in Nares Strait between Canada and Greenland, and with the USA over an area in the Beaufort Sea between Alaska and Yukon.

Both Denmark and Norway have recently developed new policies and increased their presence in the Arctic. In addition to the increased activity and interest in the area by Arctic nations, several non-Arctic nations have also shown interest in the region including China, South Korea, Japan and the countries of the European Union. The potential to take advantage of previously un-navigable shipping lanes and the possibility of exploiting natural resources appear to be the primary drivers for most of these non-Arctic nations to increase their level of interest in recent times.

The projected effects of climate change on Arctic sea ice outlined in the IPCC's *AR4*, coupled with increased tensions between the Arctic nations, have seen the United States Government take affirmative action to ensure that they remain a key player in the region. Changing conditions in the Arctic were recognized in 2007 with the release of *A Cooperative Strategy for 21st Century Seapower*. This joint USN, United States Marine Corps (USMC) and United States Coast Guard (USCG) publication focuses on the importance of seapower as a unifying force and specifically identifies the Arctic as a potential source of competition and conflict for access to shipping lanes and natural resources due to climate change. In January 2009, former President George Bush signed the *National Security Presidential Directive 66 (NSPD-66)/Homeland Security Presidential Directive 25 (HSPD-25)*, which established the policy of the USA with respect to the Arctic and recognized it as 'an Arctic nation, with varied and compelling interests in that region.' In May 2009, Task Force Climate Change (TFCC) was established to address the Navy's future actions regarding the Arctic specifically, and climate change in general. TFCC is led by the Oceanographer of the Navy and has been tasked to make recommendations to Navy leadership regarding policy, strategy, force structure and investments relating to a changing Arctic (Department of the Navy 2009). *The Arctic Roadmap*, released in November 2009, was produced by TFCC and outlines a plan to ensure naval readiness and capabilities in a changing Arctic.

Despite increasing access due to sea ice melt, the Arctic environment presents a challenging arena for naval operations. Extreme meteorological conditions pose hazards to ships and aircraft such as icing, which can adversely affect stability and lift. Icing also has the potential to significantly degrade the performance of weapons and communications systems. Increased sea ice melt and river runoff due to thawing permafrost will change the acoustic environment of the ocean, affecting sonar operations. For example, sea ice melt results in larger areas of open ocean, which are directly exposed to the effects of winds at the surface. Exposure to winds and storms potentially causes increased mixing in the upper water column, thus changing the sonic layer depth (SLD) and resulting in greater scattering of sonar at the surface due to waves. Decreased sea ice cover also results in higher ambient noise levels from wind, waves and shipping

traffic, all of which are likely to cause even greater degradation in sonar performance. Furthermore, the ability of submarines to remain visually undetected by surface ships and aircraft by hiding under areas of thick ice may no longer be a possibility.

Even with ice capable vessels, the navigability of the Arctic remains questionable, with seamounts still being discovered and only 5% of the Arctic Ocean being well surveyed (RADM D. Titley, USN, personal communication). It is likely that the Navy will be required to conduct increased surveying to obtain better bathymetry datasets. They may also be called upon to assist in search and rescue (SAR) missions as shipping traffic increases in the area. There remains an ongoing need for Navy to assist in the collection of scientific data in order to monitor future sea ice change and to assist in the improvement of Arctic atmosphere, ocean and sea ice models for operational and longer term prediction of the Arctic environment.

As recognized in *NSPD-66/HSPD-25*, the implementation of Arctic policy requires appropriate resources and assets. Although Navy submarines are active in the region for research and training purposes, surface ships are not ice strengthened and can therefore only operate in sub-Arctic conditions, or in marginal ice zones (MIZs). Aircraft are capable of operating in the region, but are limited in range and duration due to a lack of airfields (Titley and St. John 2010). The current capabilities of the U.S. to operate in the Arctic environment are limited. During recent years, the icebreaker fleet has been allowed to atrophy, with only one remaining USCG vessel, the *USCG Healy*, capable of handling heavy sea ice conditions. Furthermore, there is very little in the way of infrastructure and logistics support available in the Arctic region, including the lack of coastal installations to support SAR and very few deep water ports (Titley and St. John 2010).

The acquisition of the necessary assets, infrastructure and the appropriate training of personnel will be an expensive and slow process. Future changes in the Arctic are likely to cause increased national security concerns for the U.S., which will have important implications for Navy. The ability of the U.S. to assert its authority as an Arctic nation is currently hindered by the Senate's reluctance to ratify UNCLOS, despite support from the Department of Defense, the State Department, and the President.

2. The Southern Ocean and Antarctica

In contrast to the Arctic Ocean, the Southern Ocean surrounds the continent of Antarctica (Figure 2). Although there is no Antarctic sovereignty, the majority of Antarctica is claimed by one or more countries. Australia has the largest claim to territory in Antarctica, although this is not explicitly recognized by many other nations, including the USA. Following the International Geophysical Year (IGY) of 1957–58, the *Antarctic Treaty* was created. It was ratified in 1961 by nine member nations, including Australia and the USA, and was reaffirmed in 1991 by more than 40 nations. The treaty sets aside the continent for scientific research and prohibits military presence and activities relating to the exploitation of mineral resources.

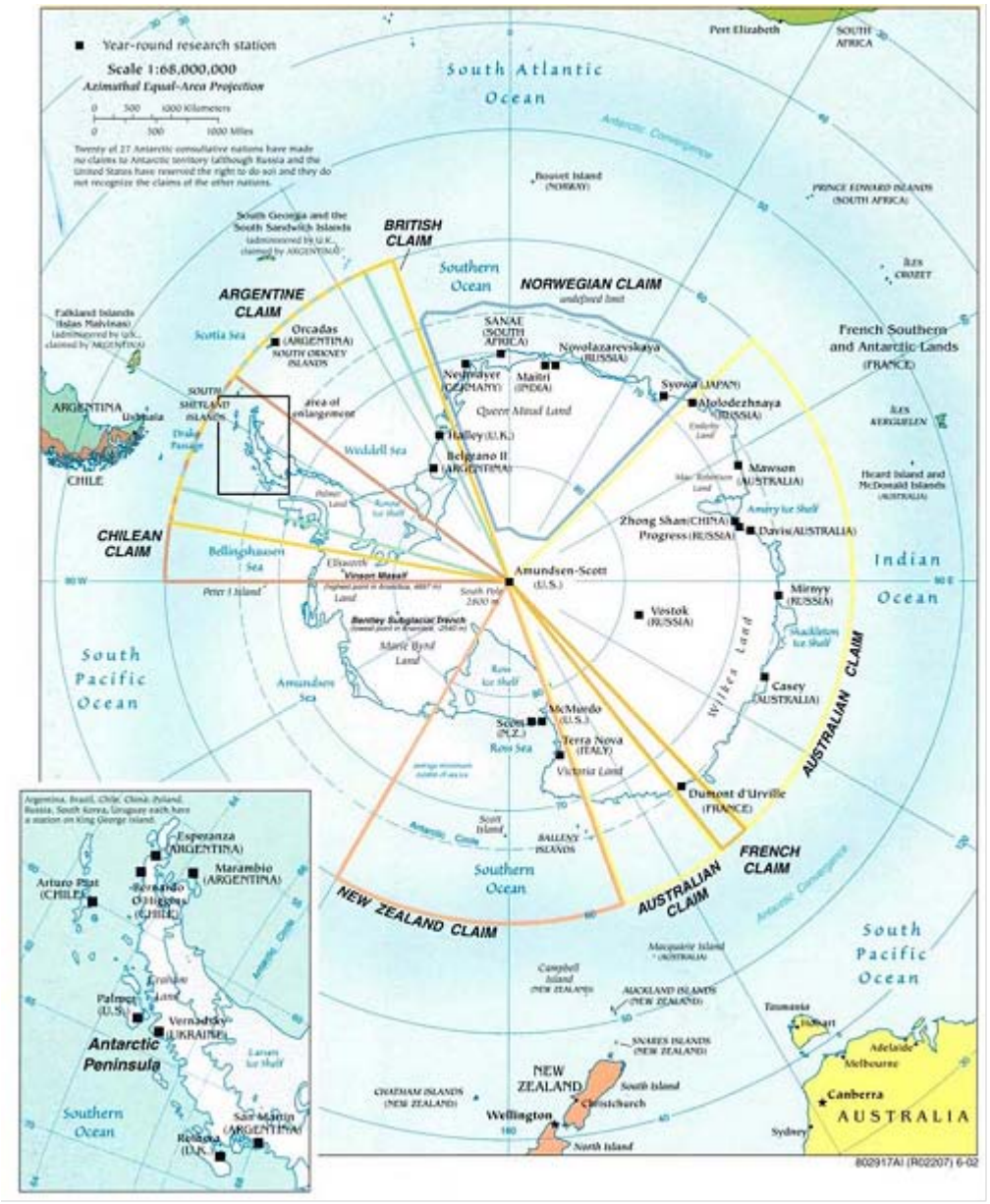

Figure 2. Map of the Antarctic Region showing territorial claims (from U.S. Central Intelligence Agency 2010)

The Southern Ocean is often considered to be one of the most unforgiving and treacherous maritime environments in the world due to the strong winds, high sea states and large swells associated with the crossing of intense cold fronts. Although the majority of this vast ocean extends well beyond the reaches of Australia's EEZ, Royal Australian Navy (RAN) ships and aircraft are called to operate there on occasion. Just as the Arctic

Ocean presents a challenging operational environment for USN operations, the Southern Ocean presents the RAN with the challenge of operating in some of the most severe weather conditions in the world. Surface ships and aircraft operating in the Southern Ocean are subject to many of the same hazards encountered in the Arctic, including icing, navigation hazards due to poorly surveyed waters and sea ice, and the potential degradation of weapons, sensors, and communications systems.

The RAN has operated in the Southern Ocean since the 1940s, when its capabilities were vital to the creation of the Australian National Antarctic Research Expedition (ANARE) scientific research stations on Heard and Macquarie Islands (Sea Power Centre 2006). During the 1950s and 1960s, RAN vessels were called upon to provide logistic support and emergency medical evacuations from the stations. During the 1990s, there were two highly publicized rescues of stranded lone yachtsmen conducted by RAN ships. In 1994, *HMAS Darwin* rescued lone yachtswoman Isabelle Autissier, and in 1997 *HMAS Adelaide* undertook one of the most complex ocean rescues ever attempted; a double rescue of around the world yacht racers Thierry Dubois and Tony Bullimore (Sea Power Centre 2006). These rescues were made possible with the support of Navy S-70B Seahawk helicopters and Royal Australian Air Force (RAAF) AP-3C Orion aircraft. As a nation that has signed and ratified UNCLOS, Australia claims a 200nm EEZ for its offshore territories and also claims sovereign rights to manage and conserve associated fish stocks in these waters. With the assistance of tanker and Australian Fisheries Management Authority (AFMA) support, since 1997 the RAN has conducted several Southern Ocean missions to deter, intercept and apprehend Foreign Fishing Vessels (FFVs) believed to be involved in the illegal acquisition of the valuable Patagonian Toothfish.

Article 1 of the *Antarctic Treaty* prohibits all military activity in Antarctica, although military personnel and equipment may be used for scientific research or any other peaceful purpose. Australian military presence in Antarctica has thus far been limited to sending personnel to the continent for expeditionary and scientific purposes, and the deployment of Deployable Geospatial Survey Teams (DGSTs) to obtain higher resolution bathymetry datasets to aid in safety of navigation. Australia has one

government leased ice breaking vessel, the *Aurora Australis*, which is under the command of the Australian Antarctic Division (AAD). The U.S. Antarctic Program has one ice strengthened research vessel and one ice breaker.

In 2041, the *Antarctic Treaty* will be reviewed, which means that it can be modified or changed. Although the *Protocol on Environmental Protection to the Antarctic Treaty* prohibits all activities relating to mineral resources except scientific, this is also due for review in 2048, potentially opening the region to mining and resource exploitation for the first time. Furthermore, many countries of the world are not signatories to the treaty, or do not recognize the claims to territory made by other nations. Although Antarctica is thought to be rich in minerals and resources, it has remained virtually untouched until present. Technological advances coupled with the expiration of current agreements may see territorial disputes not unlike those occurring in the Arctic happening in the future. Such developments are likely to see the need for increased military presence in the currently peaceful polar region.

C. DEFINING THE LIMITS OF THE POLAR OCEANS

Disagreements exist regarding the limits of the Arctic Ocean (Figure 3) and the Southern Ocean (Figure 4). The USA and Australia are member nations of the International Hydrographic Organization (IHO), who are widely considered to be the global authority on the boundaries of the world's oceans. These boundaries are described in the IHO's *Limits of the Oceans and Seas*. According to this publication, the Arctic Ocean is considered to be the smallest world ocean. Its boundaries are clearly set to encompass an almost circular area extending southwards from the North Pole, not including separately named seas. Scientists have defined the 'Arctic System' (Figure 5) as consisting of 'the geosphere and biosphere north of the boreal mean decadal 10°C sea surface isotherm, the surface air 0°C contour that encircles the North Pole, and the southern limit of terrain that drains into the High Arctic' (Roberts et al. 2010).

Figure 3. Map of the Arctic Ocean, showing the Northwest Passage (NWP) and the Northern Sea Route (NSR) (from U.S. Central Intelligence Agency 2010).

Figure 4. Map of the Southern Ocean (from U.S. Central Intelligence Agency 2010).

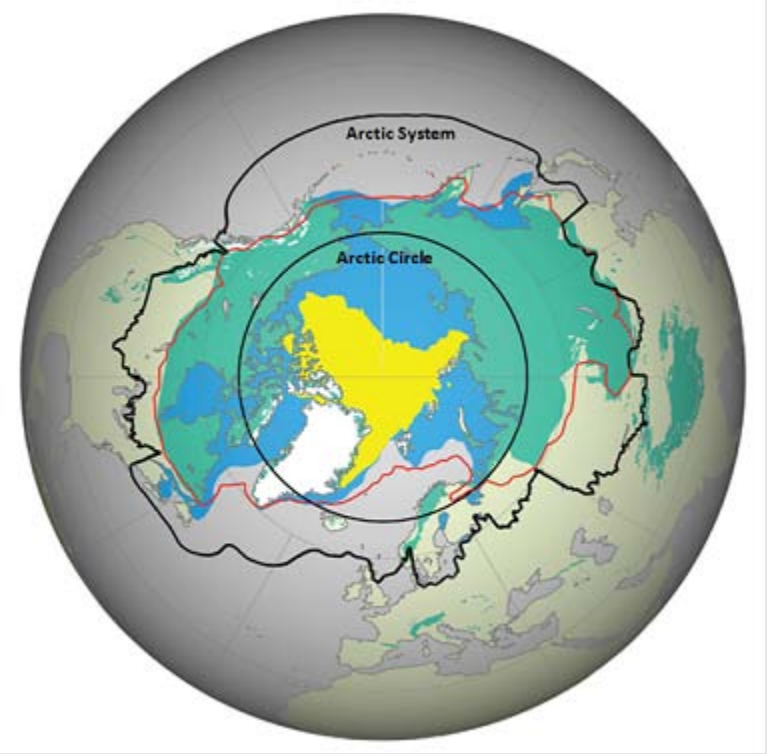

Figure 5. The Arctic System. Mean 0°C contour is shown in red, mean annual sea ice extent (1990–1999) in blue, permafrost and ground ice in green, and minimum observed sea ice extent (September 2007) in yellow (from Roberts et al. 2010).

The Southern Ocean is not defined in *Limits of the Oceans and Seas* as a world ocean at all, and the southernmost waters of the world are instead considered to be an extension of the South Pacific, South Atlantic and Indian Oceans. In 2000, the IHO defined the body of water between the Antarctic continent and 60°S latitude as the Southern Ocean. However, this definition has not yet been ratified due to a dispute with Australian authorities, who consider the Southern Ocean to lie immediately to the south of Australia. Others regard the Antarctic convergence zone, which fluctuates seasonally, to be the separation line from the other oceans.

For the purposes of this study, the Arctic Ocean is considered to consist of the area of ocean encompassed by the Arctic System. The Southern Ocean is defined as the oceanic area south of 60°S latitude, encircling Antarctica.

D. OVERVIEW

This study provides analyses and syntheses of available observational data and numerical model results to advance the understanding of critical processes and feedbacks concerning the oceanic forcing of Arctic sea ice. Qualitative comparisons and analogies or contrasts with oceanic and sea ice processes occurring in the Southern Ocean surrounding Antarctica are also made.

This thesis is organized into the following chapters: Chapter II provides a review of the current state of knowledge on sea ice variability, including a comparison of Arctic and Southern Ocean sea ice regimes; Chapter III describes the data and methodology used to conduct this research; Chapter IV presents numerical modeling and observational results from the Arctic Ocean; Chapter V consists of a discussion and summary of the results, including comparisons to previous studies and to Southern Ocean processes; Chapter VI contains conclusions and; Chapter VII makes recommendations for future research.

THIS PAGE INTENTIONALLY LEFT BLANK

II. CURRENT STATE OF KNOWLEDGE ON SEA ICE VARIABILITY

A. SEA ICE VARIABILITY IN THE ARCTIC OCEAN

Sea ice variability is often difficult to determine due to the different methods used, uncertainties in measurement techniques and the assumptions made. Despite these issues, one thing is abundantly clear: even though sea ice variability differs depending on the method of assessment, there is a general consensus that sea ice in the Arctic is declining at an alarming rate. Although observations of sea ice made using in-situ instruments are often considered to be the most accurate means of determining sea ice variability, they are difficult to obtain due to the extreme nature of the Arctic environment. They are also expensive, labor and time intensive, and provide small datasets that are limited both spatially and temporally. The birth of the satellite era enabled scientists to view almost the entire Arctic Ocean at the same time for the first time in history, and satellite imagery has become an invaluable tool for monitoring changes in sea ice cover. Since 1972, satellite passive microwave data have been used to map ice extent and concentration on a daily basis. Recent advances in GCMs and ice-ocean models have meant that past variability in sea ice can be simulated and future changes predicted more accurately. Sea ice conditions are affected by atmospheric and oceanic processes, both of which must be considered to understand sea ice variability.

1. Determining Sea Ice Variability in the Arctic Ocean

Several studies have described the annual decline of sea ice areal extent based on satellite data, in-situ observations, model predictions, or a combination of these methods (e.g., Comiso et al. 2008; Rigor and Wallace 2004; Stroeve et al. 2007). A complete understanding of the recent Arctic sea ice decline requires an evaluation not only of ice extent, but of the more challenging three dimensional problem, which includes ice thickness. Thorndike et al. (1975) recognized that many of the physical properties of sea ice depend upon its thickness. Although ice thickness is altered by both thermodynamic and mechanical processes, the major variation in ice thickness distribution is due to the

annual thermodynamic cycle, which is responsible for mass changes at the atmospheric and oceanic interfaces. Accurate estimates of sea ice thickness, however, are difficult to obtain due to sparse observations and the errors associated with the various methods of measurement. Direct methods of obtaining ice thickness estimates include upward looking sonar (ULS), ice core sampling and drifting or moored buoys, and indirect methods include remote sensing data and numerical modeling.

a. Remote Sensing Techniques

Satellite and aircraft remote sensing techniques use radar and laser altimeters to derive ice thickness from freeboard, where ice freeboard is the vertical distance between the air-snow interface and the local sea surface (Kwok and Cunningham 2008). Ice freeboard generally consists of a floating sea ice layer with a snow layer on top. The advantage of remote sensing observations is that they cover much greater areal extent than measurements made in-situ and take a relatively short period of time to obtain. For example, ICESat (Ice, Cloud and land Elevation Satellite) covers 93% of the Arctic (Kwok et al 2009). Kwok and Cunningham (2008) estimated ice thickness and snow depth from four ICESat campaigns, where freeboard and thickness from space is retrieved from laser altimeter on ICESat. Although they were able to distinguish between first year and multiyear ice due to their different reflectivities, any long term trends in ice thickness were difficult to estimate, due to the short period of observations. More recent estimates of sea ice thickness and volume were made by Kwok and Rothrock (2009) and Kwok et al. (2009) who compared ICESat campaigns to submarine cruise data. Their results indicated a trend towards thinner, more seasonal ice in the Arctic. The ICESat was launched in 2003 and ICESat-II will not be launched until 2015, and the operational periods do not provide continuous coverage. This method of determining ice thickness therefore has promising potential for monitoring current and future trends in the Arctic, but does not provide an insight into the rapid sea ice decline over the past few decades.

RADARSAT Geophysical Processor System (RGPS) measurements are another relatively recently developed remote sensing technique for assessing sea ice drift and deformation processes. RADARSAT was launched in 1996 and provides almost

basin-scale coverage of the Arctic Ocean at high resolution of about 100m (Kwok et al. 2008). This method provides one of the only available means of seeing small scale processes such as leads and ridging and rafting, which all affect ice thickness. Kwok et al. (2008) compared RGPS three day ice trajectories over six winters from 1997 to 2002 with simulated thickness fields from four numerical models, including the Naval Postgraduate School (NPS) 1/12 degree model. Results showed a noticeable negative trend in mean ice thickness over the period, as well as representing fracture patterns in the ice cover. Although RGPS is useful for examining small scale deformation at basin scales and on seasonal timescales, the importance of producing these patterns for improving climate simulations remains uncertain (Kwok et al. 2008).

b. Submarine Upward Looking Sonar (ULS)

Ice thickness, and therefore trends in sea ice variability, can also be determined from ice draft measurements. Ice draft is the amount of sea ice below the surface of the ocean and constitutes approximately 89% of total thickness (Rothrock and Wensnahan 2007), and it varies with snow loading and ice density. Observations of sea ice draft have been made using ULS on Navy submarines and on moorings. ULS data from Royal Navy (RN) and USN submarines operating in the Arctic has been collected since the Cold War era, and continues to be collected during SAMs under SCICEX Phase II. Some of this data has been declassified and made available to the scientific community. Ice draft data from about 40 submarine cruises between 1958 and 2000, which covers over 120 000km of track, or about 38% of the Arctic Ocean, has been released. The interpretation of submarine data, however, is complicated by sparse sampling (Serreze et al. 2007). There are large variations in the time intervals between the submarine cruises, and the seasons and regions in which they were conducted. Although the results from the data should therefore be interpreted cautiously, ULS data from submarines is arguably the most extensive observational dataset available in terms of spatial and temporal coverage and is therefore useful for determining long term trends in sea ice variability. It may also be one of the most accurate sources for determining sea ice thickness.

Rothrock et al. (1999) compared summer and autumn sea ice submarine draft data from the earliest 18 years of data to that acquired during SCICEX cruises during the mid 1990s. They determined that the mean draft at the end of the melt season over the deep Arctic decreased by 1.3m, or 40%, between the two time periods, with the greatest decreases in the central and eastern Arctic. The thinning of sea ice was attributed to increases in Arctic heat flux from atmospheric and oceanic sources. A more comprehensive study of the variability of sea ice thickness was conducted by Rothrock et al. (2008), based on a quarter of a century of submarine data. Their results showed that annual mean ice draft declined from a peak of 3.42m in 1980 to a minimum of 2.29m in 2000, which is equivalent to a decrease of 1.13m in draft, or 1.25m in thickness over a 20 year period. In this case it was hypothesized that the large change in ice thickness may be due to a cyclical or random variation, or simply due to natural variability.

McNamara (2006) compared submarine ice draft measurements, electromagnetic (EM) induction ice thickness measurements and ICESat data to results from the NPS 1/12 degree coupled ice-ocean model. The observational data validated the model results, which indicated an accelerated thinning trend in Arctic sea ice since the mid 1990s. The results of this study also demonstrated that ice thickness decreased at twice the rate of ice area during the period 1987 to 2002, reiterating the importance of considering sea ice from a three dimensional aspect. This work was followed by Whelan (2007), who conducted a regional and seasonal comparison of additional submarine draft measurements to NPS model output from 1979 to 2000. An overall decline in sea ice thickness of 44% (from a mean value of 4.5m to 2.5m) was determined for this period.

In their aforementioned study, Kwok and Rothrock (2009) compared ice thickness determined from ICESat data to that from submarine records. Their results indicated a peak winter ice thickness of 3.64m in 1980, decreasing to 2.89m in 2008, and they attributed the rapid decline in ice thickness to a significantly increased coverage of thinner seasonal ice during the period. These ice thickness values are comparable to those of Rothrock et al. (2008). The change in the relative quantities of first year and multiyear ice were the focus of Kwok et al. (2009), who compared ULS data from submarine cruises and moored buoys to remote sensing data from ICESat. This time period

encompasses the two years of minimum recorded ice extent in the Arctic - 2005 and 2007. Their results showed a 42% decrease in multiyear ice over the period and a significant increase in the area and volume of first year, or seasonal ice, which became the dominant type of ice cover by 2008. The dramatic decline in ice thickness and volume in recent years was attributed to the near zero replenishment of multiyear ice following the summers of 2005 and 2007, and the inability of the Arctic Ocean to maintain a balance between export, melt and replenishment.

c. Buoy Measurements

In-situ measurements by oceanographic instruments form an integral part of the Arctic Ocean observing system and also provide a means of verifying numerical model results. In the harsh conditions of the Arctic, instrumentation is difficult to deploy and recover, and is prone to destruction or sensor failure due to extreme weather and ice deformation. Buoys moored to the seafloor, such as ULSs, are one example of an Eulerian measurement technique used to monitor the characteristic of sea ice as it drifts above. The recently observed decline in sea ice has prompted the development of several relatively new instruments. These include the ice-tethered profiler (ITP) and the ice mass-balance buoy (IMB), Lagrangian observation systems that move with an ice floe, making high resolution measurements of sea ice and ocean characteristics. These particular instruments are described in further detail in Chapter III. Although they provide a vital means of monitoring sea ice variability, it should be noted that their datasets are limited both spatially and temporally, and by the precision and accuracy of the instrument in question. Measurements made with ice-tethered instruments might also be biased toward thicker ice floes in order to assure a longer life of the instrument.

d. Numerical Modeling

The advantage of numerical models is that they often provide better spatial and temporal coverage than observations and can also be made to make future predictions of sea ice variability. However, many climate models are configured at coarse resolutions and sometimes use crude parameterizations of the processes that affect ice thickness and ocean conditions, thereby limiting their representation of past and present sea ice

variability (Maslowski et al. 2007). A comparison of sea ice simulations from several IPCC AR4 GCMs shows that there is considerable scatter among the models, especially under global warming conditions (Zhang and Walsh 2006). The ability to resolve mesoscale features affecting sea ice, such as oceanic eddies and narrow boundary currents, is vital to the accurate representation of sea ice variability in model results. At high latitudes, this is complicated by the small Rossby radius of deformation (of order 10km), which determines the size of eddies. In order to resolve such features, a high resolution ice-ocean model is therefore required.

In their 2003 study, Maslowski and Lipscomb compared 9km and 18km ice-ocean models. This research showed that the higher resolution model improved the representation of ice deformation and drift, polynyas, ice concentration and ice thickness. Results from Maslowski et al. (2004) using the same 9km model in the vicinity of the Barents Sea and Fram Strait demonstrated the full extent of the contribution of the Barents Sea branch of Atlantic Water into the Arctic Ocean for the first time. This contribution is a potential source of heat, salt and mass transport, all of which affect sea ice variability, at least in the eastern Arctic Ocean. Following this, the comparison of observations with a high resolution ice-ocean model suggested that sea ice thickness especially in the western Arctic may be declining at an even faster rate than ice extent (Maslowski et al. 2007; Stroeve and Maslowski 2008).

Given that the Rossby radius of deformation for the Arctic Ocean is of order 10km, a model at 9km resolution is not able to fully resolve many small scale features. A recent comparison of high resolution model results with observations showed that doubling the horizontal resolution from 18km to 9km increases the mean eddy kinetic energy (EKE) by an order of magnitude or more (Maslowski et al. 2008). The recognition that the processes related to small scale features such as eddies may play an important role in sea ice variability has driven further advancements in high resolution ice-ocean models. One example is the recent development of the 1/48 degree (2.3km horizontal resolution) NPS coupled ice-ocean model.

2. The Role of Atmospheric Processes in the Arctic Ocean

There is no doubt that atmospheric processes play an important role in the variability of sea ice. Thinning ice has been attributed to changes in climate indices such as the North Atlantic Oscillation (NAO), the Arctic Oscillation (AO) and the Pacific Decadal Oscillation (PDO), the effects of which are described in more detail later in this chapter. For example, Rigor and Wallace (2004), Lindsay and Zhang (2005) and Serreze et al. (2007) all attribute declining sea ice during the period from the 1970s to the 1990s to a strongly positive phase of the AO/NAO. Other atmospheric factors affecting sea ice variability include surface air temperature (SAT) and wind forcing. Francis et al. (2005) conducted a regional analysis of satellite derived winds and radiative forcing over a 25 year period in order to determine the factors driving sea ice retreat. They found that downward longwave flux anomalies explained approximately 40% of sea ice variability, although wind forcing was found to be the primary driver in some regions. This was followed by a similar study by Francis and Hunter (2006), which confirmed the positive correlation between sea ice retreat and downward longwave flux.

More recent investigations into the atmospheric effects driving sea ice variability have seen a shift in the way of thinking away from a system driven purely by atmospheric effects and towards one that is also affected by oceanic processes. For example, Francis and Hunter (2007) focused specifically on the drivers of declining sea ice in the Barents and Bering Seas and determined that in addition to wind anomalies, sea surface temperature (SST) variations also play an important role in ice variability, especially in winter. Deser and Teng (2008) analyzed satellite derived sea ice concentration data over a 28 year period with the aim of determining the role of atmospheric forcing in sea ice variability. Their results also indicated that sea ice decline is not directly attributable to a trend in the overlying atmospheric circulation, and that oceanic forcing plays a vital role, once again especially in winter. Furthermore, model results (Stroeve and Maslowski 2007) suggest that atmospheric forcing accounts for less than half of the variance in Arctic sea ice cover, and a recent study conducted by Tseng (2010) using partial covariance analysis made a similar determination.

3. The Role of Oceanic Processes in the Arctic Ocean

Based on the preceding summary, it is clear that atmospheric processes alone do not account for all observed sea ice variability, especially in the case of reduced ice growth or melt in winter, when air temperatures are much too cold to melt ice from above and there is no incoming solar radiation. Atmospheric events, such as storms, affect sea ice over relatively short timescales of hours to days. Conversely, the ocean has a much longer 'memory' than the atmosphere, and some oceanic events persist for weeks to years, potentially affecting sea ice variability throughout this time.

In 1997-98 a yearlong field experiment, the Surface Heat Budget of the Arctic Ocean (SHEBA) was conducted on a drifting ice pack in the Arctic Ocean in order to better understand the physical processes that determine the surface energy budget and sea-ice mass balance in the Arctic Ocean (Uttal et al. 2002). This was one of the largest interdisciplinary and comprehensive efforts ever conducted in the Arctic and included atmosphere, ice and ocean measurements down to a depth of 500m. A recent study by Shaw et al. (2009) used observations from the SHEBA experiment to focus on the role of the upper ocean in the energy budget of Arctic sea ice in the western Arctic. Their heat flux estimates indicated that the dominant source of heat for melting ice from below was the absorption of solar radiation by the upper ocean, followed by the lateral advection of warm water of Pacific origin. A comparison of observational and model results suggested that 16 to 24% of ocean-to-ice heat flux was supplied by the entrainment of heat from below the mixed layer, and that this entrainment was largest during winter. Furthermore, heat flux estimates from the SHEBA year indicate that the ocean and atmosphere play roughly equal roles in melting sea ice.

Results from Shimada et al. (2006) for a similar time period also imply that atmospheric forcing only partially explains the recent changes in sea ice cover and that an area of anomalous sea ice reduction in the Canada Basin corresponds with an area where warm Pacific Summer Water (PSW) is observed just below the mixed layer. They suggest that the warming of the upper ocean during this period was due to a positive feedback mechanism initiated by delayed sea ice formation in early winter. Additionally, the analysis of surface and bottom melt observations from IMBs in the Beaufort Sea

show that the transfer of heat from the upper ocean to the bottom of the ice potentially causes a large amount of bottom ablation (Perovich et al. 2008). In this case, the record minimum ice extent in 2007 is attributed to the positive ice-albedo feedback effect causing solar heating of the upper ocean, which is then transferred to the underside of the ice.

Recent analyses of measurements from the Canada Basin reiterate the contribution of a warming ocean to the bottom melting of sea ice. Observations from conductivity temperature depth (CTD) sensors and ITPs suggest that the warming of the near-surface temperature maximum (NSTM), which is found at depths of approximately 25 to 35m, has caused increased ice melt during recent years (Jackson et al. 2010). The NSTM is seen as a mechanism for storing heat below the surface mixed layer from solar radiation in summer, and may persist year round, entraining heat into the surface mixed layer and melting the underside of the ice. The comparison of ITP and IMB data with a one-dimensional model by Toole et al. (2010) also demonstrates that Arctic sea ice is most sensitive to changes in ocean mixed layer heat, especially in summer due to solar heating of the upper ocean opening leads. This study focused on the strong stratification at the mixed layer base, which is thought to limit the flux of deep ocean heat to the bottom of the ice.

The aforementioned studies all recognize the vital role that oceanic processes play in sea ice variability, and most attribute increases in oceanic heat to the ice-albedo feedback mechanism. However, this feedback does not fully explain basal ice melting, since solar radiation requires areas of open leads in order to be able to penetrate the ocean surface. In some instances, there must be a source of oceanic heat being entrained into the mixed layer from below, especially in the case of winter reduction of sea ice growth or melt, when there is no incoming solar radiation. We hypothesize that mesoscale eddies may be a significant source of heat via upward entrainment into the mixed layer. Such eddies have the potential to erode the pycnocline, thus reducing or eliminating the density stratification.

The analyses of ITP measurements in the Canada Basin have indicated that shallow eddies can change the stratification of the halocline and may be a preconditioning mechanism for higher heat fluxes and the potential melt of ice from below (Timmermans et al. 2008). Maslowski and Clement Kinney (2010) compared 1/12 degree NPS model results to observations in the western Arctic in order to demonstrate the influence of oceanic heating on sea ice variability. Their results also implied that oceanic heat sources may precondition the ice for summer melt and they suggest that up to 60% of the total variance in sea ice thickness in the region can be attributed to the distribution of warm water below ice originating from the Chukchi Shelf and advected by mesoscale eddies.

B. SEA ICE VARIABILITY IN THE SOUTHERN OCEAN

Sea ice in the Southern Ocean surrounding Antarctica is largely seasonal and there are only a few areas in the Weddell, Bellingshausen, Amundsen and Ross Seas where multiyear ice survives the annual melt. The region of Southern Ocean where sea ice exists is not as indicative of changing ice cover as the Arctic Ocean. There is in fact some evidence that sea ice in the Southern Hemisphere may have increased slightly under the global warming conditions of the last few decades, which is in stark contrast to the recent decline observed in the polar regions of the Northern Hemisphere. The Southern Ocean is one of the most poorly observed regions on earth and in-situ sea ice measurements are therefore sparse. Furthermore, few models accurately represent Antarctic sea ice extent (Stroeve et al. 2007). The dynamics and thermodynamics affecting sea ice variability differ between the regions surrounding the Antarctic continent and for this reason many past studies have focused on a particular area, or sea. In the Southern Ocean, sea ice surface melting is small due to very cold surface air temperatures, even in summer. It has been long recognized that oceanic heat, which melts ice from below, is the primary factor affecting sea ice variability in the southern polar region.

1. Determining Sea Ice Variability in the Southern Ocean

The results of studies of sea ice extent in the Southern Ocean are ambiguous and inconsistent. Some historic records indicate that sea ice in the region was significantly further north in the past, which may have corresponded to the Little Ice Age, a period of significant cooling several centuries ago. Estimates of more recent variability in sea ice extent vary between finding no significant changes, to noticeable increases over the past few decades, despite a prevailing warming trend in both atmosphere and ocean temperatures. As for the Arctic, satellite data coupled with in-situ observations, have become a useful tool for monitoring sea ice extent in the Southern Ocean.

Comparisons of ship reports from the expeditions of early explorers in the late eighteenth and early nineteenth centuries to satellite derived ice edge in the 1970s show that although there were particularly heavy ice conditions in the Weddell and Amundsen Seas on occasion, there is no clear cut evidence of significantly more extensive ice overall in early times (Parkinson 1990). A comparison of sea ice extent derived from whaling ship records with that from satellite data suggests that there was no significant deviation in mean sea ice extent from the pre-1950s to the post 1970s (Ackley et al. 2003). A 30 year study of satellite observations by Cavalieri and Parkinson (2003) showed an overall increase in Antarctic sea ice extent from 1972 to 2002, and a similar study conducted by Liu et al. (2004) also indicated an overall increase in ice extent during the satellite era. Both of these studies noted that variations in ice extent differ between regions, and attributed the trends to the effects of long term climate variability. The comparison of passive microwave ice edge against in-situ observations from ships, however, suggests that the results from even the same satellite datasets are inconsistent due to the different algorithms used and because the emissivity of sea ice is highly variable, especially during the melt season (Worby and Comiso 2004).

Few observations of sea ice thickness in the ocean surrounding Antarctica have been made and most previous studies have combined limited observational data with model results to concentrate on specific regions and seasons. Measurements by submarine ULS are not available, or have not been attempted for the Southern Ocean, and buoy measurements are sparse. Most available thickness observations for the region have

been made by ships. Due to some fundamental differences in the dynamic and thermodynamic conditions, Southern Ocean sea ice is generally not as thick as Arctic Ocean sea ice, except in some of the regional seas, where multiyear ice exists. However, as for the Arctic Ocean, there has been some recognition of the importance of monitoring sea ice thickness, especially in the regions of multiyear ice, in order to determine long term trends under global warming conditions.

Studies into ice thickness over the past few decades have shown that despite differences in location, average thicknesses and the processes determining those thicknesses are not that dissimilar between the regions surrounding Antarctica. During the Winter Weddell Sea Project (WWSP) of 1986, scientists conducted a transect across the entire width of the sea in midwinter, measuring ice thickness by direct drilling and helicopter radar profiling (Wadhams et al. 1987). This study was one of the first of its kind and revealed some important findings about the ice thickness distribution in the region. It was determined that most of the sea ice was concentrated into a thickness range of 0.4 to 0.6m in winter, and that growth rates were small due to high ocean heat fluxes. Results from analyses of data collected from a 1993 winter voyage into the Bellingshausen and Amundsen Seas showed a slightly larger dominant ice thickness category of >0.7m, and the process of floe thickening was attributed to ice deformation in this region (Worby et al. 1996).

From the data available to date, there is no clear evidence of recent changes in the thickness to which first year ice grows, or changes to the thickness of limited multiyear ice in the Southern Ocean. Driven by the incentive that there was no Antarctic sea ice thickness climatology available to modelers and that changes in ice thickness may be going unnoticed, in 1997 the Antarctic Sea Ice Processes and Climate (ASPeCt) program was established to collate data from icebreakers. The analyses by Worby et al. (2008) of more than two decades of data show that the largest variability in ice thickness over all regions occurs in summer, when ice concentrations are lowest. The ice thickness distribution showed the least variability in the western Weddell Sea, which contains the most multiyear ice and is therefore ice covered for most of the year, unlike the majority

of the Southern Ocean. In the remaining regions, where predominantly seasonal ice exists, there were similar cycles of variability and mean annual thickness.

2. The Role of Atmospheric Processes in the Southern Ocean

As for the Arctic Ocean, variability in Southern Ocean sea ice is linked to climatic conditions and is affected by long term changes in atmospheric circulation on time scales of months to decades. Anomalies in sea ice cover have been linked to several modes of climate variability including the El Nino Southern Oscillation (ENSO), the Antarctic Oscillation (AAO) and the Antarctic Circumpolar Wave (ACW). The effects of these phenomena on sea ice in the Southern Ocean are described in more detail later in this chapter.

SATs over the Antarctic have increased by 0.5°C over the last 50 years, with an increase of ~0.03°C per year over the ice covered areas of the Southern Ocean (Zhang 2007). Other atmospheric changes, such as the passage of storms surrounding the sea ice zone, cause frequent changes in wind intensity, wind direction, and temperature, which can result in daily shifts in ice edge location of up to 1° of latitude (Worby and Comiso 2004). Although changing atmospheric conditions and long term climate variability are important, they do not fully explain Southern Ocean sea ice variability, especially its seasonality. Despite the recent warming trend, SATs over the far Southern Ocean remain largely below freezing year round in the sea ice regions, indicating that oceanic forcing must play a vital role in the annual melt cycle.

3. The Role of Oceanic Processes in the Southern Ocean

Since the 1950s the Southern Ocean has been warming faster than the other oceans of the world (Zhang 2007). Up to 90% of the sea ice cover in the southern polar region melts annually, and oceanic processes have long been recognized as a major contributor to this seasonality. Allison (1979) recognized that the classical relationship between the thickness of sea ice and air temperature, Stefan's Law, cannot be applied to Southern Ocean sea ice. This law greatly overestimates the growth rate of Antarctic sea ice because it neglects the transfer of oceanic heat to the underside of the ice.

The Weddell Sea, which has both seasonal and multiyear ice, has been the focus of several studies into the effects of oceanic heat on sea ice. Weddell Deep Water (WDW) comprises a core oceanic layer within the Weddell Gyre and is characterized by a local temperature maximum of greater than 0°C and low oxygen content (Gordon and Huber 1995). The analyses of observations from the Weddell Sea in the early 1980s showed that the entrainment of relatively warm WDW into the mixed layer causes ice melt, increased convection, and aids in the formation of polynyas, especially in winter (Gordon and Huber 1984; Gordon et al. 1984). A later investigation of the same observations suggested that the mechanisms for the entrainment of WDW into the mixed layer were turbulence, due to ice motion, and convection, from ice formation (Gordon and Huber 1990). The limited thickness of the sea ice cover in the Southern Ocean was attributed to the mixed layer entrainment of relatively warm, salty deep water and to a network of negative feedbacks. A further study using thickness observations from ice core sampling in a region of the Weddell Sea to the west of Maud Rise concluded that high oceanic heat fluxes have a vital role in the early removal of Southern Ocean sea ice at the end of winter, and that atmospheric conditions alone cannot account for ice melt (Gordon and Huber 1995).

The hypothesis that the large persistent Weddell Polynya of the 1970s may have preconditioned the water column in the region for thin ice cover and significantly altered deep water production that persisted nearly two decades later, led to the Antarctic Zone Flux (ANZFLUX) experiment of winter 1994. This experiment was conducted in the Weddell Sea with the goal of measuring and understanding the processes maintaining the relatively high heat flux out of the deep ocean during winter. Initial analyses of results suggested that anomalously large heat fluxes into the mixed layer were driven by high levels of turbulent mixing during storm events (McPhee et al. 1996). Further analyses of flux measurements made during the experiment confirmed that heat flux from well below the mixed layer largely determines the character of seasonal ice cover in the Weddell Sea, and that winter ice growth is severely restricted by oceanic heat from below (McPhee et al. 1999). The physical processes supporting ocean heat flux are still not fully understood,

which has led to a present study of the small to large-scale processes controlling the surface layer buoyancy budget in the Weddell Sea (Stanton and Shaw 2010).

Results from the aforementioned studies, coupled with the knowledge that the Weddell Sea is an extreme case rather than being representative of the Southern Ocean as a whole, has driven scientists to continue their investigation into the oceanic processes affecting sea ice variability in other regions. In 2007, an array of instruments including IMBs and ULSs were deployed in the Bellingshausen and Amundsen Seas for a period of two months. Initial analyses of these observations have shown that the oceanic heat flux in these regions is affected by the entrainment of deep water caused by diffusive, turbulent mixing, or convective overturning processes (Murphy et al. 2010). Further investigation into other regions is required in order to fully understand the regional processes controlling sea ice variability. Results yielded thus far, however, strongly imply that relatively warm ocean temperatures limit the growth of ice in winter and are the principal cause of ice melting. This is in sharp contrast to the Arctic, where the influences of oceanic processes on sea ice have been seldom considered to be a primary driver for the recent decline.

C. COMPARISON OF ARCTIC OCEAN AND SOUTHERN OCEAN SEA ICE REGIMES

There are some fundamental differences between the sea ice regimes of the Northern and Southern Hemispheres that need to be taken into consideration when making analogies or contrasts between the two regions. One of the most striking differences lies in the geography of the regions. The Arctic Ocean is a relatively shallow basin surrounded by continents, with few passages for exchange with the rest of the world ocean. The much deeper Southern Ocean surrounds the continent of Antarctica, making it the only ocean that encircles the globe, and it is open to exchanges with the Indian, Atlantic and Pacific Oceans. Apart from the contrasting geography, there are other factors that should be considered when comparing the polar regions, including the effects of global warming, modes of climate variability, water masses and ocean

circulation, water column structure and sea ice characteristics. The aim of this section is to provide an overview of some of the similarities and differences between the polar oceans that potentially affect sea ice variability.

1. Effects of Global Warming

Sea ice extent in the Arctic and Southern Oceans is characterized by variations from year to year. Under the global warming conditions of the past few decades, however, Arctic sea ice has declined significantly, while the Southern Ocean has shown a very small increasing trend. Although it may seem counter intuitive, this observed hemispheric asymmetry is consistent with modeled responses to increasing CO_2 (Cavalieri and Parkinson 2003). In the Arctic Ocean, sea ice reduction has been attributed to a combination of increased air and sea temperatures, due to GHG emissions, coupled with natural variability and a series of positive feedbacks. In the Southern Ocean, it has been suggested that cooling of the upper atmosphere due to ozone depletion, combined with GHG increases, have caused the strengthening and poleward shift of the westerly circumpolar winds, leading to increased coastal sea ice production (Overland et al. 2008). An alternative explanation is offered in the modeling study by Zhang (2007), who proposes a feedback where increased SATs cause increased melting of sea ice, which in turn increases thermohaline stratification and suppresses convective overturning, thereby inhibiting the upward transport of oceanic heat that is usually the major contributor to sea ice melt in the Southern Ocean.

There is also some evidence to suggest that anthropogenic warming has caused increases in glacial flow in both hemispheres, which may have caused large areas of land fast ice and ice sheet to break away from continental boundaries in recent times. Several massive icebergs have broken off ice shelves in the Ross Sea over the past few years, drifting north towards Australia and New Zealand. In August 2010, the largest iceberg in almost fifty years broke away from the Petermann Glacier on the northwest coast of Greenland, the cause of which was attributed to warm ocean temperatures melting the ice beneath the glacial surface (CBC News 2010).

2. Modes of Climate Variability

Although they do not fully explain sea ice variability in either hemisphere, the effects of long term modes of climate variability on changing ice conditions should be considered. In the Arctic Ocean, variations in sea ice may partially be due to dominant modes of variability such as the NAO, the AO, and the PDO. Changes in Southern Ocean sea ice have been attributed to ENSO and other long term atmospheric variations which alter Southern Hemisphere tropospheric circulation, such as the AAO and the ACW.

The AO is closely related to the NAO and the combined effects of these phenomena are referred to as the Northern Annular Mode (NAM). These oscillations have positive and negative phases, which alternate over time periods of weeks to decades. The strong positive phase of the AO during the 1990s is thought by many to account for much of the decrease in Arctic sea ice extent over recent years (Cavalieri and Parkinson 2003). During the positive phase, or cyclonic mode of the AO, the Beaufort Gyre is shifted to the southwest and the divergence of ice and water from the centre of the gyre results in shorter residence times for sea ice within the Arctic and in increased ice melt. The PDO is an even longer term pattern of climate variability affecting the Arctic, and is characterized by cool and warm phases that can persist for up to twenty to thirty years, potentially affecting sea ice variability throughout this period.

In the Southern Ocean the AAO, which is also known as the Southern Annular Mode (SAM), is a dominant mode of climate variability which occurs on timescales of weeks to years. Forcing due to GHG and aerosols gives rise to a positive trend in the SAM (Simmonds 2003). The positive phase of the SAM is characterized by a strong pressure gradient, which blocks storms and keeps central Antarctica cold, and a positive SAM during recent years has been suggested as another reason why Southern Ocean sea ice does not appear to have been affected by global warming to the same extent as the Arctic. Furthermore, analyses of satellite data has shown that over a 24 year period, a positive SAM coupled with a slightly negative ENSO produced regional ice trends in the seas surrounding the Antarctic continent (Kwok and Comiso 2002; Liu et al. 2004). Another phenomenon that is also thought to affect regional variability in sea ice over

periods of four to five years is the ACW, a term coined by White and Peterson (1996) to describe a system of coupled anomalies which propagate eastward across the Southern Ocean with the circumpolar flow.

The various modes of climate variability play an important role in both hemispheres and associations between climate anomalies and the behavior of sea ice are evident, but their influence alone does not explain many changes in sea ice. For example, the fact that Arctic sea ice has continued to decline despite a shift to a more neutral or negative phase in the NAM in recent years suggests that this is not the only mechanism affecting the ice. However, positive phases may play an important role in preconditioning the ocean for future melt by leaving the Arctic with thinner ice which is more vulnerable to melt in summer. Although some links between phases of climate variability and regional sea ice trends have been made in the Southern Ocean, regional ice trends are also very sensitive to the influence of topographic effects, such as katabatic winds, and to the intensity and path of low-pressure systems.

3. Ocean Circulation

Many characteristics of the global ocean reflect the influences of the polar oceans. Deep and bottom waters formed in the polar regions form part of the global thermohaline circulation and are transported around the world via the 'Great Ocean Conveyor' (Broecker 1992). Two of the world's deepest water masses, North Atlantic Deep Water (NADW) and Antarctic Bottom Water (AABW) form as a result of convective and sea ice processes in the polar regions of the northern and southern hemispheres respectively. High salinity, low nutrient NADW is formed due to deep convection caused by intense cooling in the Labrador and Nordic Seas, whilst high salinity, high density AABW is a product of ice production and brine rejection in the vicinity of the continental shelf surrounding Antarctica (Goosse and Fichefet 1999). Variability in oceanic and sea ice processes in the polar regions has the potential to impact the formation and properties of these water masses, thereby having long term trends for global ocean circulation.

The Arctic and Southern Oceans are both characterized by complex ocean circulation systems, including gyres and currents, many of which vary due to seasonal effects and on timescales of weeks to decades in response to atmospheric and oceanic forcing. For example, in the western and central Arctic, the combined effects of the Beaufort Gyre and the Transpolar Drift (Figure 6), which exports ice into the North Atlantic, has significant influence on the transport and residence time of sea ice within the Arctic Ocean. Unprecedented melting, combined with a shift and significant acceleration of the Transpolar Drift, are thought to have been a major contributor to the dramatic decrease in Arctic sea ice during recent years (Gascard et al. 2008). In the Southern Ocean, the strong eastward flow of the Antarctic Circumpolar Current (ACC), which is delineated by strong ocean fronts (Figure 7), provides an inter-basin connection for the world's oceans, therefore influencing the global transport of heat, freshwater and other properties (Rintoul et al. 2001). The circulation of ocean and ice in the regional seas surrounding Antarctica is largely dominated by cyclonic gyres and by the Antarctic Coastal Current, which flows westward around the continent.

Figure 6. Arctic Ocean circulation, showing the Beaufort Gyre and the Transpolar Drift (from Arctic Monitoring and Assessment Programme (AMAP) 1998).

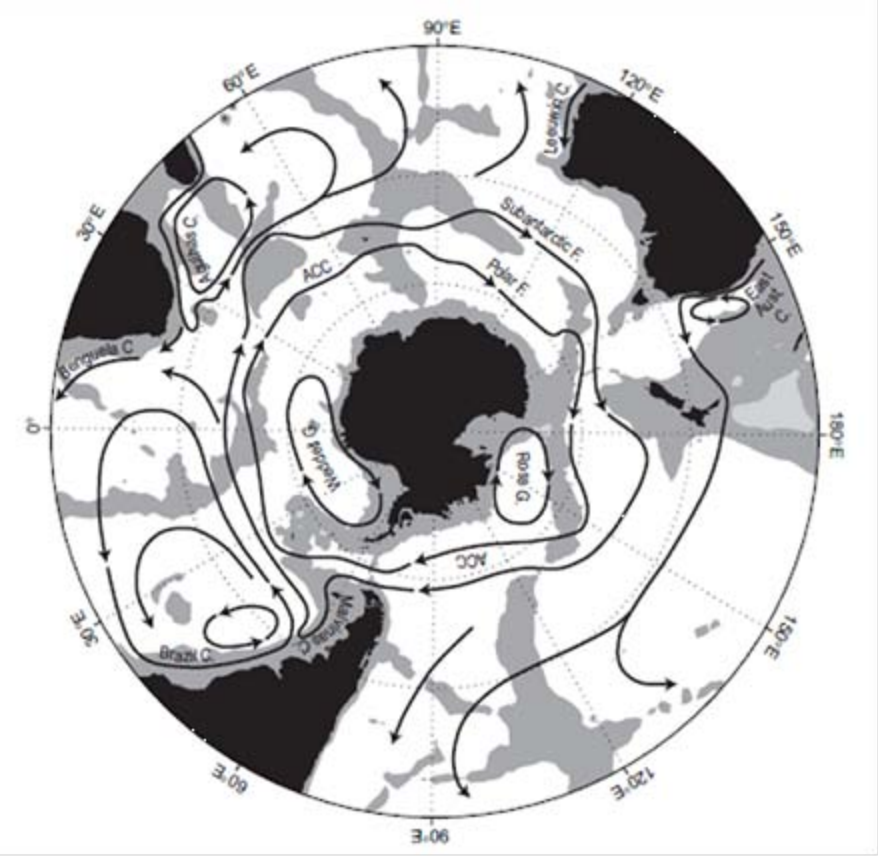

Figure 7. Southern Ocean circulation, showing the ACC and associated fronts, and the Ross and Weddell Sea Gyres (from Rintoul et al. 2001).

4. Upper Water Column Characteristics

One of the most striking contrasts between the oceanic characteristics of the Arctic and Southern Oceans lies in the structure of the upper water column. In the Arctic Ocean, a Cold Halocline Layer (CHL) exists between depths of about 50 to 200m, which marks the transition between cold, fresh polar surface water and warm, salty water of Atlantic origin (Brandon et al. 2010). This layer is thought to inhibit the upward mixing of warm Atlantic water into the mixed layer due to its steep density gradient, therefore minimizing the oceanic heat available to melt sea ice. The absence of a CHL would enable heat to penetrate the mixed layer, potentially leading to substantial ice melt due to oceanic sources, similar to that seen in the Southern Ocean. Observational evidence from

the Eurasian Basin suggests that the CHL retreated during the 1990s to cover significantly less area, potentially changing the mass balance of sea ice in the region (Steele and Boyd 1998).

Due to strong stratification, mixed layer depths (MLDs) in the Arctic are typically restricted to a maximum of 30 to 40m, and convection is limited. In comparison, in the Southern Ocean, the absence of a CHL and the passage of intense storms leads to vigorous mixing, resulting in average MLDs greater than 100m. Furthermore, the upper ocean in the Arctic is also affected by large volumes of freshwater input due to several large river runoffs from the surrounding continents. This forms a layer of cold fresh water at the ocean surface, contributing to greater stratification than in the Southern Ocean where such freshwater sources are absent.

5. Sea Ice Characteristics

There are several characteristics that are unique to each of the polar oceans, which potentially affect the formation and variability of sea ice. From summer to winter in the Arctic, sea ice extent doubles in size, and for the Southern Ocean, it increases by about five times the size (Figure 8). Due to differences in atmospheric and oceanic circulation, sea ice in the Arctic is asymmetric, with more ice in some areas than in others, whilst the sea ice surrounding Antarctica is almost symmetric around the pole. Apart from being out of phase by six months, the seasonal distributions of sea ice in each hemisphere are also different. In the northern hemisphere, the growth period for sea ice is generally as long as the melt or decay period, but in the southern hemisphere, the growth season takes about seven months and the decay period only five months, which can be partially attributed to contrasting geographical and environmental factors (Comiso 2010). Traditionally, Arctic Ocean ice cover was characterized by large areas of thick, multiyear ice that survived the summer melt season although in recent decades it has been moving towards a thinner, more seasonal regime that is characteristic of most of the sea ice in the Southern Ocean.

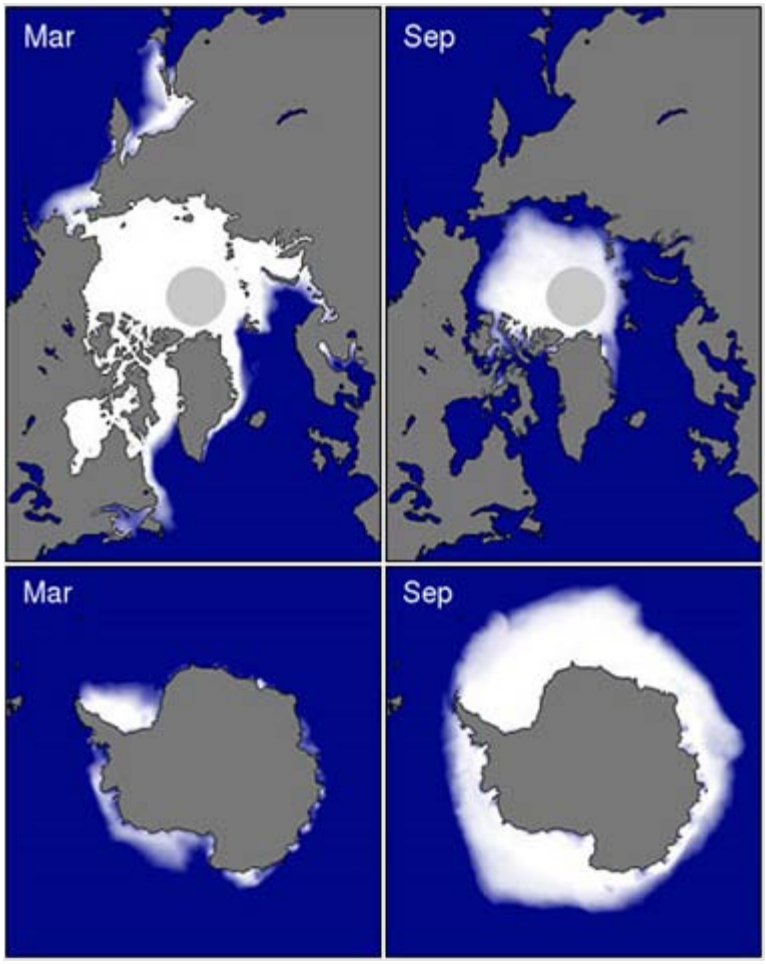

Figure 8. Minimum and maximum sea ice cover for the Arctic Ocean (top) and the Southern Ocean (bottom) (from NSIDC 2010).

The formation mechanisms, which affect the characteristics of sea ice, are also somewhat different in each of the polar oceans. In general, sea ice is formed when seawater reaches freezing point, frazil ice crystals form in supercooled water, and brine rejection occurs. Deformation processes, such as ridging and rafting, result in the formation and thickening of sea ice. However, a fundamental difference between the two hemispheres occurs due to the role that snow plays in sea ice formation. Snow has important implications for sea ice because it affects the thermal conductivity and albedo of the ice, influencing growth, melt and thickness. In the Southern Ocean, precipitation rates and therefore snowfall is higher than in the Arctic, and the formation of snow-ice is common. Snow-ice forms when a mass of relatively thick snow cover depresses the sea

surface below sea level, flooding the ice and resulting in the infiltration of seawater into cracks and brine drainage channels, which forms slush before freezing into ice (Massom et al. 2001). Flooding of sea ice is rare in the Arctic, but in the Southern Ocean it contributes significantly to the total mass of the ice.

It is clear that the Arctic and Southern Oceans are inherently different in many ways. There are obvious differences in the geography and the effects of global warming at high latitudes in both hemispheres, and contrasts can be made between the atmosphere, ocean and ice characteristics. Perhaps more importantly, there are many similarities between the polar oceans, which may hold the key to explaining the drivers of recent Arctic sea ice decline. The fact that the Arctic Ocean appears to be on a trajectory towards the type of seasonal ice cover that is characteristic of the Southern Ocean is justification in itself for further investigation into the analogous processes occurring in both sea ice regimes.

THIS PAGE INTENTIONALLY LEFT BLANK

III. DESCRIPTION OF DATA AND METHODOLOGY

A. NAVAL POSTGRADUATE SCHOOL (NPS) PAN-ARCTIC COUPLED ICE-OCEAN MODEL

The NPS pan-Arctic coupled ice-ocean model, which is also known as the NPS Arctic Modeling Effort (NAME), was developed to provide high resolution simulations of ocean and sea ice processes in the Northern Hemisphere. The model domain (Figure 9) encompasses all major inflow and outflow areas of the Arctic Ocean and the surrounding seasonally ice covered seas (Maslowski et al. 2004). Model bathymetry derives from the 2.5km resolution International Bathymetric Chart of the Arctic Ocean (IBCAO) digital bathymetry dataset. The model is forced using daily atmospheric fields from the European Centre for Medium-range Weather Forecasts (ECMWF) reanalysis data. Although the model does not allow any transfer across lateral boundaries, including river runoff, it does include an artificial channel connecting the North Atlantic and the North Pacific, in order to balance the net northward water transport through Bering Strait.

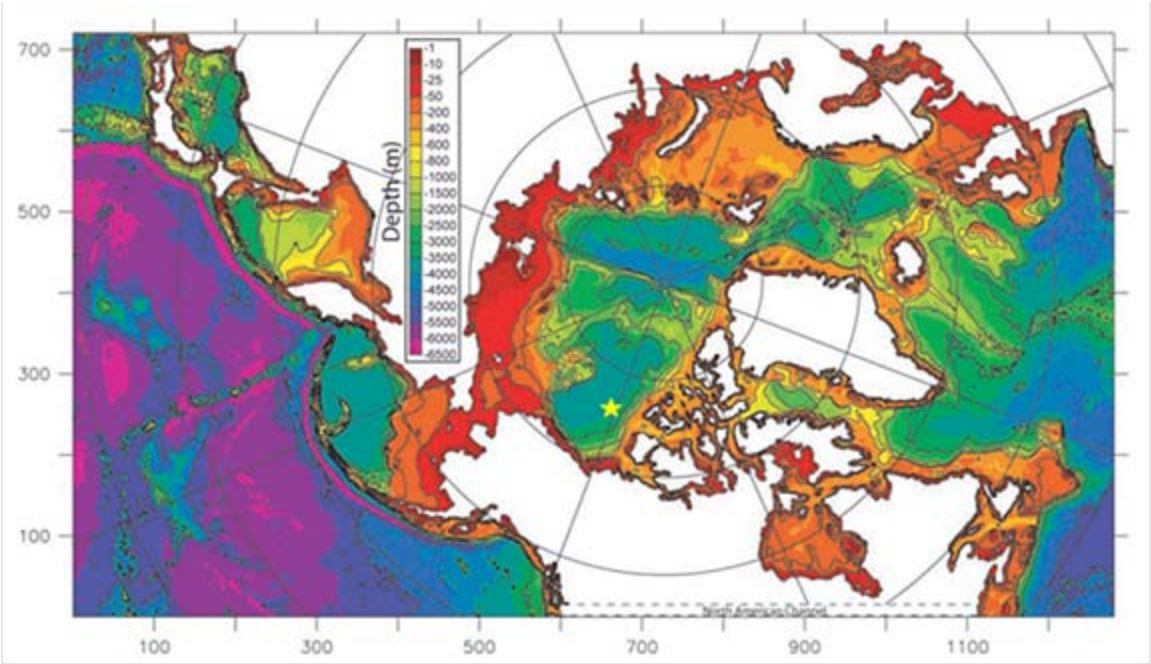

Figure 9. NPS 1/12 (~9km) model domain and bathymetry (from Maslowski et al. 2004). The dashed lines indicate the artificial channel connecting the North Atlantic and the North Pacific and the yellow star marks the position of a 5x5 grid cell area used as a region of focus for model case studies.

The model is configured on a rotated spherical co-ordinate grid and can be run at a high horizontal resolution of 1/12^{o} (~9km), or an ultra-high resolution of 1/48^{o} (~2.3km). The 1/12^{o} model covers 1280x720 horizontal grid cells and has 45 vertical levels, with eight levels in the upper 50m and 15 levels in the upper 200m of the ocean. Model output is available thus far for a 26 year period from 1979 to 2004. This version of the model is considered to be 'eddy permitting', as the horizontal resolution enables mesoscale features of approximately 36km (or four grid points) to be resolved. Smaller scale features are not well represented (if at all) at this resolution (Maslowski et al. 2004). Further information about the NPS 1/12^{o} model can be found in Maslowski and Lipscomb (2003), Maslowski et al. (2004), and Maslowski et al. (2008).

The 1/48^{o} model covers 5120x2880 grid cells (over the same domain as the 1/12° model) and has 48 vertical levels, with three extra levels in the upper 10m compared with the 1/12° model. Model output thus far is available for the one year period of 1983. This

version of the model is 'eddy resolving' due to its ability to resolve features of approximately 10km, and this higher resolution model is more likely to identify and better represent small scale features than the coarser resolution model. Further information about the NPS $1/48^{o}$ model will be provided at http://www.oc.nps.edu/NAME/name.html as it becomes available.

The NPS model output datasets used in this study include daily, monthly, annual and 26 year mean ice and ocean data from the 9km model, which are used to determine seasonal and decadal trends, and to investigate the occurrence of mesoscale events on a daily basis. Daily and monthly mean ice and ocean data from the 2.3km model are used to make comparisons to the 9km model results for the period of 1983.

B. ICE-TETHERED PROFILER (ITP)

The ITP (Figure 10) was developed as part of the global ocean observing system (GOOS) to provide high vertical resolution (better than 1m) measurements of ice covered oceans for periods of up to three years. The ITP is a Lagrangian measurement system which is tethered to, and drifts with, a multiyear ice floe. The system includes an underwater profiling unit that is comprised of a CTD and other instrumentation as required. Typical profiling speed is $0.25ms^{-1}$ and measurements are made at depths of approximately 5 to 750m, generally at six to twelve hourly intervals. Data are transferred from the ITP to shore in near real time via satellite link. The accuracy of the ITP data is limited by several factors and the data used in this research was adjusted for uncertainties as detailed by Krishfield et al. (2008b).

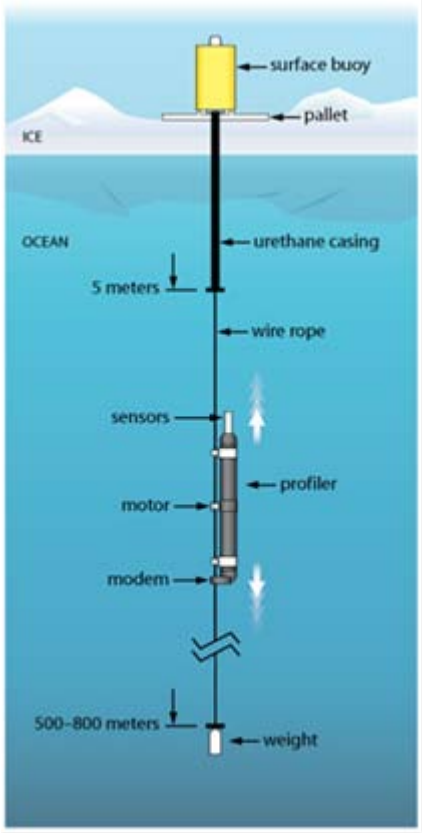

Figure 10. ITP schematic (from http://www.whoi.edu/itp).

The ITP data analyzed here were collected and made available by the ITP Program based at the Woods Hole Oceanographic Institution (WHOI) (http://www.whoi.edu/itp). Since their inception in 2004, ITPs have been deployed in several areas of the Arctic Ocean including the Beaufort Sea, the Central Arctic and the North Pole regions. ITP data is available at three levels of processing: Level 1 (raw data), Level 2 (real time data) and Level 3 (archive data). Level 3 data are from completed missions and have been corrected for sensor response, adjusted for regional conductivity based on historical hydrographic data, and have been edited to provide the best estimates of ocean properties (WHOI 2010). The ITP data used in this research are Level 3 data from ITPs 1, 3 and 6 (Beaufort Sea region) and ITP10 (central Arctic region) and Level 1 raw location data from ITP1. Further details regarding the ITP system and data are available at the above website and in Toole et al. (2006), Krishfield et al. (2008), and Toole et al. (2010).

C. ICE MASS-BALANCE BUOY (IMB)

The IMB (Figure 11) is also a Lagrangian measurement system that is tethered to a moving ice floe in order to measure thermodynamic changes in the mass balance of the sea ice cover. The system measures atmospheric parameters (air temperature and mean sea level pressure) and includes a string of thermistors spaced at 10cm intervals to measure ice and upper ocean temperatures from the top of the ice to depths of 3.8m. The accuracy of the thermistors is better than 0.1^{o}C (Perovich et al. 2009). Acoustic rangefinders measure the positions of the top and bottom of the ice and the uncertainty in the amount of basal ice loss or gain is estimated to be +/-1cm over a full season (Toole et al. 2010). Data is transmitted to shore via an Argos transmitter and satellite system.

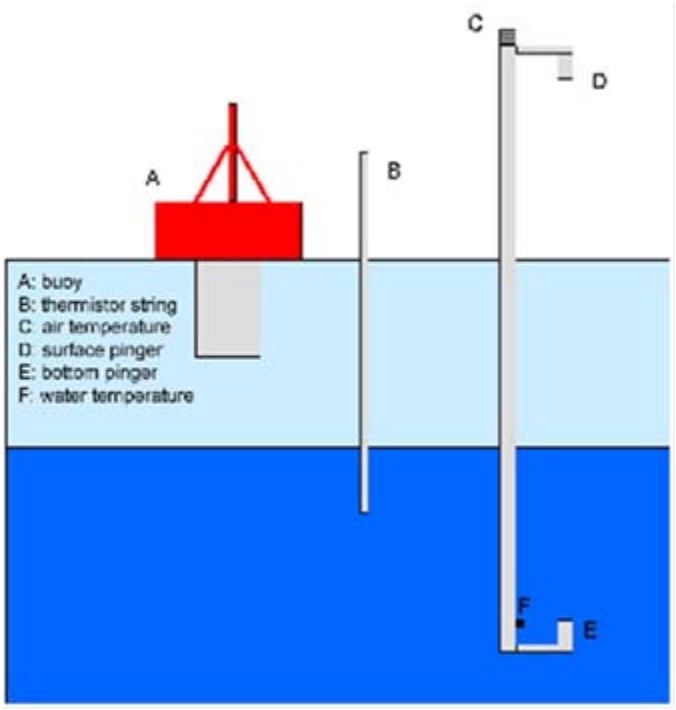

Figure 11. IMB schematic (from http://imb.crrel.usace.army.mil/buoyinst.htm).

The IMB data presented here were provided by the Cold Regions Research and Engineering Laboratory (CRREL) (Perovich et al. 2009). Since their inception in 1997, over 40 IMBs have been deployed in various areas of the Arctic Ocean, and five in the Southern Ocean. The IMB data used in this study are from IMBs 2005C, 2005B, 2006C and 2007H, which were co-located with ITPs 1, 3, 6 and 10, respectively (Figure 12).

Further details regarding the IMB system and data are available at http://imb.crrel.usace.army.mil/index.htm and in Richter-Menge et al. (2006), and Toole et al. (2010).

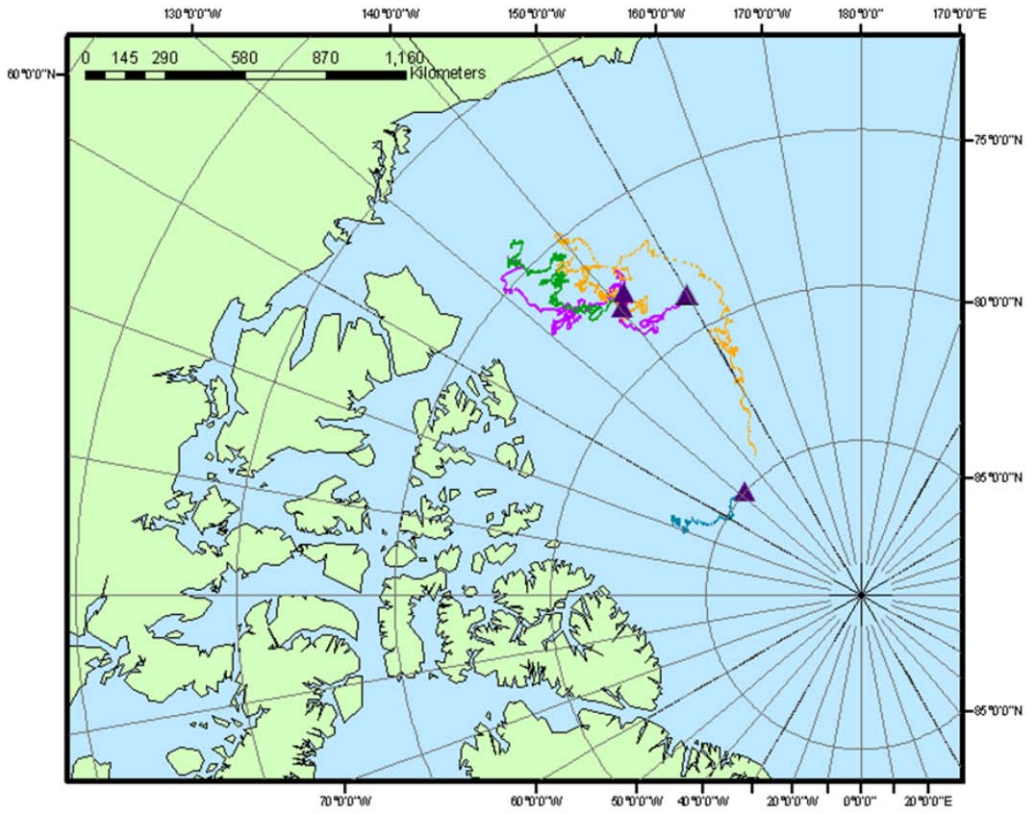

Figure 12. Map of the western and central Arctic Ocean showing drift tracks of ITP1/IMB2005C (pink), ITP3/IMB2005B (green), ITP6/IMB2006C (orange) and ITP10/IMB2007H (blue). Purple triangles indicate start positions.

D. METHODOLOGY

Due to the fact that sea ice melt has been particularly pronounced in the western Arctic over recent years, we focus on co-located ITPs and IMBs in the Beaufort Sea and also include one ITP/IMB pair that was located further north in the central Arctic to provide a means of regional comparison. The NPS model domain was reduced to focus on a region of the western and central Arctic Ocean that encompasses the areas covered by the ITPs and IMBs.

Most of the instruments selected survived a period of at least one year, allowing seasonal differences in the structure of the upper water column and the sea ice characteristics to be identified. The hypothesis that entrainment events driven by mesoscale eddies may locally be a significant contributor to sea ice melt, or a limiting factor for ice growth in winter, led to the identification of several case studies of interest. These case studies were initially selected by visually identifying periods of a few days duration where there was noticeable warming and freshening of the upper water column that appeared to be driven by an oceanic source and that was occurring during the winter, where winter is considered to be from December to May. Analysis of daily model output focused on periods that corresponded with similar times of the year to the ITP/IMB case studies.

In order to ensure a good means of comparison, wherever possible the same calculations were used to determine oceanic parameters from the observational data and from the model output. For example, potential density was derived from model and ITP salinity, temperature and pressure data using the same simplified equation of state. The speed of the sea ice from observational and model data is also of interest because it may be indicative of the passage of extreme weather events, such as storms, which in turn affect the distribution of oceanic heat in the upper water column beneath the ice. In order to determine whether periods of increased heat in the upper water column were driven by particularly fast moving ice, floe speed (FS) (ms^{-1}) for each co-located ITP/IMB case and for the model output was determined from horizontal velocity using the following equation:

$$FS = \sqrt{u^2 + v^2} \tag{1}$$

where u and v are the horizontal components of velocity (ms^{-1}) in the x and y directions respectively. Furthermore, to influence the growth or melt of sea ice, heat must be entrained into the mixed layer at the underside of the ice. The oceanic properties of, and changes to, the mixed layer are therefore of interest, especially during any potential entrainment events. The mixed layer depth (MLD) (m) was calculated from single ITP

profiles and from model output using the method described by Shaw et al. (2009), where the MLD is defined as the depth at which density increases from its surface value to 20% of the difference between the 100m and surface values.

Several calculations were made using only the NPS model data. Model ice and ocean data were used to calculate sea ice thickness, sea surface height anomaly (SSHA), total kinetic energy (TKE) and eddy kinetic energy (EKE). SSHA and EKE are useful parameters for identifying regions of active mixing and the possible entrainment of heat into the mixed layer, which may be associated with mesoscale eddy activity. Daily SSHAs (cm) were calculated from daily mean sea surface height (SSH) with reference to the monthly mean SSH. TKE (cm^2s^{-2}) was determined using the following equation:

$$TKE = \frac{u^2 + v^2}{2} \tag{2}$$

and daily EKE (cm^2s^{-2}) was found using:

$$EKE = \frac{u'^2 + v'^2}{2} \tag{3}$$

where *u'* and *v'* are daily fluctuations in velocity (cms^{-1}), determined from the difference between the daily and monthly mean horizontal velocity components. Furthermore, in order to find any obvious correlation between changes in ice thickness and changes in upper ocean salinity, fresh water content (FWC) (m) was found using the method described by Proshutinsky et al. (2009) where:

$$FWC = \int_{z2}^{z1} \frac{[Sref - S(z)]}{Sref} dz \tag{4}$$

and *Sref* is 34.8psu, *S(z)* is the salinity of the water at depth *z*, *z1*=0 (the surface) and *z2* is the depth level where *S(z)=Sref*.

Other ice and ocean parameters were calculated using only observational data from the ITPs and IMBs. In order to determine if the water within the mixed layer was at

or above the freezing point, the difference between the potential temperature θ (°C) and the freezing temperature T_f (°C) at the surface was determined where:

$$T_f = -0.054S \tag{5}$$

and S is salinity (psu) from ITP measurements. Heat content Q (Jm^{-2}) was calculated per unit area over the depth of the mixed layer (denoted by subscript ML) using the equation adapted from Shaw et al. (2009):

$$Q = c_w \overline{\rho_{ML}} \sigma T_{ML} h_{ML} \tag{6}$$

where the specific heat of seawater c_w is set to a constant value of $4186 Jkg^{-1}{}^{\circ}C^{-1}$, ρ is density ($kgm^{-3}$), σT is departure from freezing point (°C) and h is depth (m). Once heat content was determined, and assuming that there is no atmospheric contribution and that all oceanic heat goes into melting ice, the depth of basal ice melted Δh_{bot} (m) was calculated as follows:

$$\triangle h_{bot} = \frac{Q}{\overline{\rho_{ML} L_f}} \tag{7}$$

where the latent heat of fusion for sea ice L_f with a salinity of 6psu is set to a constant value of $2.7 \times 10^5 Jkg^{-1}$. Additionally, the volume of water from sea ice melt (where sea ice is assumed to be of salinity 6psu) that is required to reduce salinity from the 'before' entrainment value of salinity to the 'during' entrainment value of salinity per unit area over a given depth was determined using a simple conservation of volume calculation.

Ocean heat flux F_0 (Wm^{-2}) near the ice-ocean interface was also determined from ITP data using the method described by McPhee et al. (2003), where turbulent heat flux is a product of interfacial friction velocity and the elevation of the mixed layer above freezing given by:

$$F_0 = \rho c_w c_H u_* \sigma T \tag{8}$$

where c_H is the dimensionless bulk heat transfer co–efficient (equal to 0.0057) and u_* is the interface friction velocity (ms^{-1}). Friction velocity is derived using the Rossby

similarity method described by McPhee et al. (1999), where friction velocity is a function of ice velocity relative to the geostrophic flow (in this case assumed to be equal to the actual ice speed), the coriolis parameter *f*, the hydraulic roughness of the underside of the ice z_0 (assumed to be 0.01m for multiyear ice), and neutral static stability constants.

Furthermore, in order to determine whether inertial oscillations had a significant influence on the drift trajectory of the ITPs/IMBs, position data for the instruments of interest were analyzed. Results indicate that inertial oscillations play a negligible role in the movement of the Lagrangian drifters, especially during the winter. Further information regarding the methods used to determine the significance of inertial oscillations and some example results are included in Appendix A.

IV. RESULTS

Results from the NPS model and from ITP and IMB observations from the central and western Arctic Ocean are presented in this chapter, including winter case studies which focus on the Beaufort Sea. A more detailed analysis and discussion of these results, including a comparison to previous studies and to processes occurring in the Southern Ocean, is in Chapter V.

A. MODEL RESULTS

Results from the 9km and 2.3km NPS models are presented in this section. In the following text, the former model configuration is referred to as 'eddy permitting' and the latter as 'eddy resolving'. Although the model output spans a 26-year period that precedes that of the ITP and IMB observations, the focus on winter months over a similar region of interest allows some analogies to be made between the two datasets. The model results also provide a more complete regional overview of expected sea ice and ocean conditions than those available from the in-situ measurements, which are limited both spatially and temporally. For completeness, and to provide a means of seasonal comparison, some summer (September) model results are included in Appendix B.

1. Decadal Variation in Sea Ice and Ocean - Winter 9km Model Results

In order to assess the modeled changes in sea ice and ocean, decadal variation in winter sea ice thickness, salinity and fresh water content (FWC) was investigated for the western and central Arctic Ocean. Results are presented for the early winter month of December (Figures 13 to 15) and the late winter month of May (Figures 16 to 18).

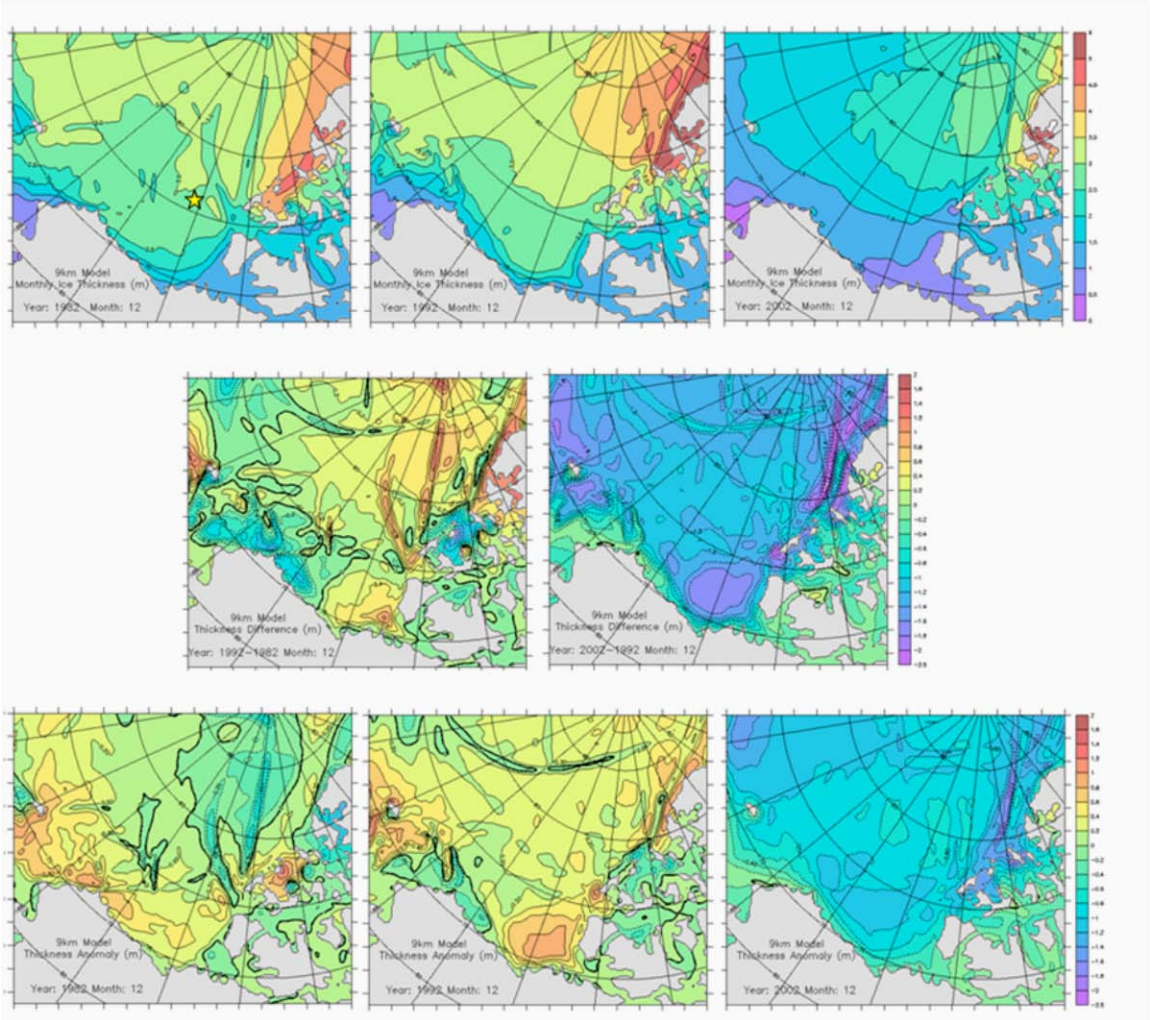

Figure 13. Decadal variation in monthly mean sea ice thickness for December for 9km model. Panels show mean ice thickness for December 1982 (top left), December 1992 (top center) and December 2002 (top right), thickness difference for December 1992 minus December 1982 (middle left) and for December 2002 minus December 1992 (middle right), and thickness anomaly (monthly mean minus 26 year December mean) for December 1982 (bottom left), December 1992 (bottom center) and December 2002 (bottom right). Yellow star on top left panel shows approximate position of 5x5 grid cell area in the vicinity of ~76°N 136°W.

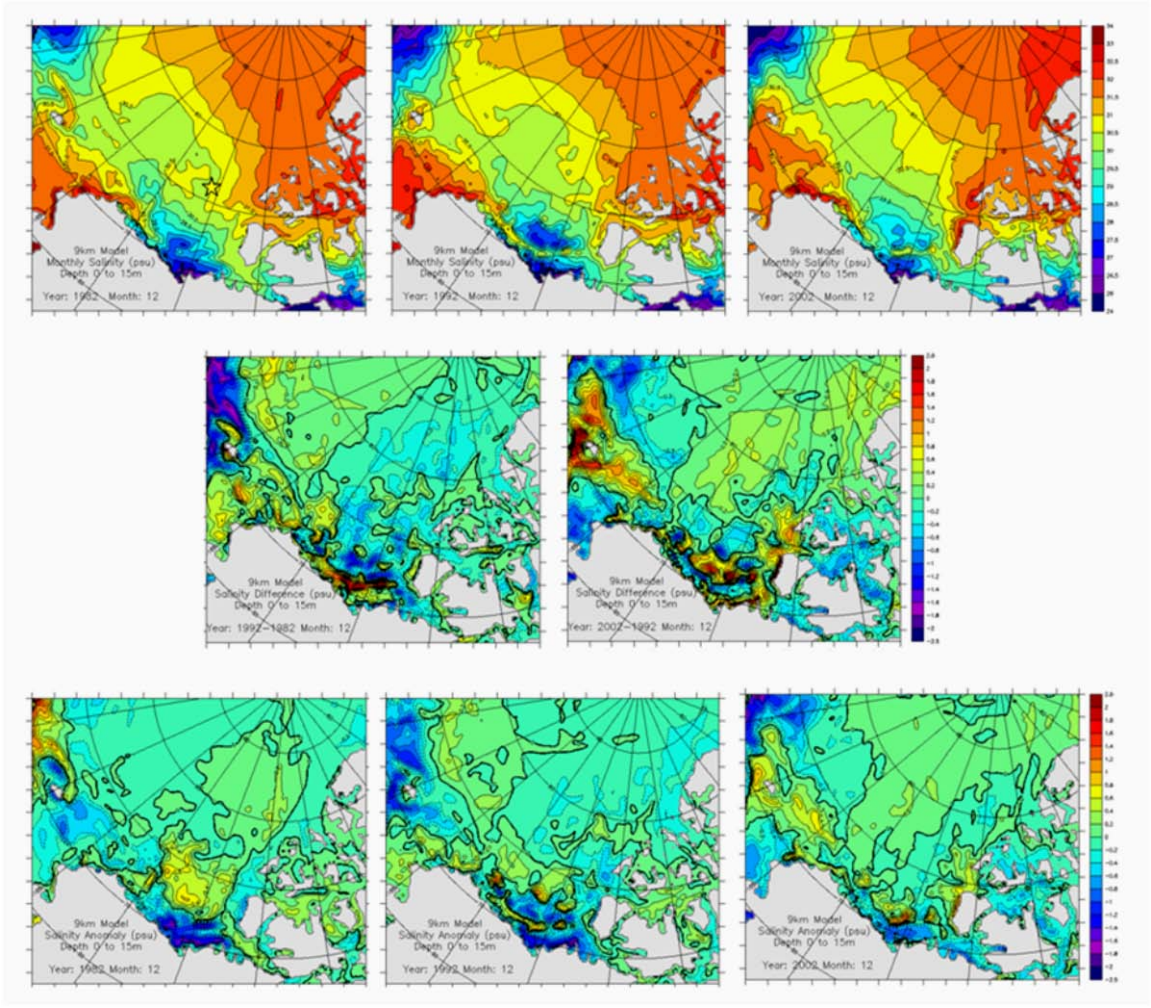

Figure 14. Decadal variation in monthly mean salinity (average 0 to 15m depth) for December for 9km model. Panels show mean salinity for December 1982 (top left), December 1992 (top center) and December 2002 (top right), salinity difference for December 1992 minus December 1982 (middle left) and for December 2002 minus Dec 1992 (middle right), and salinity anomaly (monthly mean minus 26 year December mean) for December 1982 (bottom left), December 1992 (bottom center) and December 2002 (bottom right). Yellow star on top left panel shows approximate position of 5x5 grid cell area in the vicinity of 76°N 136°W.

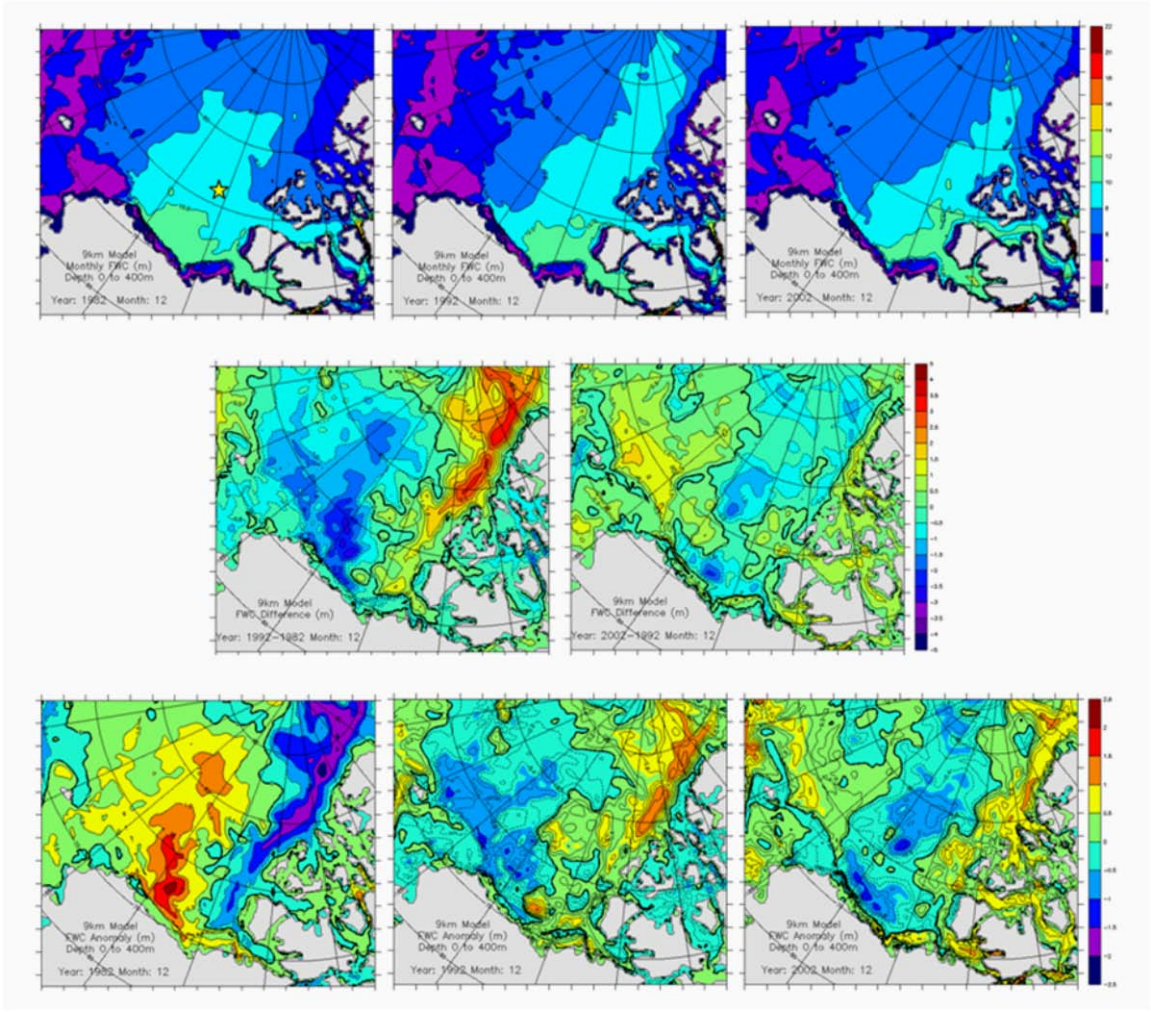

Figure 15. Decadal variation in monthly mean FWC (0 to 400m depth) for December for 9km model. Panels show mean FWC for December 1982 (top left), December 1992 (top center) and December 2002 (top right), FWC difference for December 1992 minus December 1982 (middle left) and for December 2002 minus December 1992 (middle right), and FWC anomaly (monthly mean minus 26 year December mean) for December 1982 (bottom left), December 1992 (bottom center) and December 2002 (bottom right). Yellow star on top left panel shows approximate position of 5x5 grid cell area in the vicinity of 76°N 136°W.

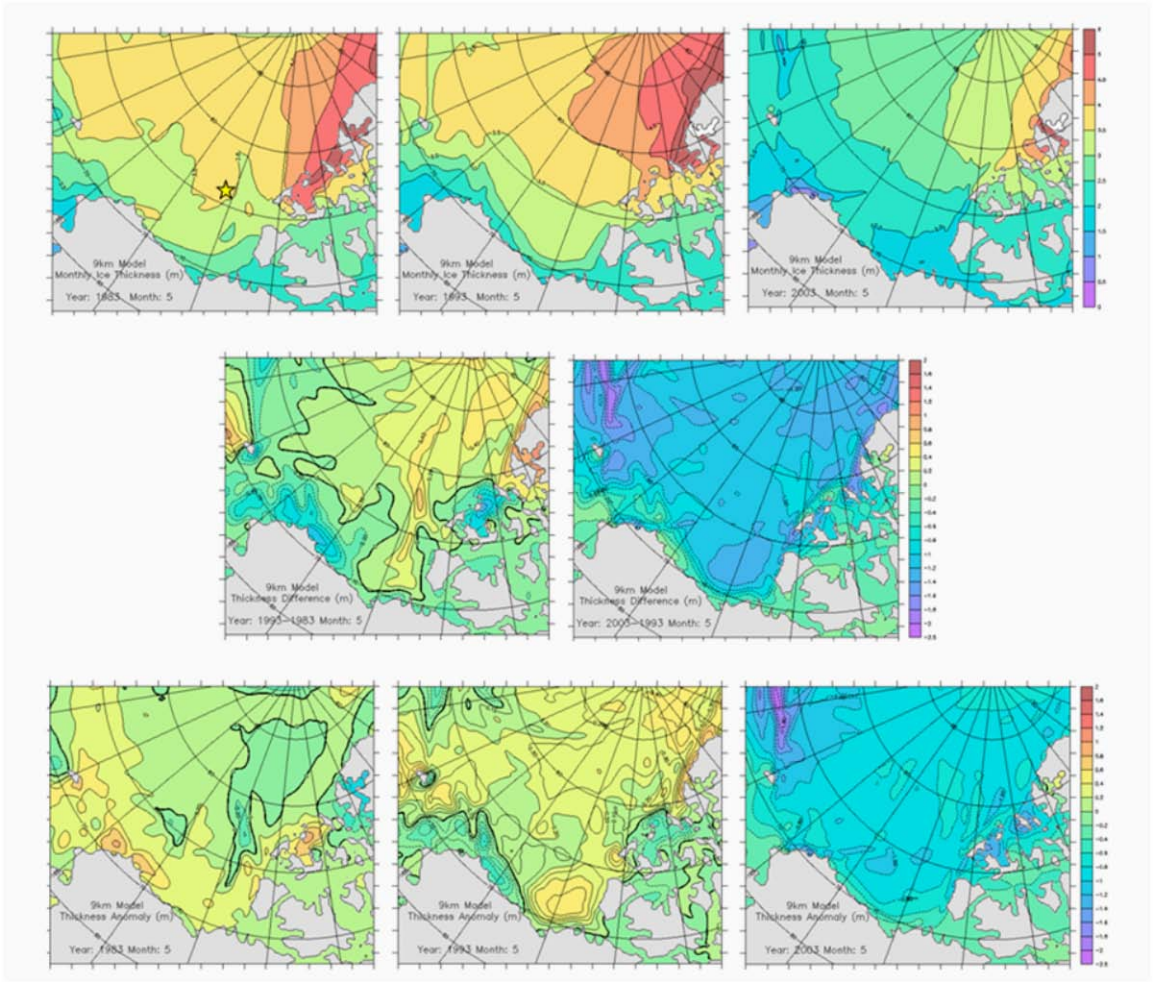

Figure 16. Decadal variation in monthly mean sea ice thickness for May for 9km model. Panels show mean ice thickness for May 1983 (top left), May 1993 (top center) and May 2003 (top right), thickness difference for May 1993 minus May 1983 (middle left) and for May 2003 minus May 1993 (middle right), and thickness anomaly (monthly mean minus 26 year May mean) for May 1983 (bottom left), May 1993 (bottom center) and May 2003 (bottom right). Yellow star on top left panel shows approximate position of 5x5 grid cell area in the vicinity of 76°N 136°W.

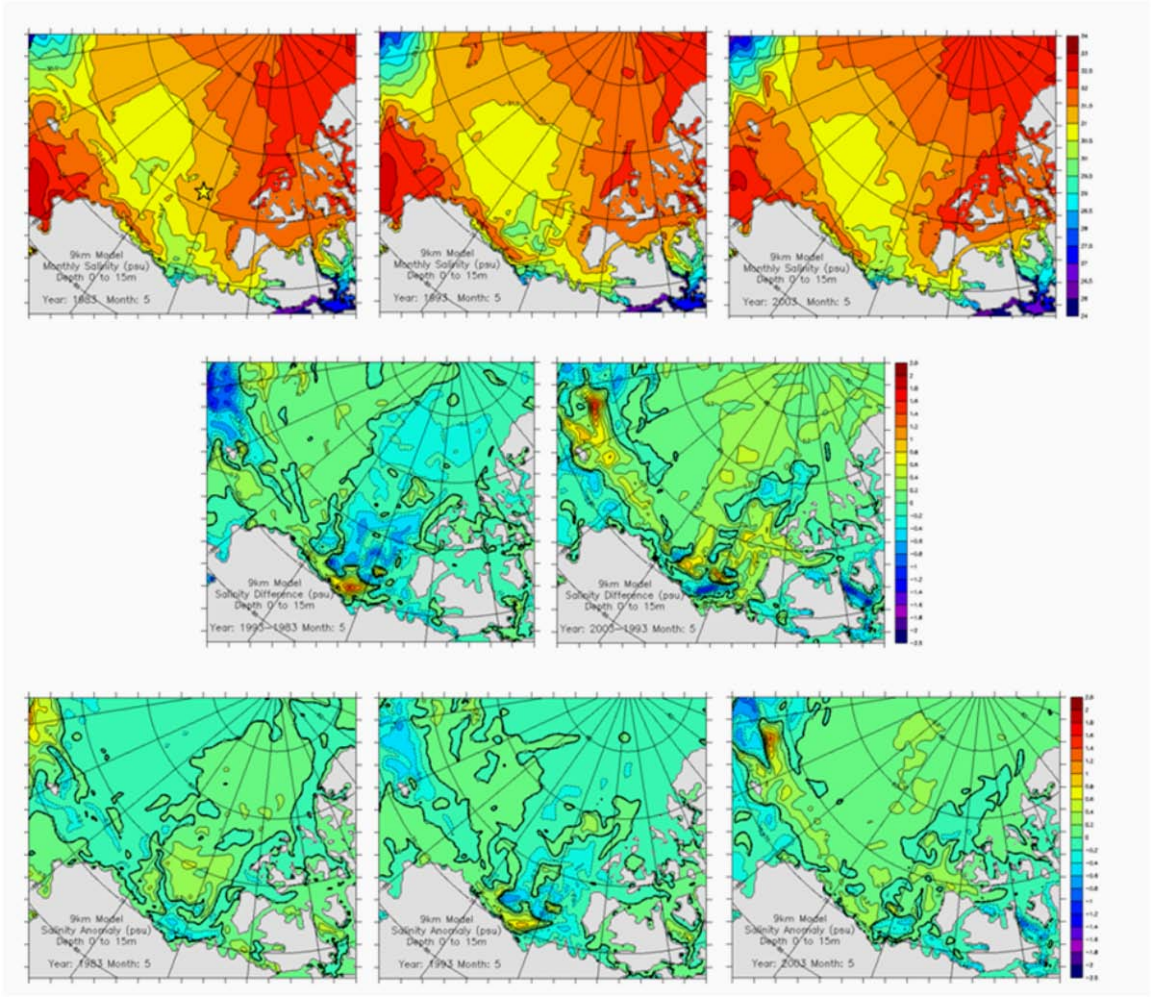

Figure 17. Decadal variation in monthly mean salinity (average 0 to 15m depth) for May for 9km model. Panels show mean salinity for May 1983 (top left), May 1993 (top center) and May 2003 (top right), salinity difference for May 1993 minus May 1983 (middle left) and for May 2003 minus May 1993 (middle right), and salinity anomaly (monthly mean minus 26 year May mean) for May 1983 (bottom left), May 1993 (bottom center) and May 2003 (bottom right). Yellow star on top left panel shows approximate position of 5x5 grid cell area in the vicinity of 76°N 136°W.

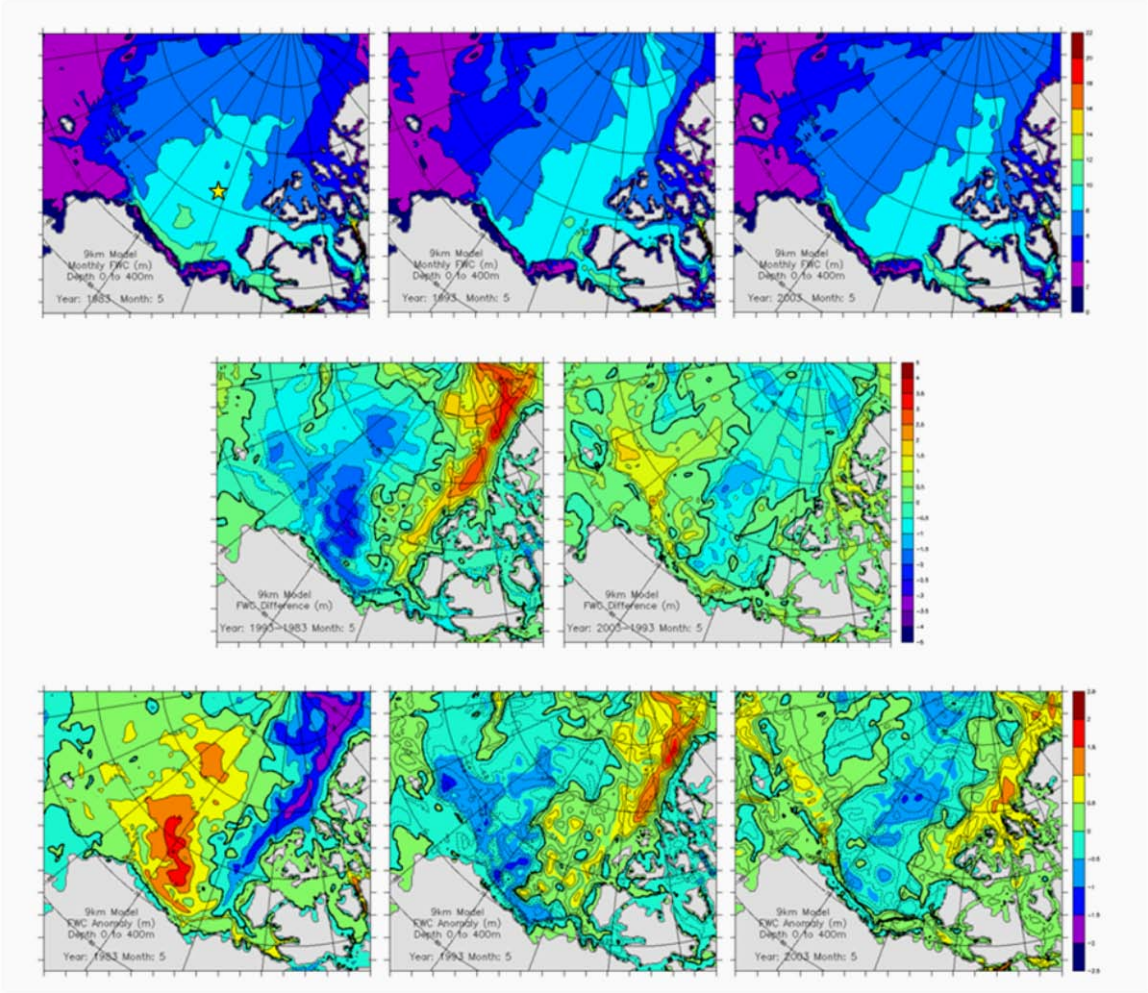

Figure 18. Decadal variation in monthly mean FWC (0 to 400m depth) for May for 9km model. Panels show mean FWC for May 1983 (top left), May 1993 (top center) and May 2003 (top right), FWC difference for May 1993 minus May 1983 (middle left) and for May 2003 minus May 1993 (middle right), and FWC anomaly (monthly mean minus 26 year May mean) for May 1983 (bottom left), May 1993 (bottom center) and May 2003 (bottom right). Yellow star on top left panel shows approximate position of 5x5 grid cell area in the vicinity of 76°N 136°W.

Analysis of the decadal variation in modeled December (early winter) ice thickness (Figure 13) indicates that there were no significant changes or clear trends in the distribution of ice thickness between December 1982 and December 1992, although the magnitude of the thickness in some areas of the central Arctic Ocean increased by 0.5 to 1.5m over this decade. More significant changes in thickness distribution and magnitude (large scale thinning) are evident between December 1992 and December

2002. Ice thickness decreased over the entire western and central Arctic region by 2002, with the largest differences being apparent in the Chukchi and southern Beaufort Seas (~2m decrease), and in the eastern Beaufort Sea in the vicinity of the Canadian Arctic Archipelago (CAA) (up to 2.5m decrease). Corresponding plots of average upper 15m salinity and FWC for December (Figures 14 and 15) show less definitive trends than those seen in ice thickness. In general, for all decades the areas of lowest salinity were in the vicinity of the MacKenzie and Kolyma River outflows, whilst the highest salinities occurred on the Chukchi Shelf, the CAA and the central Arctic regions. It may seem intuitive that thinner ice in the western and central Arctic Ocean in recent decades should result in lower salinity and higher FWC due to melt, but model results suggest that this is not necessarily the case. Direct correlations between ice thickness and upper ocean salinity and FWC may not be evident because salinity and FWC are not only influenced by melting ice, but also by river runoff, precipitation rates and by runoff from land, which are not well known in the Arctic region, especially over decadal timescales (Maslowski et al. 2007). Lateral advection and large scale circulation changes may also add to the complexity of analyzing Arctic salinity and FWC.

Similar analysis of the modeled decadal variation in May (late winter) sea ice thickness (Figure 16) shows a similar trend as that detected in the December results. Although the thickness magnitudes were greater for all three decades under late winter conditions in comparison to early winter conditions, monthly mean ice thicknesses for May once again show a slight increase (of 0.2 to 0.4m) from 1983 to 1993 over much of the domain and an overall decrease (of 0.2 to 2.5m) from 1993 to 2003. The greatest thickness decrease in this case occurred in the East Siberian Sea. Modeled salinity and FWC for May (Figures 17 and 18) again paints a complicated picture, with no clear decadal trends correlating directly with changes to sea ice thickness or distribution. Results show that the previously identified areas of low salinity due to river runoff were not as significant under late winter conditions, and that FWC was also substantially lower along the Alaskan coast and into the Beaufort Sea for all decades in May when compared to December.

To further assess long term variability, monthly mean ice and ocean data from the 9km model were analyzed for twelve month periods during 1982/83, 1992/93 and 2002/03. The variation in several ice and ocean parameters for these times (and for 2003/04) over a 5x5 grid cell area (~2144km^2) in the central Beaufort Sea at approximately 76°N 136°W is shown in Figure 19. This position is in the vicinity of the winter entrainment case studies presented in Section B of this chapter from ITP and IMB observations. These annual time series at decadal intervals for the area in the Beaufort Sea yield similar results to those previously described over the larger region of the western and central Arctic, with a trend towards thinner ice in recent years. There is a corresponding trend towards faster ice speed with decreased ice thickness. The model output also suggests that TKE was low during the winter months for all years. As seen in the previous results, there is once again no obvious trend in upper ocean salinity. Winter mixed layer depths were shallowest (~20m) in 1982/83 and deepest in 2002/3 (~45m), which corresponds to the periods of thickest and thinnest ice respectively. Deeper mixed layer depths in recent years may partially be attributed to lower concentrations of sea ice and larger areas of open water, which are directly exposed to the effects of wind-induced mixing at the surface.

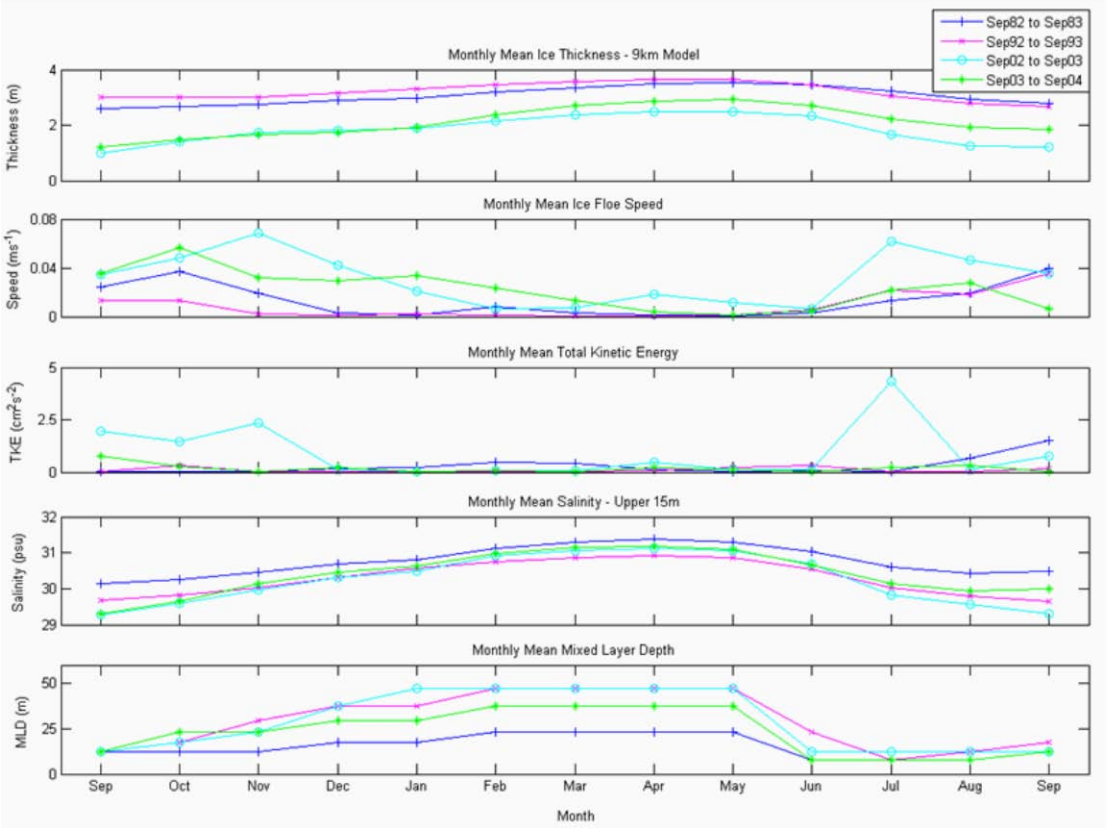

Figure 19. Decadal variation in monthly mean ice thickness, floe speed, TKE, salinity (averaged over 0 to 15m depth) and mixed layer depth for 5x5 grid cell area in the vicinity of 75°N 136°W.

2. Annual Variation in Sea Ice and Ocean - Winter 9km Model Results

Annual variations in winter monthly mean ice thickness, ice floe speed and upper ocean (averaged over 0 to 15m depth) salinity are shown in Figures 20 to 22 respectively for the 9km model over a period of 26 years (1979 to 2004). These results show the average values over the aforementioned 5x5 grid cell area in the central Beaufort Sea. Linear trend lines were fitted to each dataset for the periods 1979 to 1993 and 1993 to 2004, based on the significant increase seen in modeled ice floe speed from 1993 onwards. Interestingly, for each parameter, the February monthly mean appears to best represent the overall winter mean.

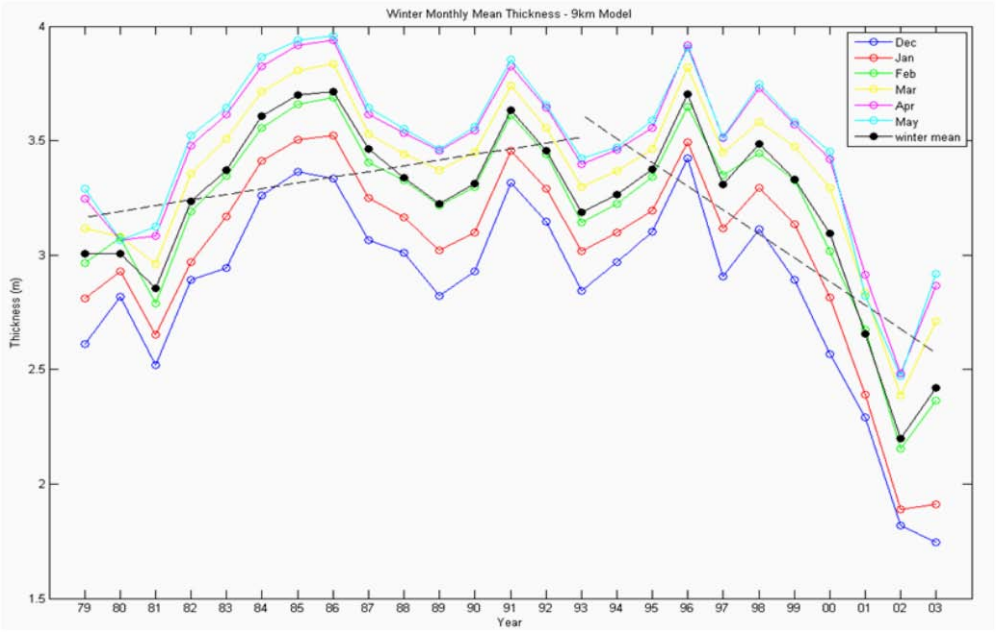

Figure 20. Annual variation in winter monthly mean sea ice thickness for 9km model for 5x5 grid cell area in the vicinity of 75°N 136°W. Linear trend for periods 1979 to 1993 and 1993 to 2004 is shown as dashed black line.

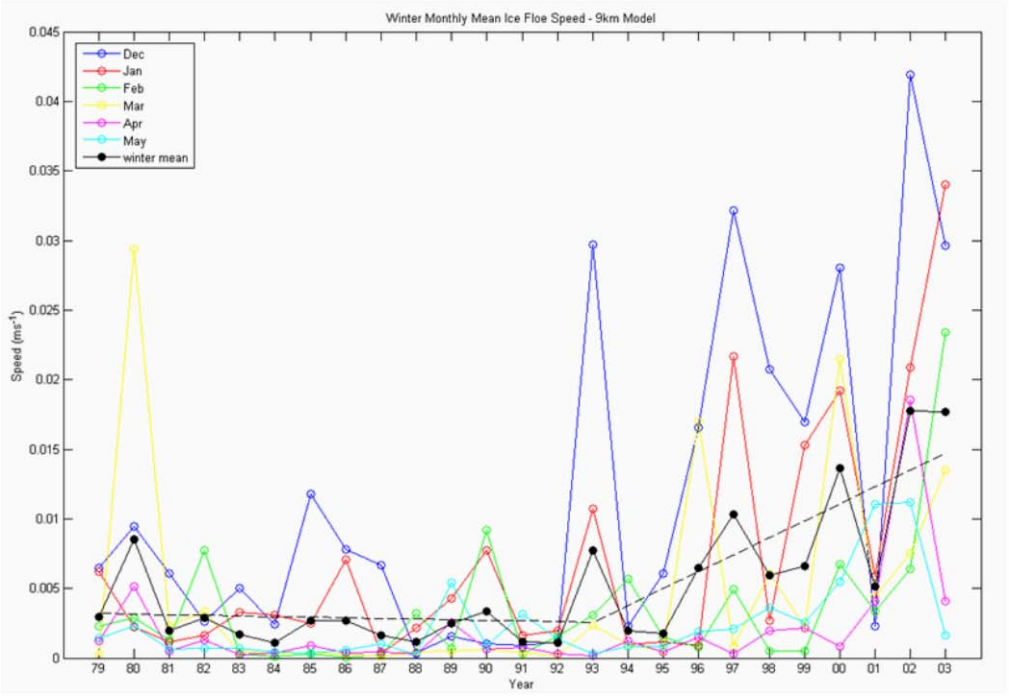

Figure 21. Annual variation in winter monthly mean ice floe speed for 9km model for 5x5 grid cell area in the vicinity of 75°N 136°W. Linear trend for periods 1979 to 1993 and 1993 to 2004 is shown as dashed black line.

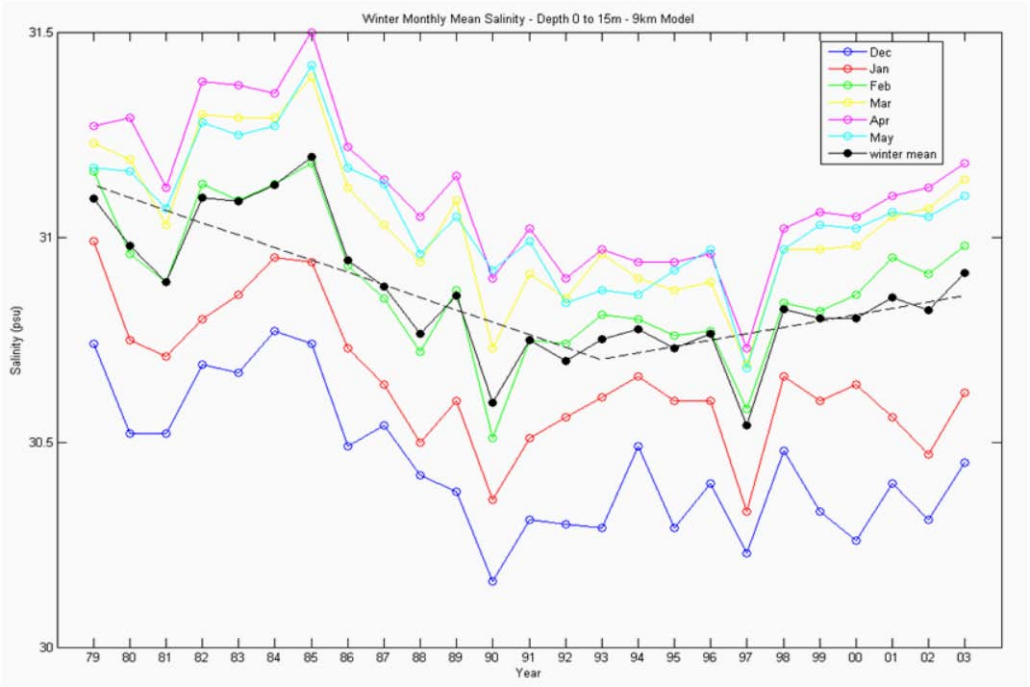

Figure 22. Annual variation in winter monthly mean salinity (average 0 to 15m depth) for 9km model for 5x5 grid cell area in the vicinity of 75°N 136°W. Linear trend for periods 1979 to 1993 and 1993 to 2004 is shown as dashed black line.

The 26-year time series of mean thicknesses (Figure 20) show the expected increase in ice thickness with the progression of the winter months, with the thinnest ice in December and the thickest ice in April/May each year. The modeled results suggest that the mean winter ice thickness increased during the mid 1980s (reaching a maximum thickness of 3.7m in 1986), before significantly declining from the late 1990s onwards (reaching a minimum thickness of 2.2m in 2002). Trends in monthly mean ice floe speed (Figure 21) once again mirror those seen in thickness, with modeled ice floe speed showing a steady increase from the mid 1990s onwards. These results, coupled with the faster floe speeds in early winter across the entire 26-year time series suggest that thinner ice moves faster. Although the modeled ice floe speed is useful for demonstrating general trends, it should be noted that previous analyses of NPS model results (e.g., Maslowski and Lipscomb 2003) found that ice floe speed is underestimated by the model by at least an order of magnitude in most instances. Model results for average salinity (Figure 22) over the upper 15m of ocean (i.e., within the surface mixed layer) show a general trend of decreasing salinity with increasing thickness, followed by a period of increasing salinity

corresponding with the period of ice thickness decrease. The increase in salinity that began during the mid 1990s may be explained by increased brine rejection during winter ice production in a regime of thinner ice conditions, or could once again possibly be due to changes in the large scale atmospheric and oceanic circulation, advective processes, or river runoff.

3. Case Study 1: December 1983 - 9km and 2.3km Model Results

Since mesoscale eddies may provide a mechanism for the entrainment of warm water into the mixed layer, EKE derived from the 9km and 2.3km daily model output was investigated, with the expectation that the eddy resolving model would better resolve small-scale features than the 9km model. The analyses of model output concentrated on the winter months of 1983, since this is the only year of model output available thus far for the 2.3km model. Case Study 1 focuses on results from 19 December 1983, which corresponds to the same day in December as the first case study presented in Section B based on observational results.

Daily mean modeled EKE for the 9km and 2.3km models, and SSHA from the 9km model for 19 December 1983 are shown in Figure 23 for three different depth levels. Results from the 9km model show that surface EKE was small, but increased with depth. The highest values of EKE at depths of 20 to 26m occurred in the vicinity of the shallower regions of the Bering Sea, the Chukchi Shelf and the Alaskan Shelf, most likely due to topographical influences and the Alaskan Coastal Current (ACC). At depths of 65 to 80m, EKE was highest along the Northwind Ridge, over the Chukchi Cap and along the Alaskan Shelf into the CAA. There was some apparent eddy activity in the western and southern Beaufort Sea at sub-surface depths, but this signal did not translate into any distinguishable features in SSHA over the same region. In contrast, the 2.3km model results show high levels of surface EKE over most of the western and central Arctic, which may be due to the influence of synoptic scale meteorological influences, or due to the fact that the model is still being run in the initial spin-up mode. At 20 to 26m

and 65 to 81m, EKE was concentrated in similar regions as for the 9km model. However, smaller, more detailed, and greater numbers of features were resolved by the eddy resolving model, especially in the central Beaufort Sea.

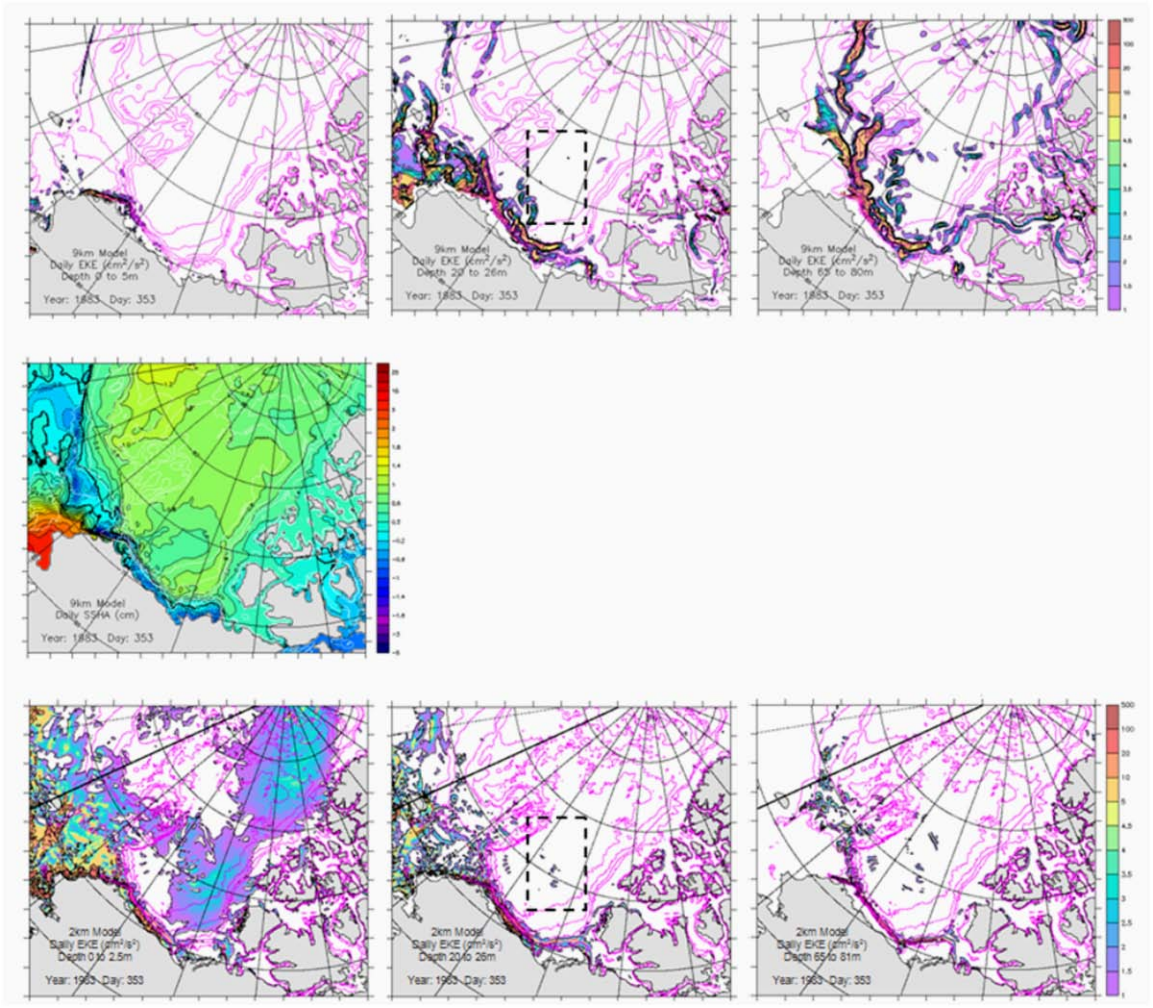

Figure 23. Daily mean model output for 19 December 1983 for 9km and 2.3 km models. Panels show 9km model results for EKE for depth 0 to 5m (top left), 20 to 26m (top center), 65 to 80m (top right) and SSHA (middle), and 2km model results for EKE for depth 0 to 2.5m (bottom left), 20 to 26m (bottom center) and 65 to 81m (bottom right). Dashed black box shows region of interest in the Beaufort Sea.

Figures 24 and 25 show model results for 19 December 1983 of EKE, currents and relative vorticity over a smaller region of the Beaufort Sea for the 9km and 2.3km models respectively. The depth range of 20 to 26m was selected for further analysis due

to its location near the bottom or just below the mixed layer and the potential for heat entrainment upwards from eddies at this depth. In order to facilitate the upwelling of warm water into the mixed layer, eddies in the Northern Hemisphere must be anticyclonic, which corresponds to areas of negative relative vorticity. The 9km model results over the selected area of the Beaufort Sea are indicative of a generally low energy environment. However, even at this eddy permitting resolution, the current vector and vorticity fields suggest that there may have been more eddy activity than is apparent from the analysis of EKE in isolation. The 2.3km model results for EKE also show relatively low energy, again possibly due to an early spin-up phase, although in this case greater numbers and smaller features were resolved, which can also be seen in the corresponding relative vorticity field. The current vectors for the eddy resolving model output show several meanders, but do not distinguish as many areas of closed circulation as seen in the 9km results.

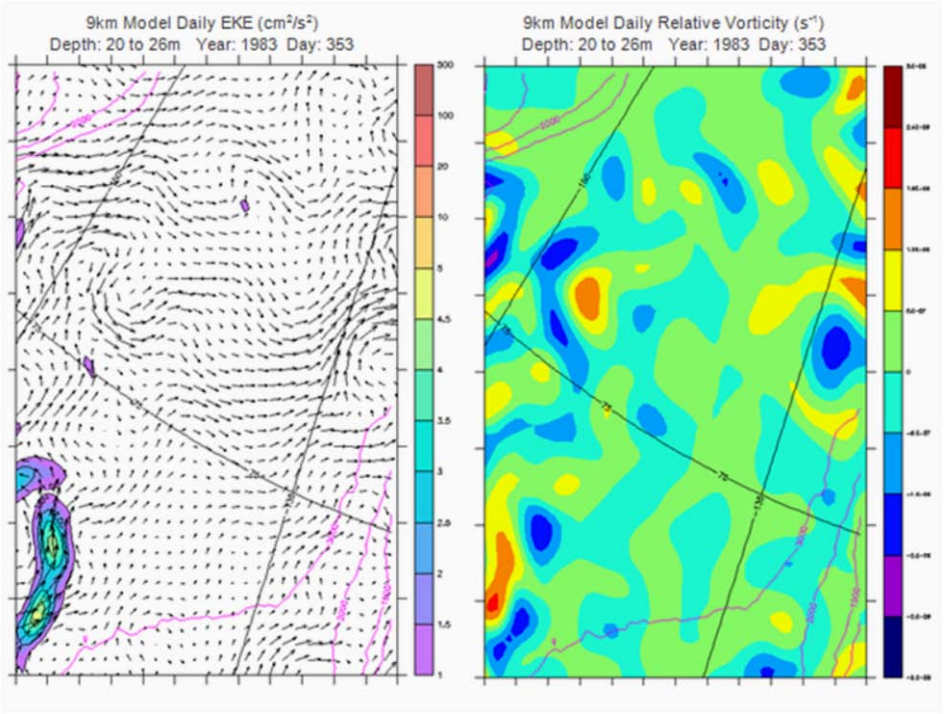

Figure 24. Daily mean model output for 19 December 1983 for the 9km model showing EKE with current vectors (left) and relative vorticity (right) at depth 20 to 26m for domain in Beaufort Sea shown by dashed black box in Figure 23.

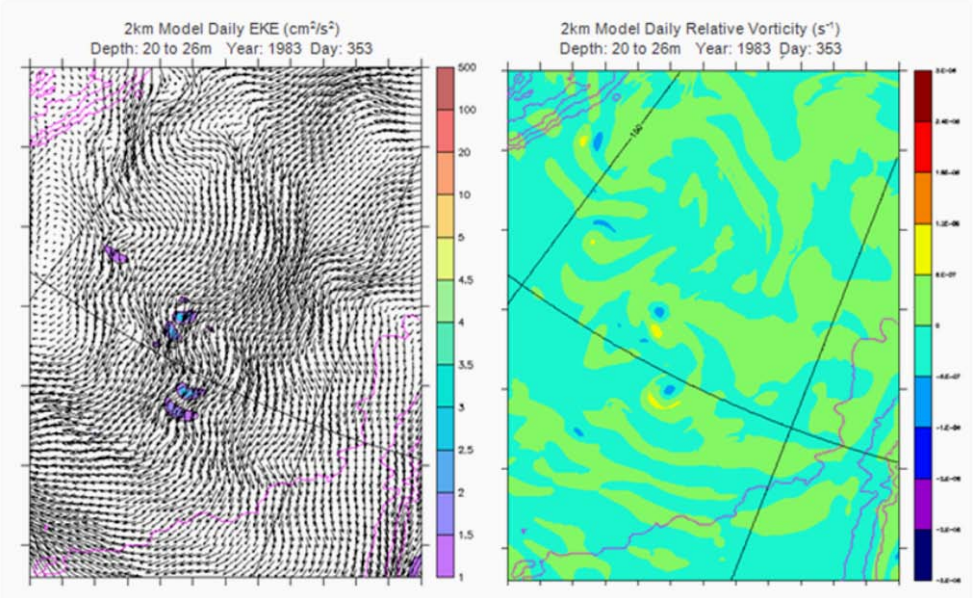

Figure 25. Daily mean model output for 19 December 1983 for the 2.3km model showing EKE with current vectors (left) and relative vorticity (right) at depth 20 to 26m for domain in Beaufort Sea shown by dashed black box in Figure 23.

4. Case Study 2: May 1983 - 9km and 2.3km Model Results

Similar analyses (Figures 26 to 28) as that done for the first case study were also conducted for Case Study 2, this time for a day in late winter (22 May 1983) corresponding to the same day of the month as the second observational case study described in the next section. The model results at all depths for both resolutions show that there was greater EKE in the Beaufort Sea than for the early winter case. This is particularly noticeable in the 2.3km output in the Beaufort Sea at sub-surface depths, where the number of small scale features resolved in the EKE field is substantial. The 20 to 26m relative vorticity fields at both resolutions show more areas of greater magnitude negative vorticity, which in some instances correlate with regions of closed circulation shown by the current vectors in the 9km model. It is once again difficult to distinguish any obvious features in the 9km SSHA, or to detect areas of closed circulation in the 2.3km model current vector field at a depth of 20 to 26m. However, the overall results are promising because they once again show substantial improvement in the representation of small scale features in the Beaufort Sea in the eddy resolving model. A comparison of the

daily EKE and relative vorticity results for both model resolutions all of the winter months yields a similar trend to that seen in the daily snapshots, where increased resolution shows an increase in EKE magnitude and in eddy numbers, in addition to resolving much smaller scale features. The spatial distribution of all of these parameters in the eddy resolving model (Figures 23, 25, 26 and 28) suggests that mesoscale eddies are common over the Chukchi Cap, the Northwind Ridge and in the southern and central Beaufort Sea. This bears consequences for their potential to facilitate vertical exchanges at depths near the bottom of the upper mixed layer.

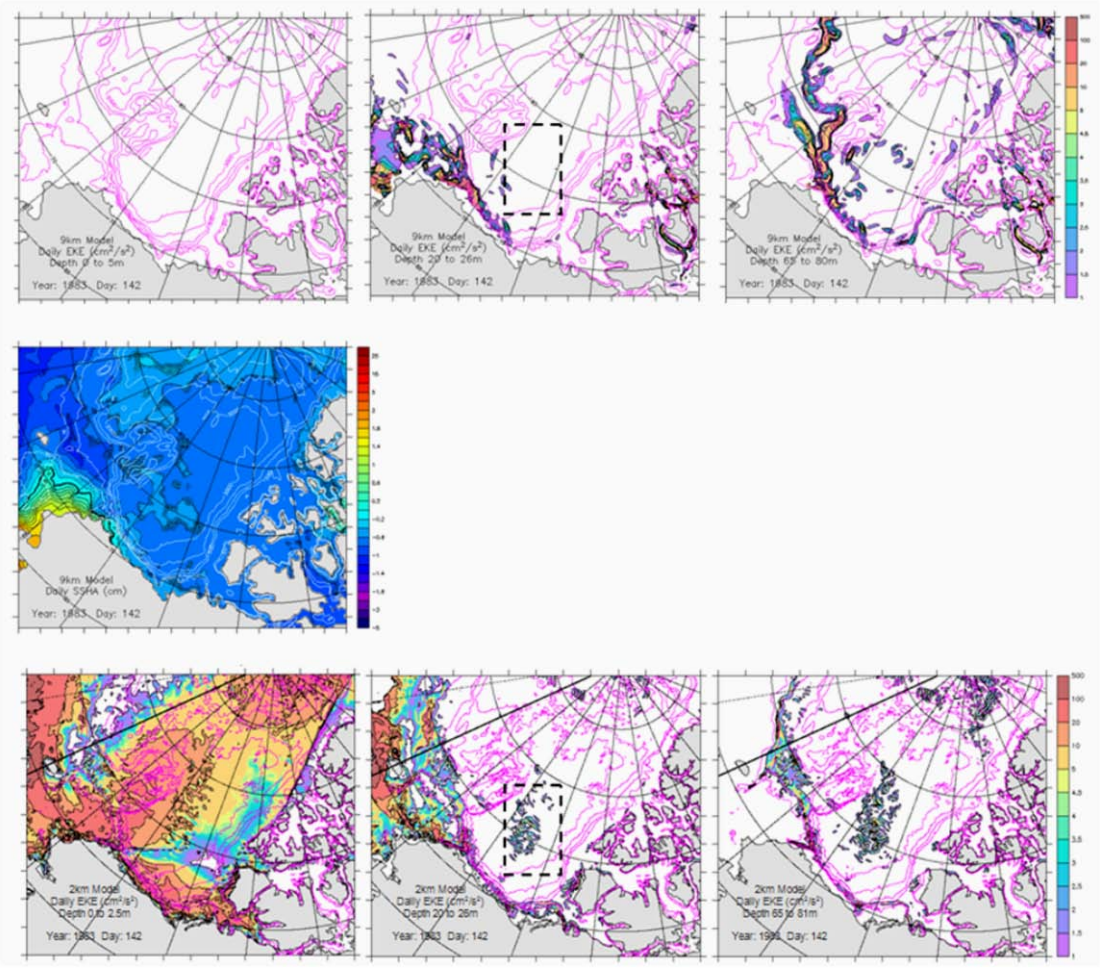

Figure 26. Daily mean model output for 22 May 1983 for 9km and 2.3 km models. Panels show 9km model results for EKE for depth 0 to 5m (top left), 20 to 26m (top center), 65 to 80m (top right) and SSHA (middle), and 2km model results for EKE for depth 0 to 2.5m (bottom left), 20 to 26m (bottom center) and 65 to 81m (bottom right). Dashed black box shows region of interest in the Beaufort Sea.

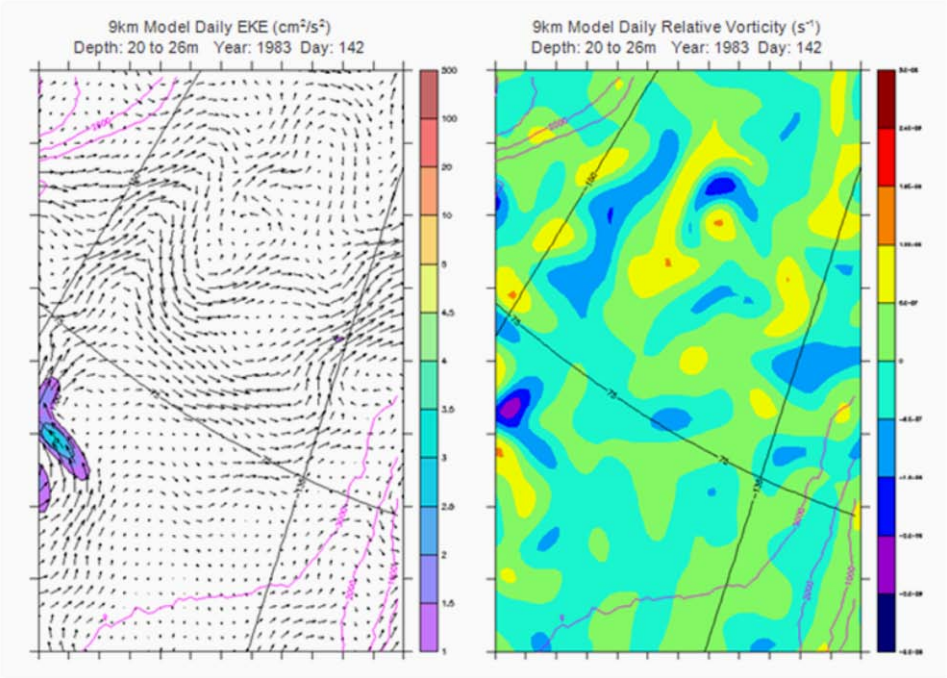

Figure 27. Daily mean model output for 22 May 1983 for the 9km model showing EKE with current vectors (left) and relative vorticity (right) at depth 20 to 26m for domain in Beaufort Sea shown by dashed black box in Figure 26.

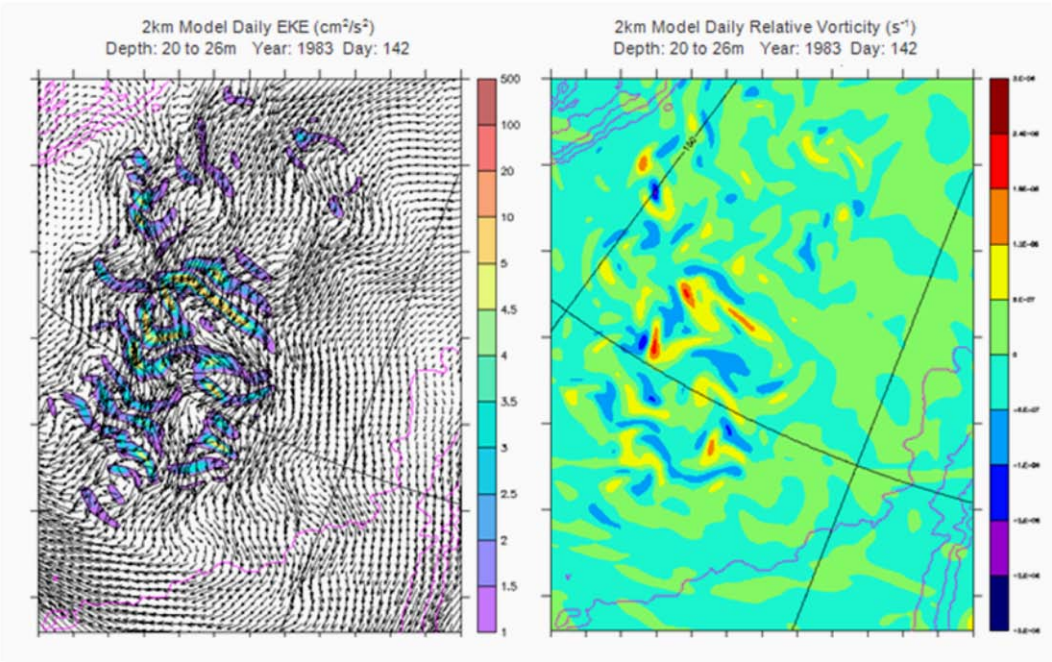

Figure 28. Daily mean model output for 22 May 1983 for the 2.3km model showing EKE with current vectors (left) and relative vorticity (right) at depth 20 to 26m for domain in Beaufort Sea shown by dashed black box in Figure 26.

B. OBSERVATIONAL RESULTS

Results from recent ITP and IMB observations in the western and central Arctic Ocean are presented in this section. These results concentrate on the relatively small areas covered by the drift trajectories of the instruments over periods of up to two years. Two winter case studies are presented for the Beaufort Sea region, with a focus on warm water entrainment into the mixed layer and the potential that an oceanic heat source (such as a warm eddy) may have to melt sea ice.

The model results presented in the previous section demonstrate the potential existence of numerous anticyclonic mesoscale eddies, particularly in the western Arctic at subsurface depths. Although in-situ instruments do not directly measure the entrainment of warm water across the base of the mixed layer, we hypothesize that entrainment is the mechanism via which the physical characteristics of the mixed layer can be significantly altered. The analyses of observations from the western Arctic show that the warming and freshening of the mixed layer occurred during periods of identified entrainment. Given that observed ice speeds were relatively slow during these times, coupled with the fact that large scale mixing of the upper ocean was not observed during these times, it is unlikely that such events were the result of synoptic scale storms. Furthermore, model results have shown that the freshening of the mixed layer of similar magnitudes to that observed from the measurements during entrainment periods is unlikely to occur during the winter, or in offshore limited areas removed from river outflow.

1. Central Arctic - ITP10 and IMB2007H

Observations from ITP10 (10 September 2007 to 24 May 2008) and IMB2007H (11 September 2007 to 24 February 2008) from the central Arctic were analyzed to show the seasonal evolution of the mixed layer in a relatively quiescent environment that is not commonly influenced by mesoscale eddies and entrainment events that are more characteristic of the western Arctic Ocean. Plots of potential temperature, salinity and potential density from ITP10 measurements (Figure 29) show that throughout most of the year a well mixed layer exists in the upper water column. PSW forms a relatively warm, salty layer well below the mixed layer in the upper halocline, at depths of about 70 to

80m and below. The remnants of summer surface heating are evident in September/October 07, and the local temperature maxima between depths of about 20 to 30m are indicative of the NSTM described by Jackson et al. (2010). The meanders in the drift track of ITP10 (Figure 30) show that the instrument may have encountered several relatively weak eddies during transit, especially in the latter part of its journey, which is possibly why they are not immediately evident from the initial analysis of temperature and salinity data.

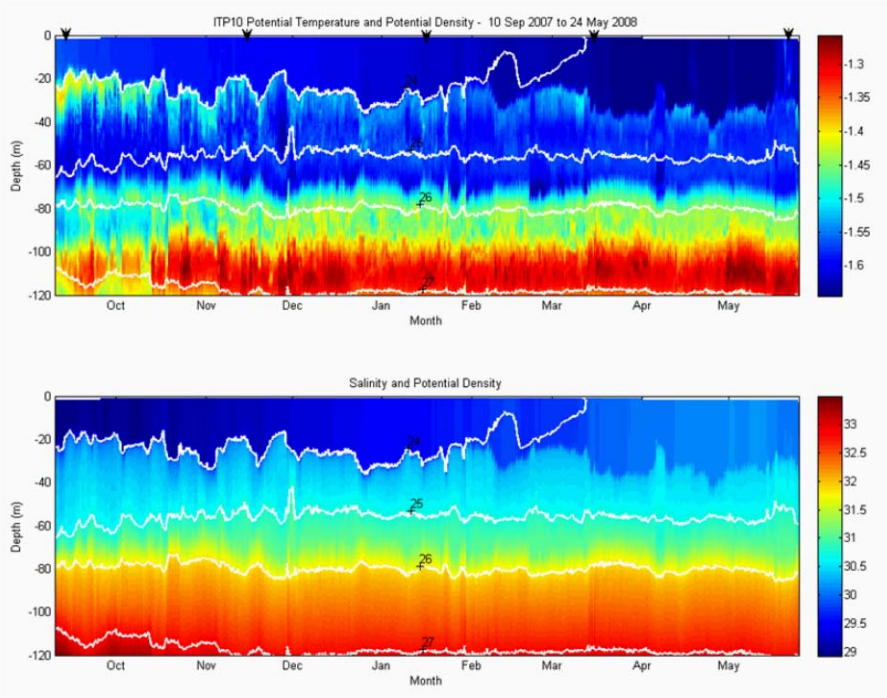

Figure 29. ITP10 potential temperature with potential density contours (shown in white, ranging from 24 to 27kgm^{-3} from top to bottom) (top) and salinity with potential density contours (bottom) for the period 10 September 2007 to 24 May 2008. Black arrows indicate profiles of interest on 15 September 2007 (profile 9), 15 November 2007 (profile 135), 15 January 2008 (profile 259), 15 March 2008 (profile 385) and 20 May 2008 (profile 526).

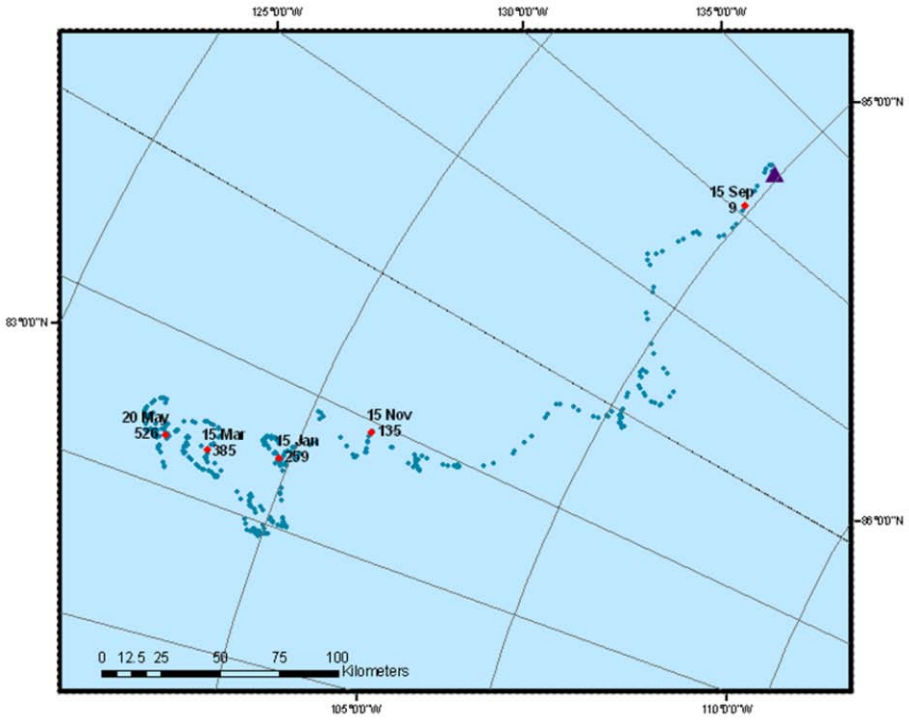

Figure 30. ITP10 drift track. Blue dots indicate all profile positions and red dots show profiles of interest (date and profile number shown). Purple triangle marks start position.

Corresponding time series of ITP10 ice floe speed, potential temperature and freezing point, and temperature above freezing point near the surface (at depth 5m) are shown in Figure 31. The mean ice floe speed for the entire time series was $0.04 ms^{-1}$. Faster average floe speeds occurred during summer and autumn, which was most likely due to lower concentrations of sea ice and greater percentages of open water during these times. The large intermittent spikes in floe speed (up to $0.2 ms^{-1}$) throughout the time series were possibly caused by the passage of synoptic scale storm events. Analysis of the near surface potential temperature and freezing point time series show that for the most of the measurement period, temperature was approximately 0.02°C below freezing point. The most likely cause of this offset is uncertainty in conductivity measurements. It can be assumed that the temperature within the mixed layer was actually at or near (within a few thousands of °C) the freezing point during the entire period when it is shown to be 0.02 to 0.03 °C colder than freezing point (Shaw et al. 2009; Toole et al. 2010).

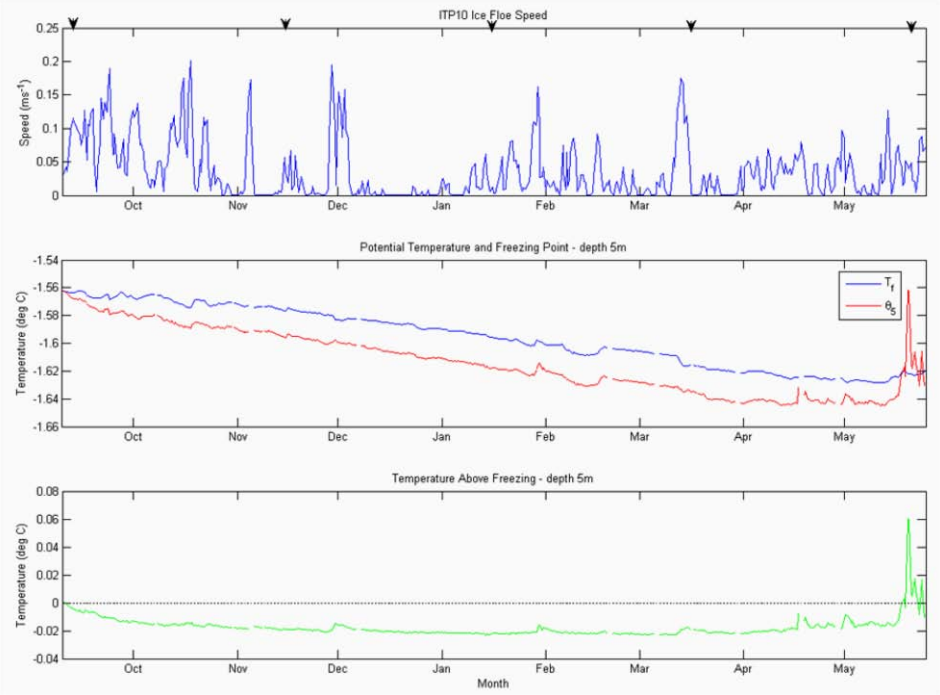

Figure 31. ITP10 ice floe speed (top), potential temperature and freezing point at depth 5m (middle) and temperature above freezing point at depth 5m, with black line showing reference point of zero (bottom). Arrows indicate profiles of interest on 15 September 2007 (profile 9), 15 November 2007 (profile 135), 15 January 2008 (profile 259), 15 March 2008 (profile 385) and 20 May 2008 (profile 526).

Vertical profiles of potential temperature, salinity and potential density to a depth of 120m at intervals of approximately two months are shown in Figure 32, and a temperature-salinity (T-S) scatter plot for the same profiles (upper 50m) is in Figure 33. Plots of potential density over the depth of the mixed layer for each profile are shown in Figure 34. This series of plots provides a 'snapshot' representation of the typical seasonal evolution of the mixed layer and upper water column in the central Arctic over a period of nine months. They show the expected cooling and deepening of the mixed layer during the transition from late summer to late winter, which was accompanied by corresponding increases in salinity and potential density. Heat content in the upper water column also followed a distinct seasonal cycle, and calculations of heat content show no clear evidence of heat penetrating the mixed layer with the exception of the final profile on 20 May 2008. This event is not considered as an entrainment case study in the following

sections due to the absence of significant freshening in the mixed layer and the fact that there are no corresponding IMB observations for this period. The characteristics of the mixed layer described above for the ITP10 profiles of interest are summarized in Table 1.

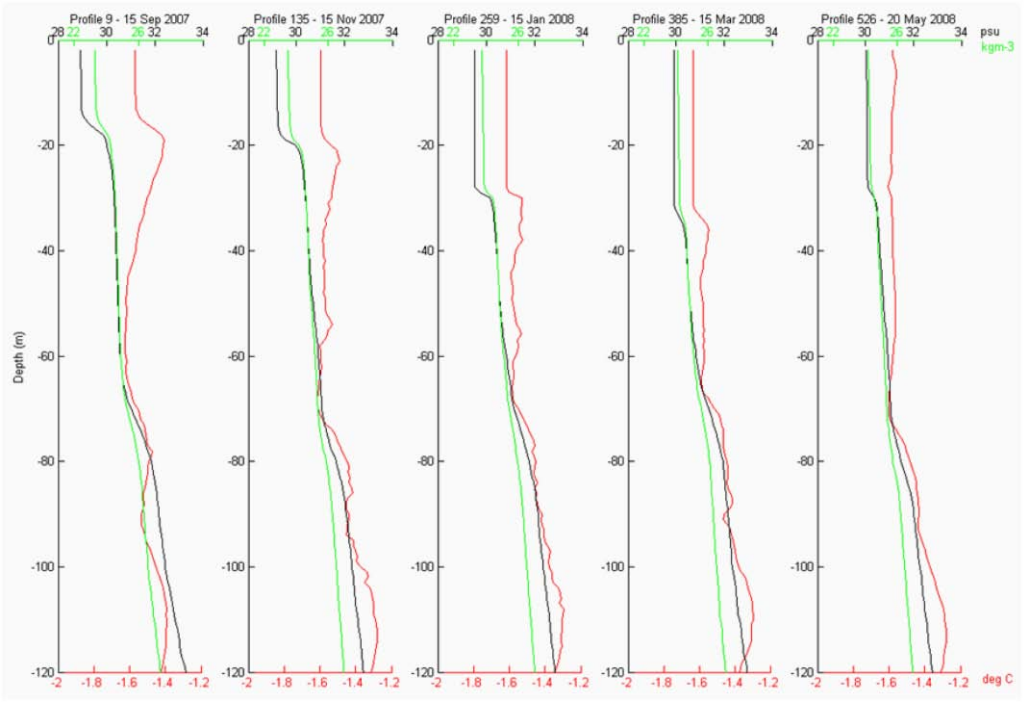

Figure 32. ITP10 vertical profiles of potential temperature (red), salinity (black) and potential density (green) for profiles of interest on 15 September 2007 (profile 9), 15 November 2007 (profile 135), 15 January 2008 (profile 259), 15 March 2008 (profile 385) and 20 May 2008 (profile 526) (from left to right).

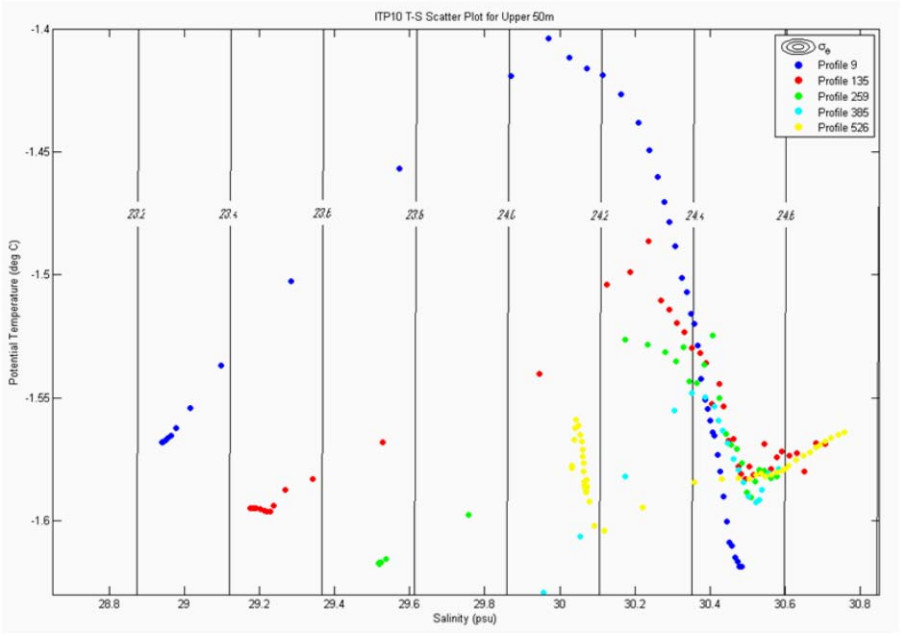

Figure 33. ITP10 T–S scatter plot for upper 50m with contours of potential density for profiles of interest on 15 September 2007 (profile 9 - blue), 15 November 2007 (profile 135 - red), 15 January 2008 (profile 259 - green), 15 March 2008 (profile 385 - cyan) and 20 May 2008 (profile 526 - yellow).

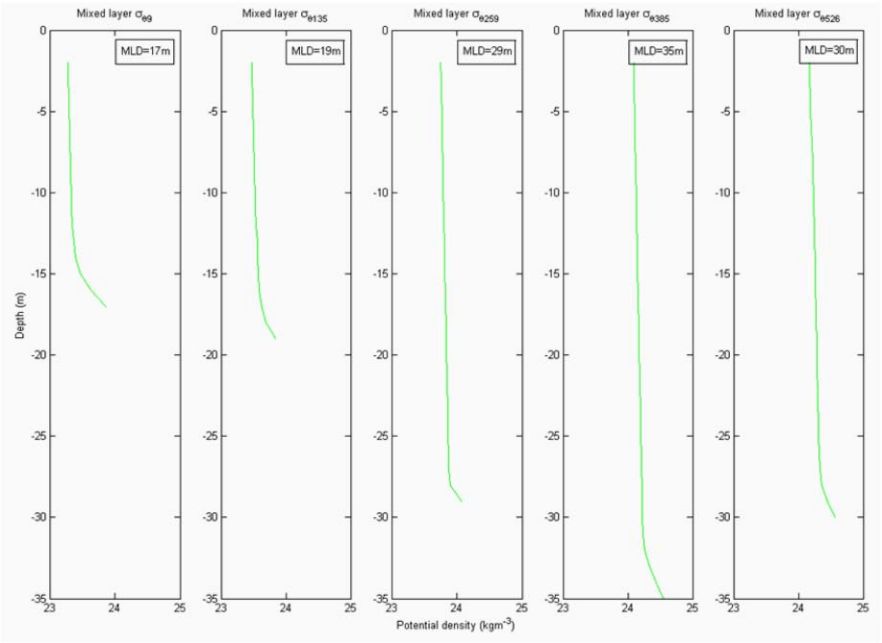

Figure 34. ITP10 mixed layer potential density for profiles of interest on 15 September 2007 (profile 9), 15 November 2007 (profile 135), 15 January 2008 (profile 259), 15 March 2008 (profile 385) and 20 May 2008 (profile 526) (from left to right).

Profile Number	Date	Mixed Layer Depth MLD (m)	Mean Potential Temperature $\overline{\theta}$ (°C)	Mean Salinity $\overline{S}$ (psu)	Mean Potential Density $\overline{\sigma_\theta}$ (kgm^{-3})	Ice Floe Speed (ms^{-1})
9	15 Sep 2007	17	-1.5100	29.3763	23.6912	0.1004
135	15 Nov 2007	19	-1.5716	29.4622	23.7619	0.0045
259	15 Jan 2008	29	-1.6173	29.5193	23.8089	0.0621
385	15 Mar 2008	35	-1.6340	29.9330	24.1451	0.1196
526	20 May 2008	30	-1.5782	30.0593	24.2467	0.0398

Table 1. ITP10 summary of mixed layer characteristics for profiles of interest on 15 September 2007 (profile 9), 15 November 2007 (profile 135), 15 January 2008 (profile 259), 15 March 2008 (profile 385) and 20 May 2008 (profile 526).

ITP10 was co-located with IMB2007H for the period September 2007 to February 2008. The IMB provides observations of the atmospheric conditions and the characteristics of the sea ice and the upper ocean above the depth of the ITP measurements. Figure 35 shows air pressure, air temperature, snow depth, ice thickness and water temperature (taken as the temperature of the first thermistor below the bottom of the ice), and Figure 36 shows sea ice temperature and the position of the ice bottom. Analysis of the IMB air pressure data does not indicate any obvious trends when compared with the ITP floe speed data making it difficult to ascertain when and if synoptic scale weather events influenced the sea ice and upper ocean. It could be expected that the passage of storms or low pressure systems may result in stronger winds and therefore faster moving ice, but this is not evident. Air temperature remained below freezing for the duration of the IMB period of observation, becoming cooler during the transition towards the winter months, and the upper ocean temperatures show a similar trend. Despite significant cooling of both air and upper ocean temperatures from October onwards, measurements of ice thickness indicate that the onset of winter sea ice growth did not occur until mid December. Relatively warm ice temperatures during the autumn suggest that the ice was affected by incident solar radiation until November, when significant cooling of the upper portion of the ice floe was observed. Furthermore, in late summer and into autumn, the ice and upper ocean temperatures were close to isothermal, but during the growth season the vertical temperature gradient through the ice was much greater than that of the ocean below the ice.

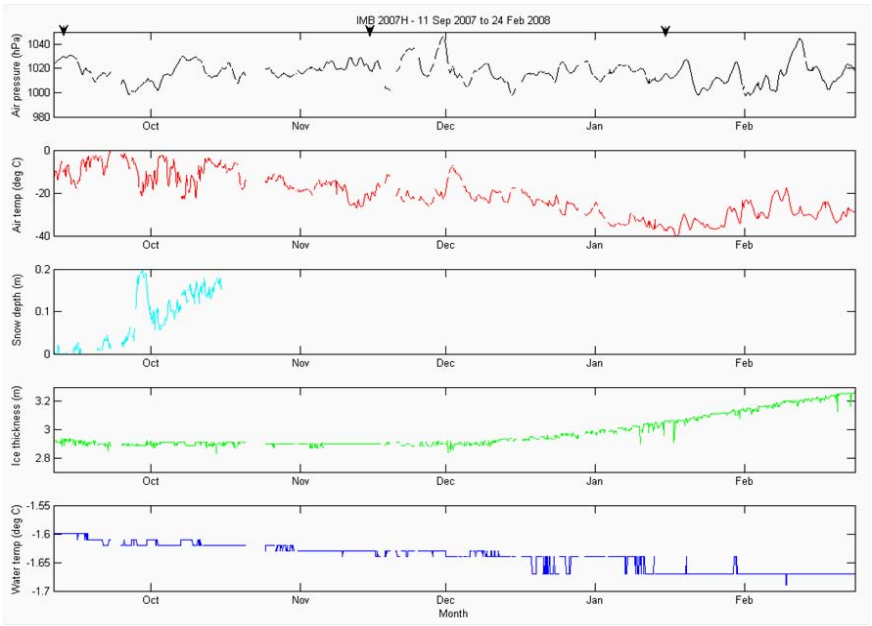

Figure 35. IMB2007H air pressure (black), air temperature (red), snow depth (cyan), ice thickness (green) and water temperature (blue) for the period 11 September 2007 to 24 February 2008. Arrows indicate positions corresponding to ITP10 profiles of interest on 15 September 2007 (profile 9), 15 November 2007 (profile 135) and 15 January 2008 (profile 259).

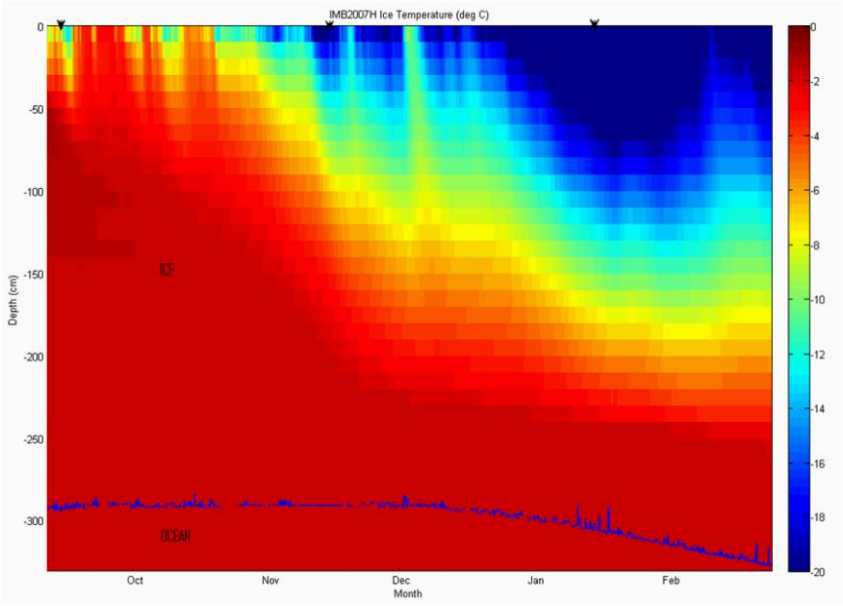

Figure 36. IMB2007H sea ice and upper ocean temperature. Blue line shows position of ice bottom and arrows indicate positions corresponding to ITP10 profiles of interest on 15 September 2007 (profile 9), 15 November 2007 (profile 135) and 15 January 2008 (profile 259).

Closer investigation of mid to late May 2008 observations from ITP10 (Figures 37 and 38) reveals that significant warming and slight freshening of the mixed layer, coupled with a warming of 0.06°C above the freezing point occurred during this time, which may be indicative of a late winter entrainment event. A relatively slow floe speed ($<0.04 ms^{-1}$) during this period suggests that the event was unlikely to be the result of lateral advection of warm water or storm induced mixing. Analysis of the ITP drift track shows that the floe followed a cyclonic path, before moving anticyclonically during the period 16 to 23 May 2008 (Figure 39), possibly showing that it encountered an eddy around 20 May. Vertical profiles made before, during and after the potential period of entrainment (Figure 40) confirm that the mixed layer warmed by 0.05°C between 16 and 20 May 2008, with an almost negligible change in salinity and potential density during this time. A calculation of heat content per unit area over the depth of the mixed layer for the profile made during the entrainment event confirms that heat penetrated throughout the mixed layer, extending all the way to the surface. Furthermore, ocean-to-ice heat flux at a depth of 5m for the same profile is estimated at $6 Wm^{-2}$, which is more than six times the monthly mean for May based on calculations from the entire May 2008 time series of profiles for ITP10 (Figure 41).

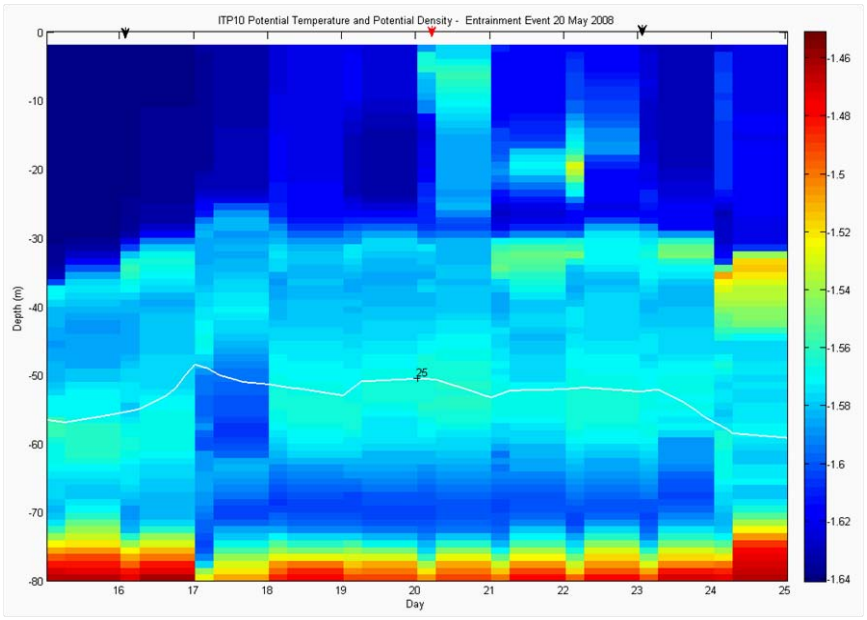

Figure 37. ITP10 potential temperature with potential density contours (shown in white with a value of 25kgm^{-3}) for the period 15 to 25 May 2008. Arrows indicate profiles of interest before (16 May, profile 517 - black), during (20 May, profile 526 - red) and after (23 May, profile 531 - black) entrainment.

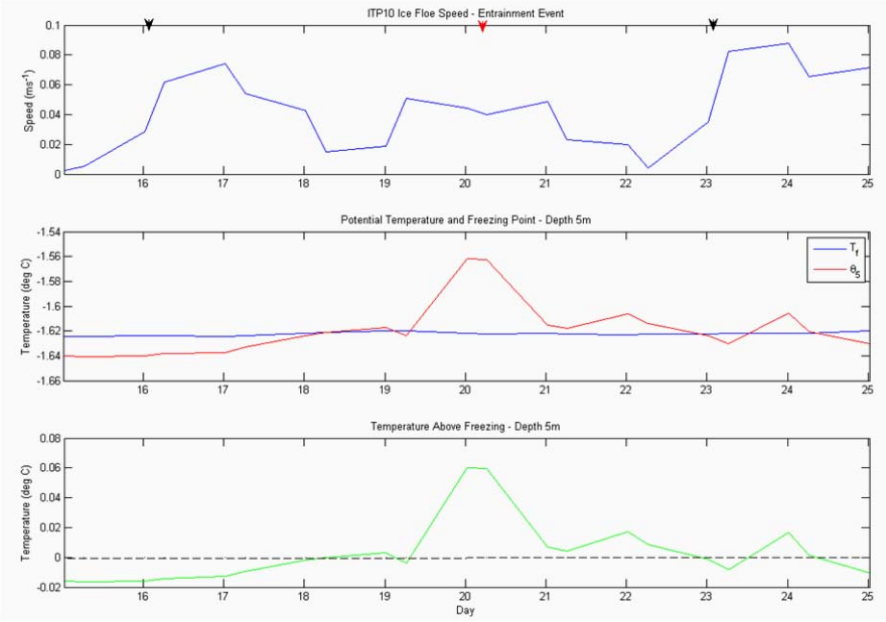

Figure 38. ITP10 ice floe speed (top), potential temperature and freezing point at depth 5m (middle) and temperature above freezing point at depth 5m, with black line showing reference point of zero (bottom) for the period 15 to 25 May 2008. Arrows indicate profiles of interest before (16 May, profile 517 - black), during (20 May, profile 526 - red) and after (23 May, profile 531 - black) entrainment.

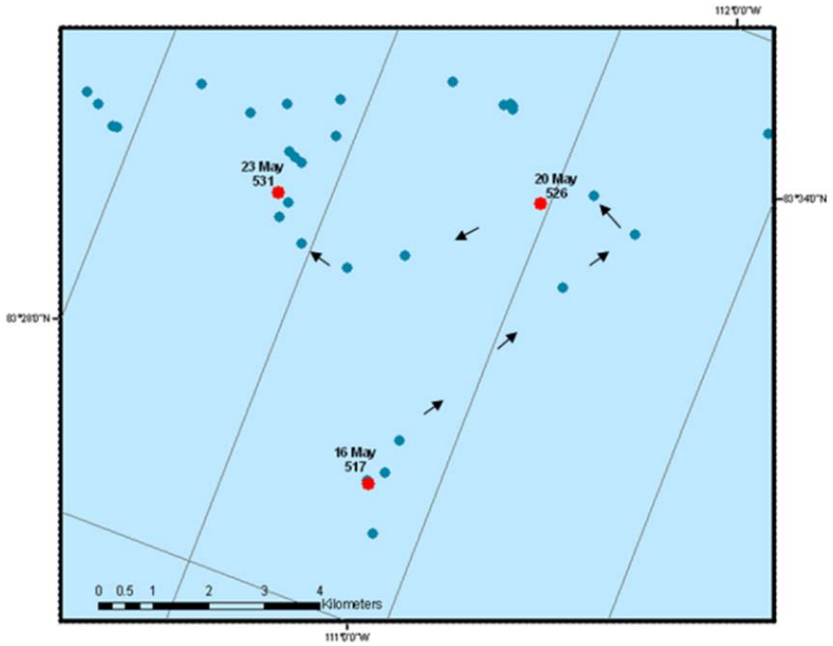

Figure 39. ITP10 drift track for period of focus. Blue dots indicate all profile positions and red dots show profiles of interest (date and profile number shown). Black arrows show actual direction of drift from 16 to 23 May 2008.

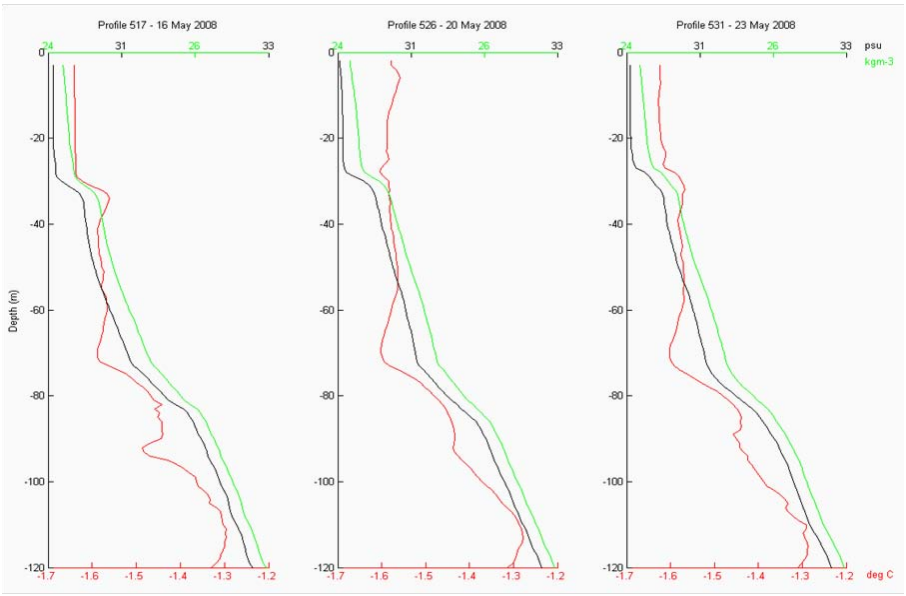

Figure 40. ITP10 vertical profiles of potential temperature (red), salinity (black) and potential density (green) for profiles of interest before (16 May, profile 517), during (20 May, profile 526) and after (23 May, profile 531) entrainment.

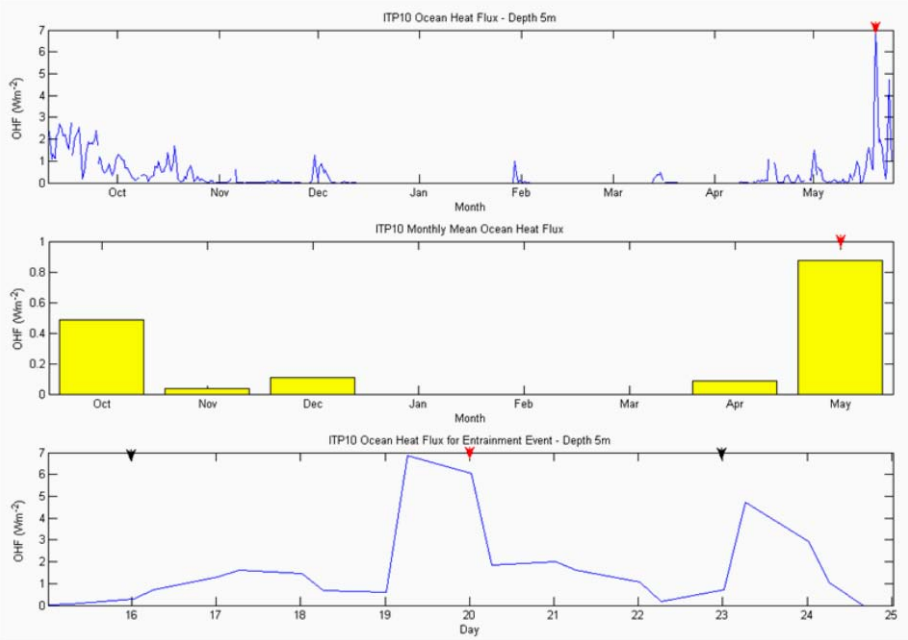

Figure 41. ITP10 ocean heat flux at depth 5m for entire time series (top), monthly mean ocean heat flux at depth 5m (middle) and ocean heat flux at depth 5m for period of entrainment during May (bottom). Red arrows show period of entrainment in May 2008.

Unfortunately it is difficult to determine whether significant sea ice melt occurred during the possible entrainment event due to the lack of any significant change in the salinity of the mixed layer and the fact that there are no corresponding IMB observations available during this period. One way to explain this could be that the eddy was recently generated and its impact on sea ice just started. However, since the time series ends shortly after the identified event, it is also uncertain whether the warming of the upper ocean is a persistent feature, which may be the result of surface heating through leads in late May as summer approaches. This particular event does, however, show that there may be potential for the bottom ablation of sea ice due to oceanic forcing, even in the relatively cold, low energy region of the central Arctic.

2. Western Arctic - ITP6 and IMB2006C

Observations from ITP6 (04 September 2006 to 03 July 2008) and IMB2006C (05 September 2006 to 22 October 2008) from the Beaufort Sea are presented to show the evolution of the mixed layer during the transition from summer to winter in the typically

more energetic environment of the western Arctic Ocean. Surviving a period of about two years, this array of instruments forms the longest time series of co-located ITP/IMB observations available thus far. Potential density, salinity and potential density plots from ITP6 (Figure 42) clearly show the effects of summer solar heating on the upper water column during the summer of 2007. The NSTM described by Jackson et al. (2010) is evident at a depth of ~25m in Sep 2007 and deepens in the following few months, before it appears to merge with the layer of PSW below in November/December 2007, as the mixed layer deepens towards late winter. The existence of a warm, salty PSW layer is particularly distinct at depths of approximately 40 to 80m from May to November 2007. Unlike the aforementioned central Arctic example, evidence of possible eddy activity is more noticeable in the ITP6 temperature data. Although it is possible that they are related to the deepening of the NSTM, local temperature maxima just below the depth of the mixed layer in late 2007 suggest the presence of warm eddies. Eddies were previously identified in the ITP6 observations by Timmermans et al. (2008), but their focus was on cold halocline eddies in September/October 2006, which are characterized by anomalously cold potential temperature and low stratification. The drift track of ITP6 (Figure 43) confirms that events identified below as possible warm eddies correspond with anticylonic meanders in the drift.

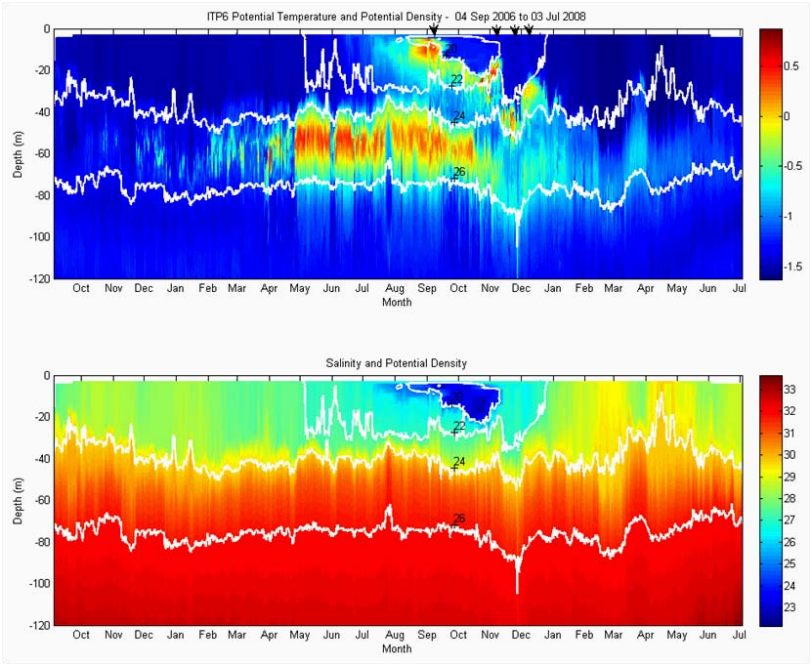

Figure 42. ITP6 potential temperature with potential density contours (shown in white, ranging from 20 to 26kgm^{-3} from top to bottom) (top) and salinity with potential density contours (bottom) for the period 04 September 2006 to 03 July 2008. Black arrows indicate profiles of interest on 04 September (profile 729), 04 November (profile 851), 23 November (profile 889) and 11 December 2007 (profile 925).

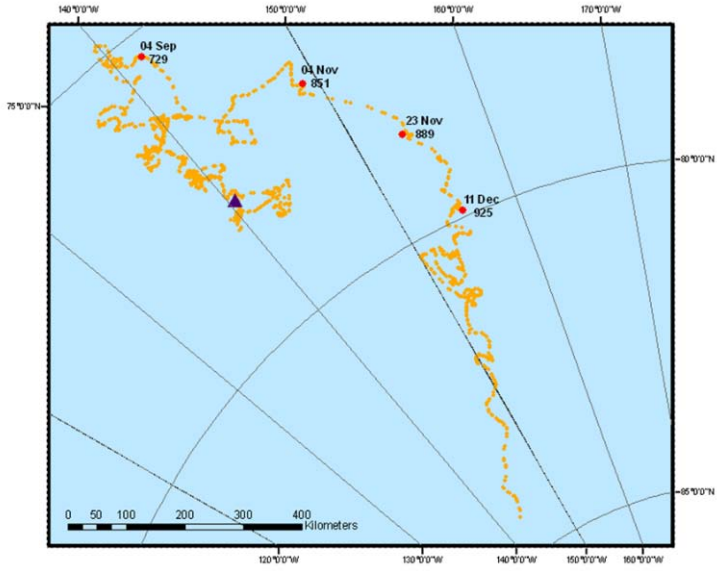

Figure 43. ITP6 drift track. Orange dots indicate all profile positions and red dots show profiles of interest (date and profile number shown). Purple triangle marks start position.

Figure 44 shows corresponding time series of ITP6 ice floe speed, potential temperature and freezing point, and temperature difference above freezing point at a depth of 5m. At 0.08ms^{-1}, the mean ice floe speed was twice as fast as that of ITP10 in the central Arctic, perhaps due to lower concentrations of sea ice and the fact that its drift was most likely affected by the underlying circulation of the Beaufort Gyre and the Transpolar Drift. Several large spikes in floe speed (~0.45ms^{-1}) during the winter of 2007/08 may be indicative of the passage of storm events. The analysis of temperature and freezing point data reveals that the temperature remained at or near freezing point until summer 2007, when large departures above freezing point occurred due to the effects of incident solar radiation. It is difficult to determine any trends in near surface temperature and freezing point for the following winter (2007/08) due to gaps in upper ocean data during this time.

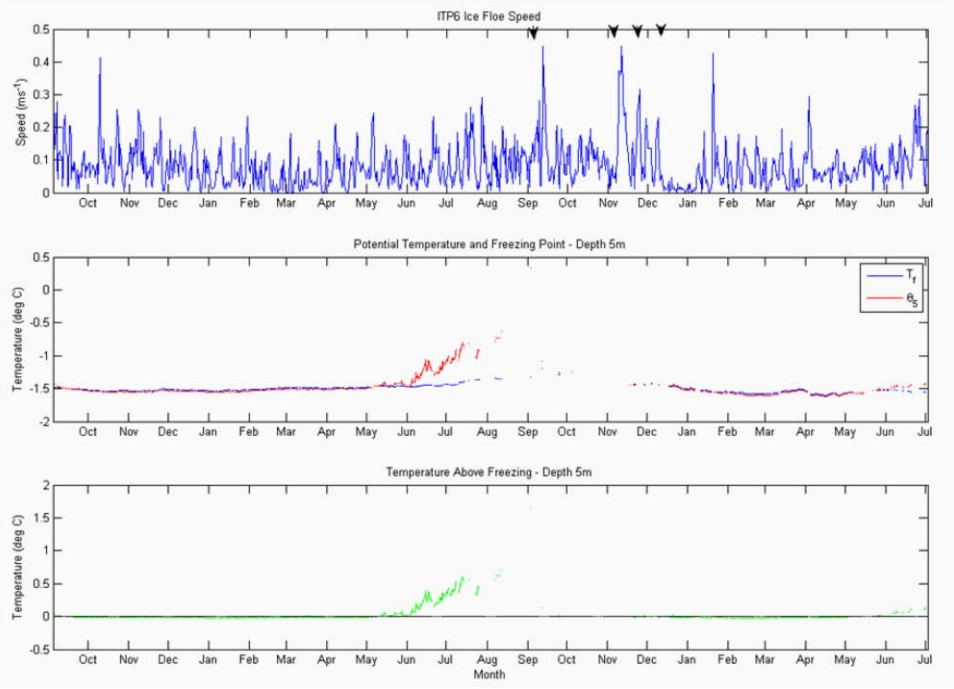

Figure 44. ITP6 ice floe speed (top), potential temperature and freezing point at depth 5m (middle) and temperature above freezing point at depth 5m, with black line showing reference point of zero (bottom). Arrows indicate profiles of interest on 04 September (profile 729), 04 November (profile 851), 23 November (profile 889) and 11 December 2007 (profile 925).

The characteristics of the mixed layer during the summer to winter transition in the Beaufort Sea region of the western Arctic are shown in the vertical profiles in Figure 45, the corresponding T-S scatter plot in Figure 46 and the plots of potential density over the depth of the mixed layer in Figure 47. The late summer profile from September 2007 shows that solar heating provided a significant warming and freshening as a result of sea ice melt on the structure of the upper water column at this time. The mixed layer became significantly deeper in late autumn, and was well mixed to a depth of 37m by late November, where it was bounded by a large temperature gradient possibly due to a deepening NSTM, an intrusion of PSW, the presence of a warm eddy, or a combination of these factors.

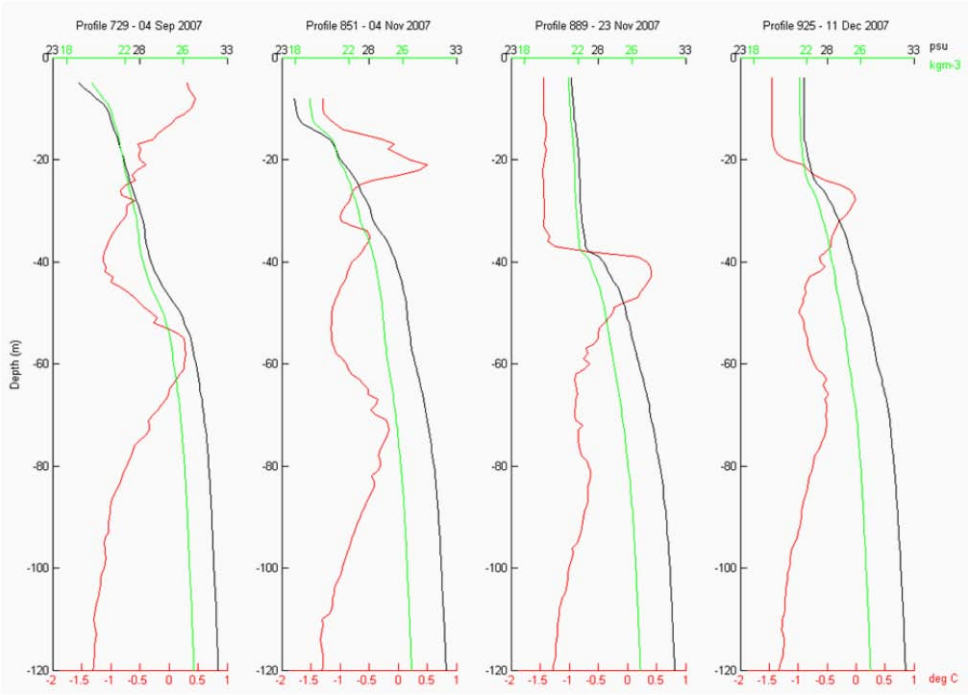

Figure 45. ITP6 vertical profiles of potential temperature (red), salinity (black) and potential density (green) for profiles of interest on 04 September (profile 729), 04 November (profile 851), 23 November (profile 889) and 11 December 2007 (profile 925) (from left to right).

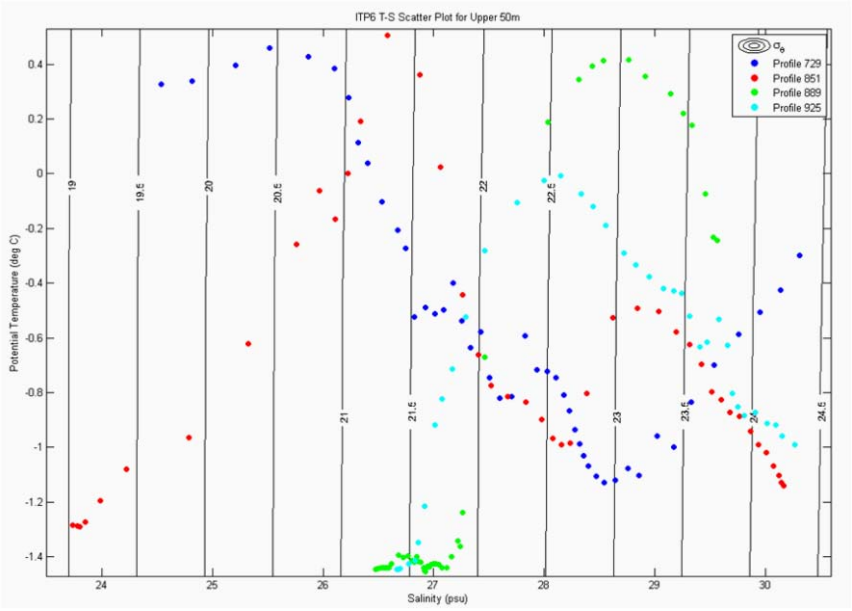

Figure 46. ITP6 scatter plot for upper 50m with contours of potential density for profiles of interest on 04 September (profile 729 - blue), 04 November (profile 851- red), 23 November (profile 889 - green) and 11 December 2007 (profile 925 - cyan).

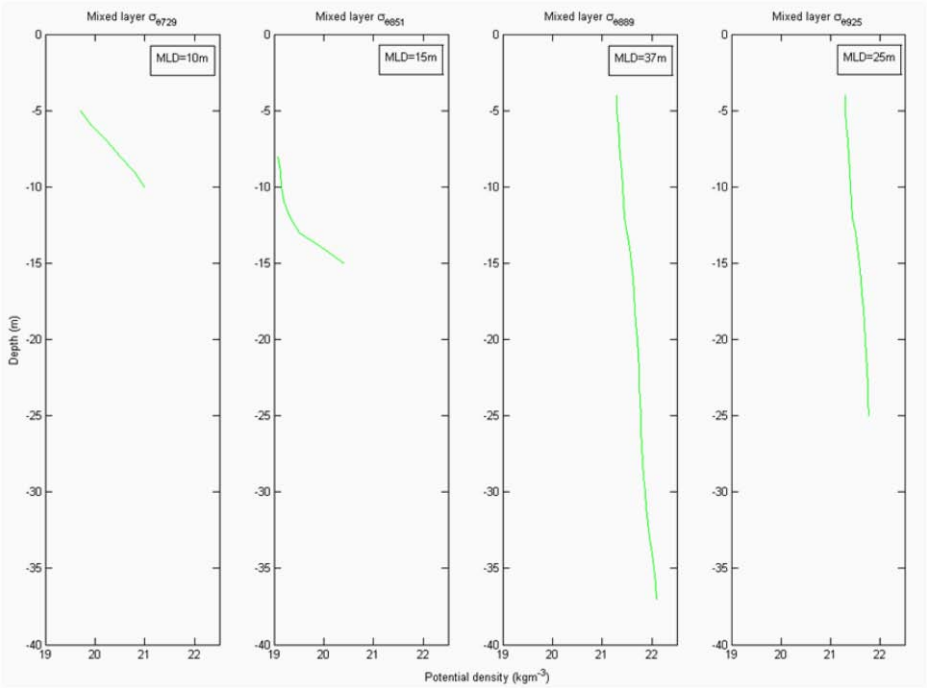

Figure 47. ITP6 mixed layer potential density for profiles of interest on 04 September (profile 729), 04 November (profile 851), 23 November (profile 889) and 11 December 2007 (profile 925) (from left to right).

During the approach to winter, the salinity and potential density of the mixed layer increased and there was weak stratification at the base of the mixed layer. As in the central Arctic example, heat content in the mixed layer followed a distinct seasonal cycle, although in this case some was available within the mixed layer at the times of all the four profiles shown in Figure 45. Furthermore, the analysis of monthly mean ocean heat fluxes (Figure 48) shows that they were several orders of magnitude larger (three to four times) in the Beaufort Sea than in the central Arctic in winter. The profile from 11 December 2007 is particularly of interest because it shows a relatively shallow mixed layer during winter, which corresponds to an area of anomalously warm temperature and low salinity previously identified in Figure 42. This feature may indicate the presence of a warm eddy, but a lack of vertical profiles either side of this event (not immediately obvious from Figure 42 due to data interpolation) make it difficult to establish a persistent or definite trend during this period. The characteristics of the mixed layer for the selected ITP6 profiles are summarized in Table 2.

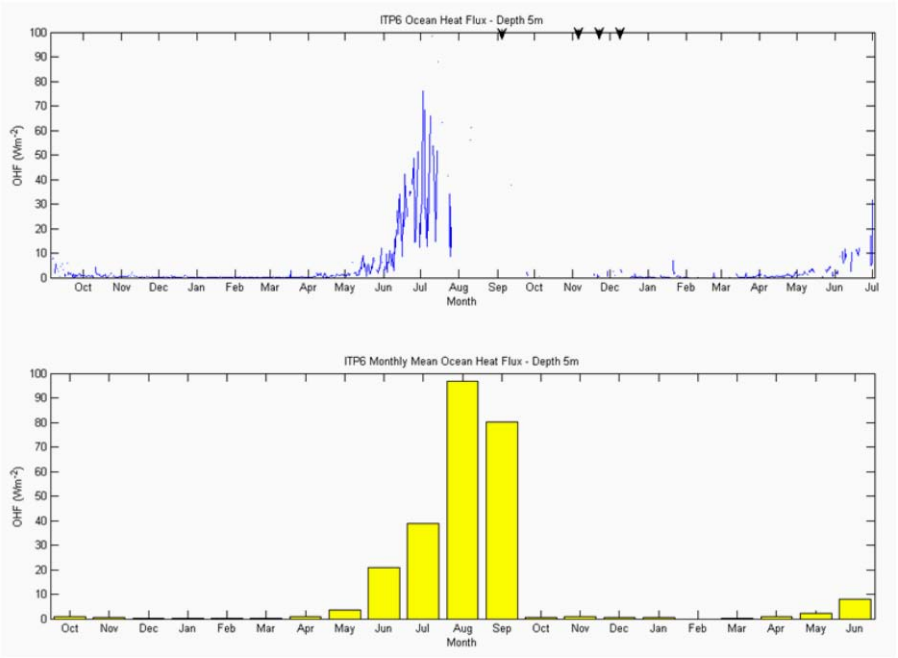

Figure 48. ITP6 ocean heat flux at depth 5m for entire time series (top) and monthly mean ocean heat flux at depth 5m (bottom). Arrows indicate profiles of interest on 04 September (profile 729), 04 November (profile 851), 23 November (profile 889) and 11 December 2007 (profile 925).

Profile Number	Date	Mixed Layer Depth MLD (m)	Mean Potential Temperature $\overline{\theta}$ (°C)	Mean Salinity $\overline{S}$ (psu)	Mean Potential Density $\overline{\sigma_\theta}$ (kgm^{-3})	Ice Floe Speed (ms^{-1})
729	04 Sep 2007	10	0.3894	25.3411	20.3618	0.0890
851	04 Nov 2007	15	-1.1245	24.1846	19.4709	0.0349
889	23 Nov 2007	37	-1.4177	26.8627	21.6887	0.0909
925	11 Dec 2007	25	-1.2387	26.8325	21.6322	0.1042

Table 2. ITP6 summary of mixed layer characteristics for profiles of interest on 04 September (profile 729), 04 November (profile 851), 23 November (profile 889) and 11 December 2007 (profile 925).

IMB2006C was co-located with ITP6 and its lifetime exceeded that of ITP6 by several months. This IMB therefore provides a good example of the seasonal cycle of atmospheric and sea ice conditions in the Beaufort Sea over a period of more than two years. Figure 49 shows meteorological observations, snow depth and water temperature for the period of observation, and Figure 50 shows sea ice temperature and ice bottom position. Once again, it is difficult to find any direct correlation between IMB air pressure and ITP floe speed. Meteorological observations show that air temperature was close to freezing in September 2007, which corresponds with the period of warm upper ocean temperatures seen in the ITP6 observations in late summer. The time series of water temperature just below the bottom of the ice shows a distinct seasonal cycle. However, Figure 50 suggests that there were large temperature differences (often >1°C) between one thermistor and the next (spaced at 10cm depth intervals apart) below the bottom of the ice. This jagged appearance may be due to an offset between thermistors that was a problem with some of the older IMBs (D. Perovich, CRREL, personal communication). As previously reported by Perovich et al. (2008) and Toole et al. (2010), measurements of the ice bottom show a very large bottom melt of 2.1m during the summer of 2007, which was well above the annual average melt conditions observed in prior years in the Beaufort Sea. As in the central Arctic case, the onset of winter ice growth in the Beaufort Sea did not occur until December. Monthly mean ocean heat fluxes derived from ice temperature and mass balance (not shown) (D. Perovich, CRREL, personal communication) are of the same order of magnitude as those calculated at 5m depth from the ITP data.

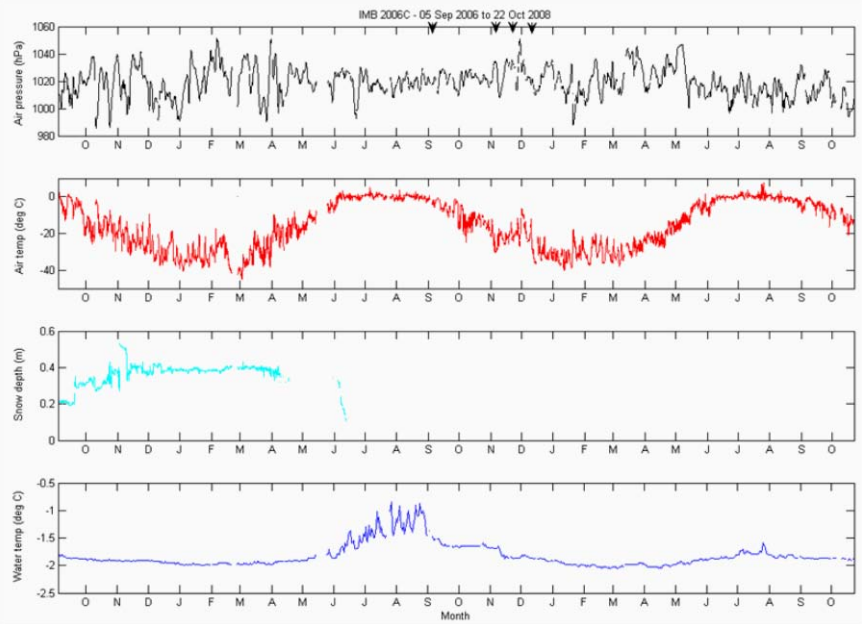

Figure 49. IMB2006C air pressure (black), air temperature (red), snow depth (cyan) and water temperature (blue) for the period 05 September 2006 to 22 October 2008. Arrows indicate positions corresponding to ITP6 profiles of interest on 04 September (profile 729), 04 November (profile 851), 23 November (profile 889) and 11 December 2007 (profile 925).

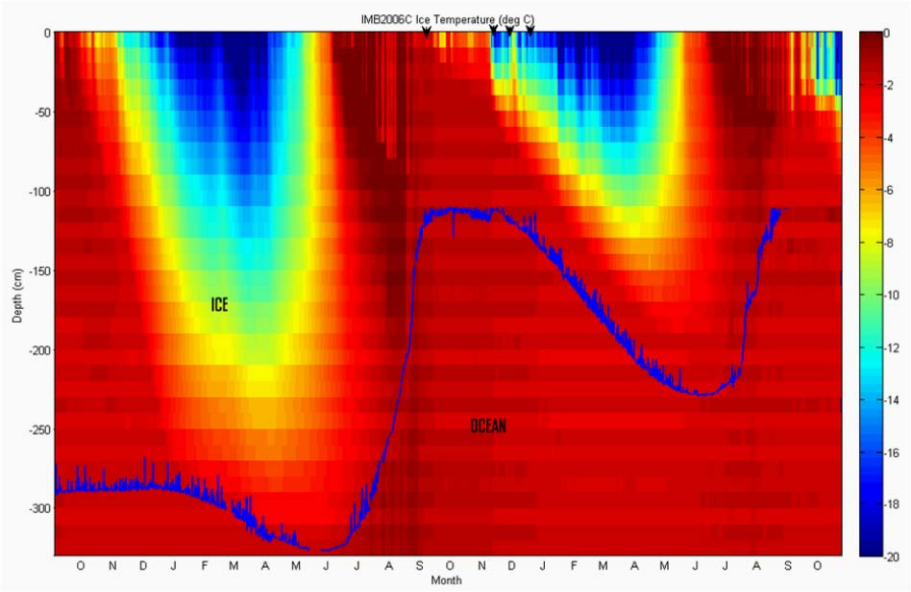

Figure 50. IMB2006C sea ice and upper ocean temperature. Blue line shows position of ice bottom and arrows indicate positions corresponding to ITP6 profiles of interest on 04 September (profile 729), 04 November (profile 851), 23 November (profile 889) and 11 December 2007 (profile 925).

3. Case Study 1: Beaufort Sea Winter - ITP3 and IMB2005B

Data from co-located instruments ITP3 (23 August 2005 to 10 September 2006) and IMB2005B (23 August 2005 to 15 May 2007) are presented as a case study of a potential entrainment event in the Beaufort Sea in winter 2005/06. We focus on an event around 19/20 December 2005, initially identified through analyses of potential temperature, salinity and potential temperature data from ITP3 (Figures 51 and 52). These data reveal an area of anomalously warm temperature centered at about 60m depth and extending upwards towards the surface, suggesting an entrainment of heat into the mixed layer. Satellite imagery (Figure 53) shows that in mid December, sea ice concentration in the vicinity of ITP3 was close to 100%. Corresponding data on floe speed, temperature and freezing point (Figure 54) indicate that the ice was not moving fast (with speeds $<0.09 ms^{-1}$) and there was also a significant (0.02°C) increase in potential temperature near the surface when compared to conditions preceding and following the event. Given the aforementioned bias resulting from the calculation of freezing point from salinity data, the increase in near surface temperature on 19 December 2007 is interpreted as a departure above the freezing point, which has the potential to melt sea ice from below.

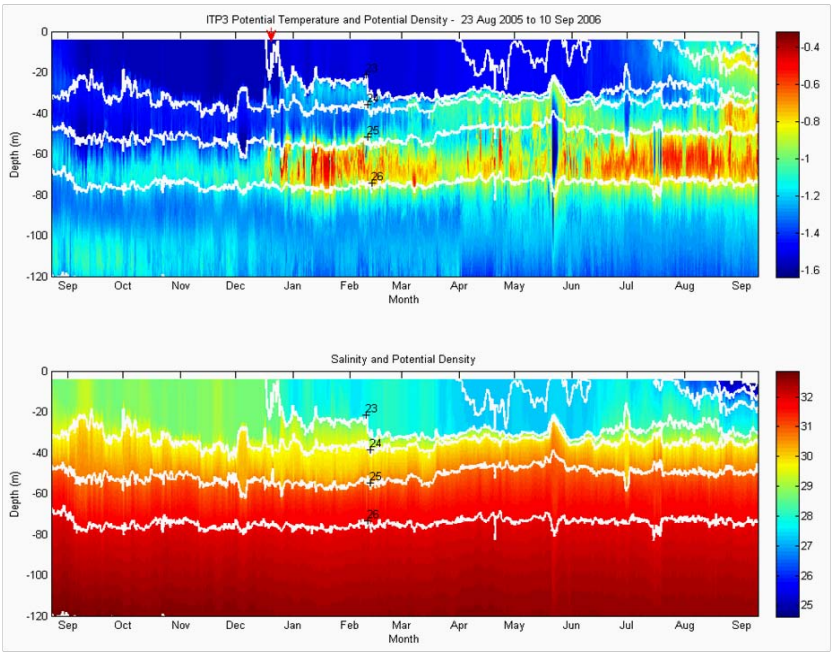

Figure 51. ITP3 potential temperature with potential density contours (shown in white, ranging from 23 to 26kgm^{-3} from top to bottom) (top) and salinity with potential density contours (bottom) for the period 23 August 2005 to 10 September 2006. Red arrow indicates entrainment event in mid December 2005.

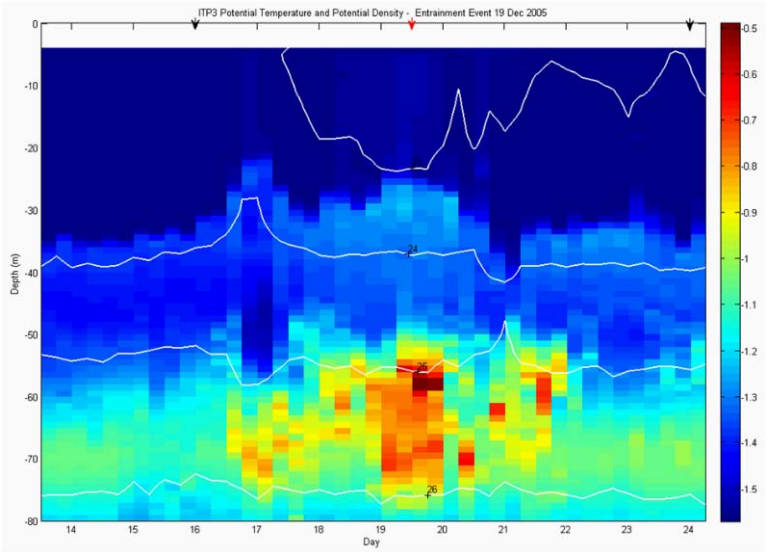

Figure 52. ITP3 potential temperature with potential density contours (shown in white, ranging from 23 to 26kgm^{-3} from top to bottom) for the period 14 to 24 December 2005. Arrows indicate profiles of interest before (16 December, profile 456-black), during (19 December, profile 474-red) and after (24 December, profile 490-black) entrainment.

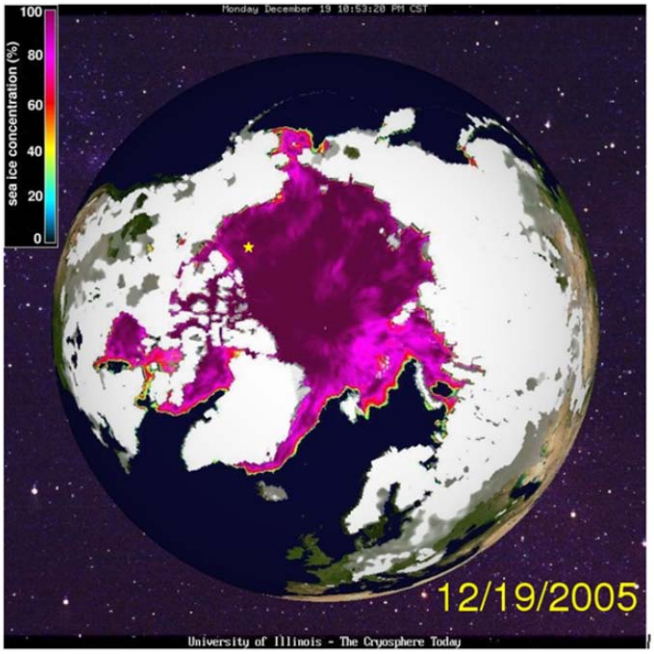

Figure 53. Sea ice concentration from satellite data on 19 December 2005. Yellow star shows ITP3 entrainment event position (from University of Illinois 2010).

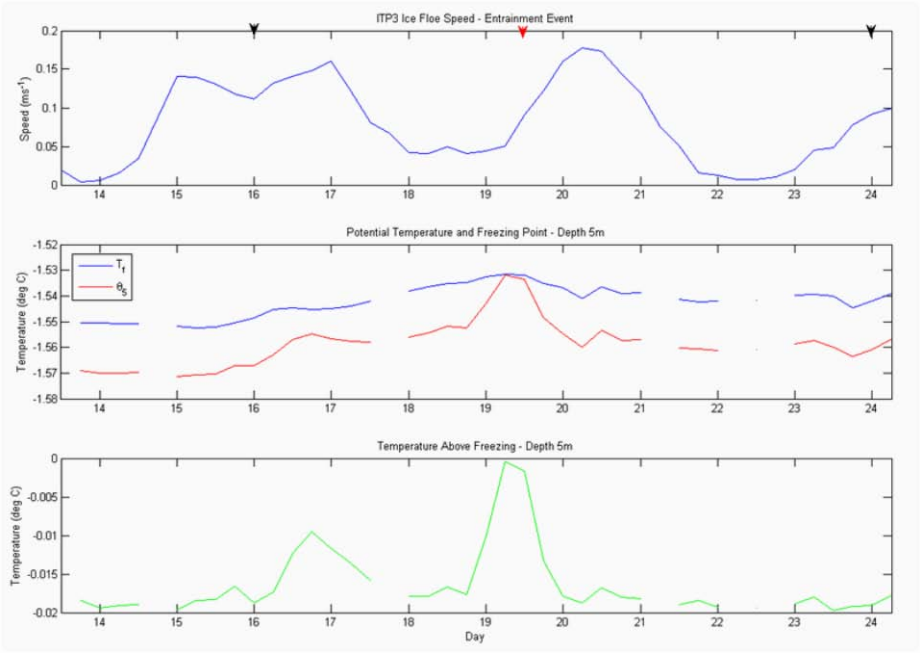

Figure 54. ITP3 ice floe speed (top), potential temperature and freezing point at depth 5m (middle) and temperature above freezing point at depth 5m (bottom) for the period 14 to 24 December 2005. Arrows indicate profiles of interest before (16 December, profile 456 - black), during (19 December, profile 474 - red) and after (24 December, profile 490 - black) entrainment.

The drift track of ITP3 (Figure 55) for the period of interest shows meanders in the drift, including drift past the eastern perimeter of an anticyclonic feature (of order 10km) on 19/20 December. The small size of the drift pattern delineated by the red arrows in Figure 55 implies the presence of a mesoscale ocean eddy rather than the effect of large scale atmospheric forcing. Furthermore, the analyses of ITP and IMB positional data (Appendix A) shows that during the winter months (December to May) inertial oscillations play a negligible role in the ice drift, hence it is unlikely that the anticylonic feature is due to inertial effects. During 19/20 December, the instrument only briefly measured the peripheral effects of the identified eddy. Further analyses of the drift track show that the ice floe encountered the same feature in mid February (two months later) when it completed a full rotation within the eddy. Given that previous observations (e.g., Timmermans et al. 2008; D'Asaro 1988) and results from the numerical model discussed in the previous section indicate that mesoscale eddies may commonly persist for periods of months, it is likely that the instrument was subjected to the effects of the same feature first in December, then again in February.

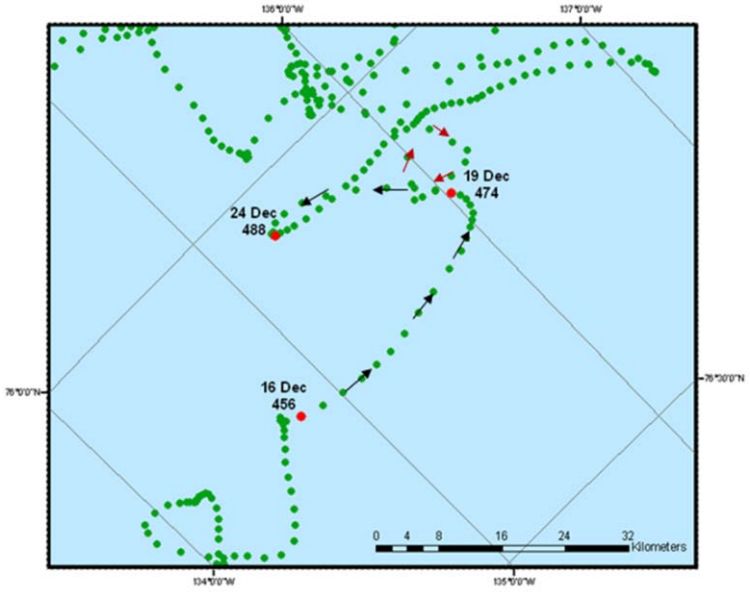

Figure 55. ITP3 drift track for period of focus. Green dots indicate all profile positions and red dots show profiles of interest (date and profile number shown). Black arrows show actual drift from 16 to 24 December 2005, and red arrow shows a drift track around an anticyclonic eddy-like feature in Februrary 2006. The instrument encountered the eastern boundary of the eddy on 19/20 December 2005.

The characteristics of the upper water column at times before (16 December, profile 456), during (19 December, profile 474) and after (24 December, profile 490) the indentified event are summarized in Table 3 over the depth of the shallowest mixed layer (27m). Corresponding vertical profiles of potential temperature, salinity and potential density are shown in Figure 56 and the temperature maximum at a depth of about 55m on 19 Dec represents the previously identified likely source of heat for the entrainment event. A T-S scatter plot and plots of potential density over the depth of the mixed layer for the same profiles are shown in Figures 57 and 58 respectively. This series of figures shows that the upper water column became significantly warmer, fresher and less dense during the entrainment event, and that the mixed layer was shallower when compared with profiles made before and after. The magnitude of the changes to the upper 27m of the water column during entrainment in comparison to before and after are more clearly shown in Figure 59 and are summarized in Table 4. Furthermore, profiles of potential temperature, salinity and potential density for a 24 hour period leading up to the 19 December entrainment profile (Figure 60) confirms that a gradual warming and freshening of the upper water column occurred throughout this time.

Profile Number	**Date**	**Mixed Layer Depth MLD (m)**	**Mean Potential Temp $\overline{\theta}$ (°C)**	**Mean Salinity $\overline{S}$ (psu)**	**Mean Potential Density $\overline{\sigma_\theta}$ (kgm^{-3})**	**Heat Content Q (Jm^{-2})**	**Ice Melt (cm)**	**Ice Floe Speed (ms^{-1})**
456	16 Dec 2005	33	-1.5713	28.7366	23.1855	0	0	0.1408
474	19 Dec 2005	27	-1.5125	28.4647	22.9640	1779300	0.6418	0.0909
490	24 Dec 2005	34	-1.5619	28.6078	23.0808	1800	0.0006	0.0205

Table 3. ITP3 summary of mixed layer characteristics for profiles of interest before (16 December, profile 456), during (19 December, profile 474) and after (24 December, profile 490) entrainment.

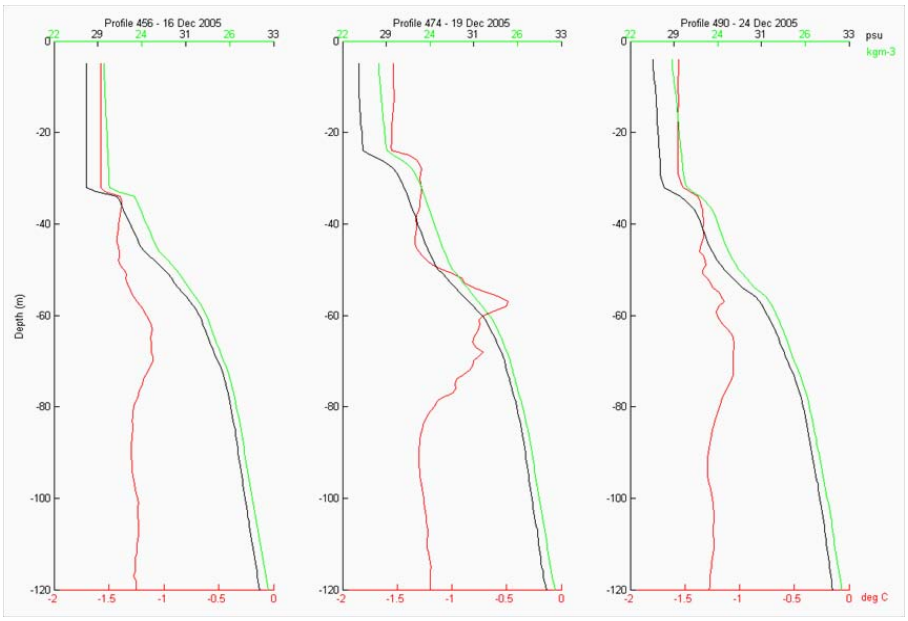

Figure 56. ITP3 vertical profiles of potential temperature (red), salinity (black) and potential density (green) for profiles of interest before (16 December, profile 456 - left), during (19 December, profile 474 - middle) and after (24 December, profile 490 - right) entrainment.

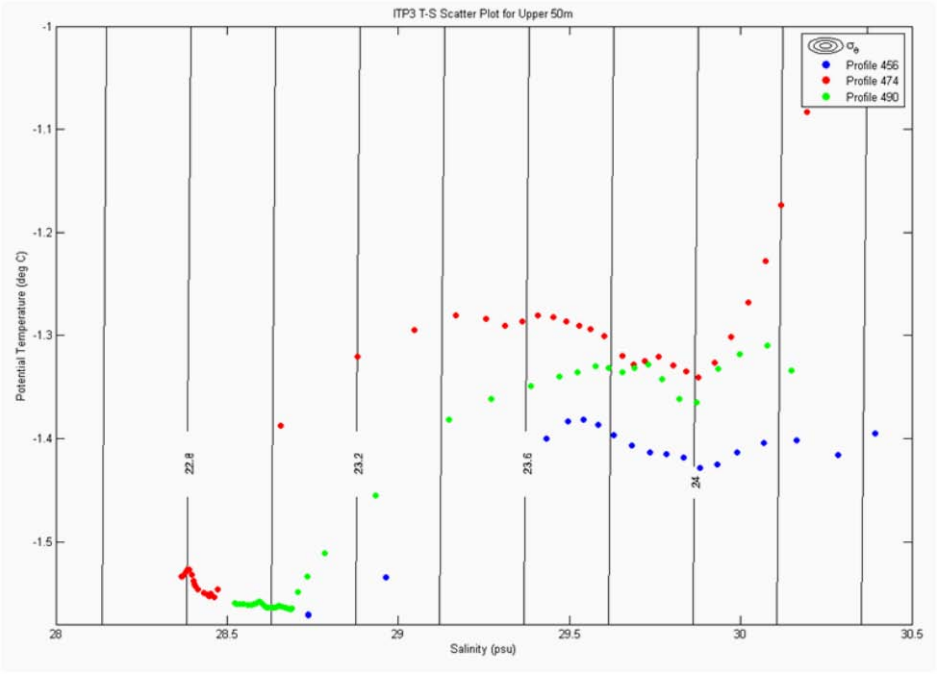

Figure 57. ITP3 scatter plot for upper 50m with contours of potential density for profiles of interest before (16 December, profile 456 - blue), during (19 December, profile 474 - red) and after (24 December, profile 490 - green) entrainment.

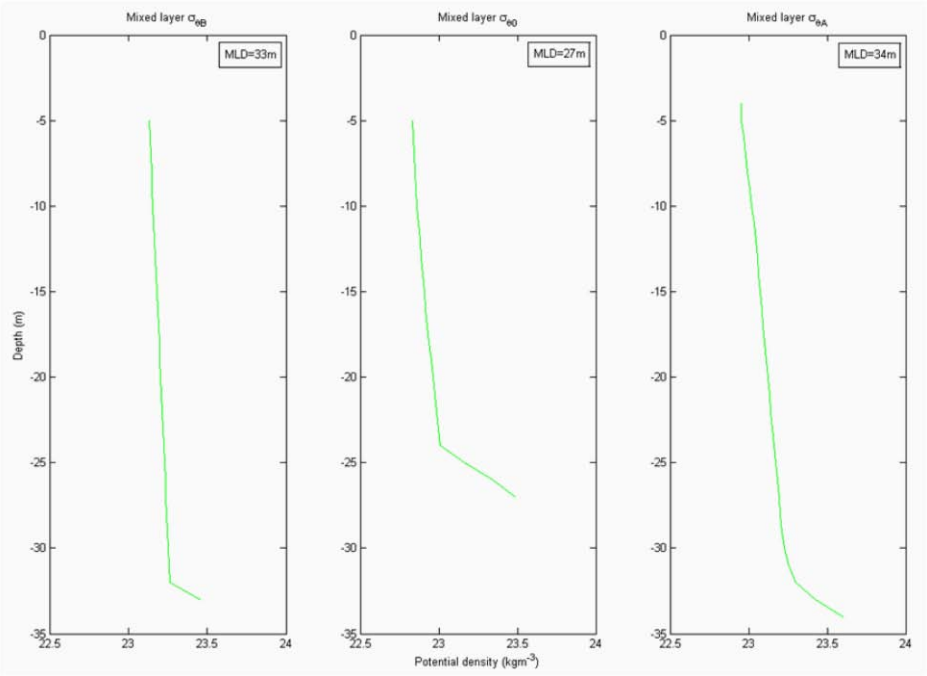

Figure 58. ITP3 mixed layer potential density for profiles of interest before (16 December, profile 456 - left), during (19 December, profile 474 - middle) and after (24 December, profile 490 - right) entrainment.

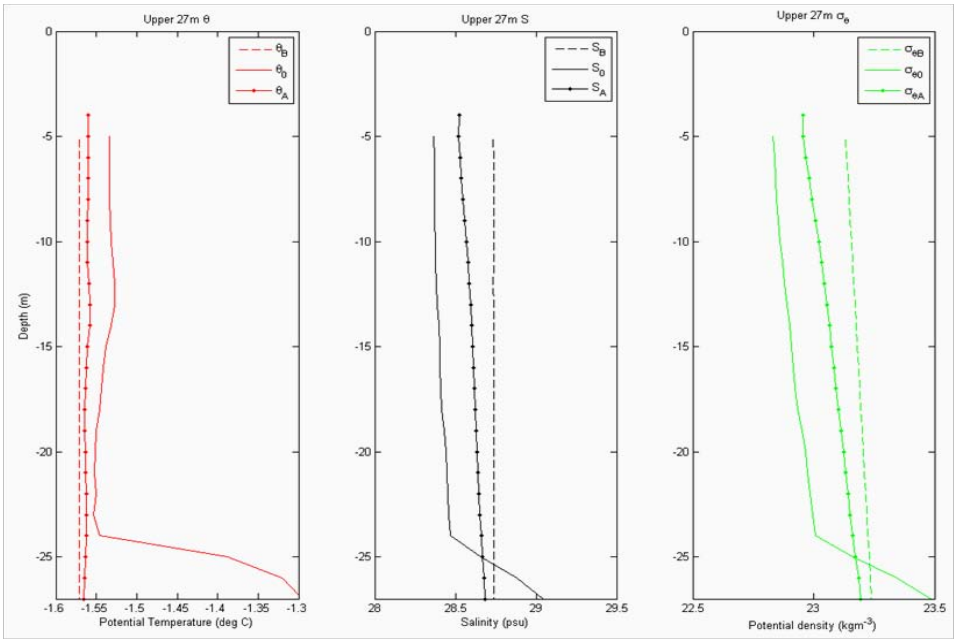

Figure 59. ITP3 upper 27m potential temperature (left), salinity (middle) and potential density (right) for profiles before (16 December, profile 456 - subscript B), during (19 December, profile 474 - subscript 0) and after (24 December, profile 490 - subscript A) entrainment.

Parameter	During minus before entrainment (profile 474-profile 456)	After minus during entrainment (profile 490-profile 474)
Potential Temperature $\overline{\theta}$ (°C)	+0.0588	-0.0494
Salinity $\overline{S}$ (psu)	-0.2719	+0.1431
Potential Density $\overline{\sigma_\theta}$ (kgm^{-3})	-0.2215	+0.1168
Heat Content Q (Jm^{-2})	+1779300	-1777500

Table 4. ITP3 differences in upper 27m characteristics from profiles made before (16 December, profile 456), during (19 December, profile 474) and after (24 December, profile 490) entrainment.

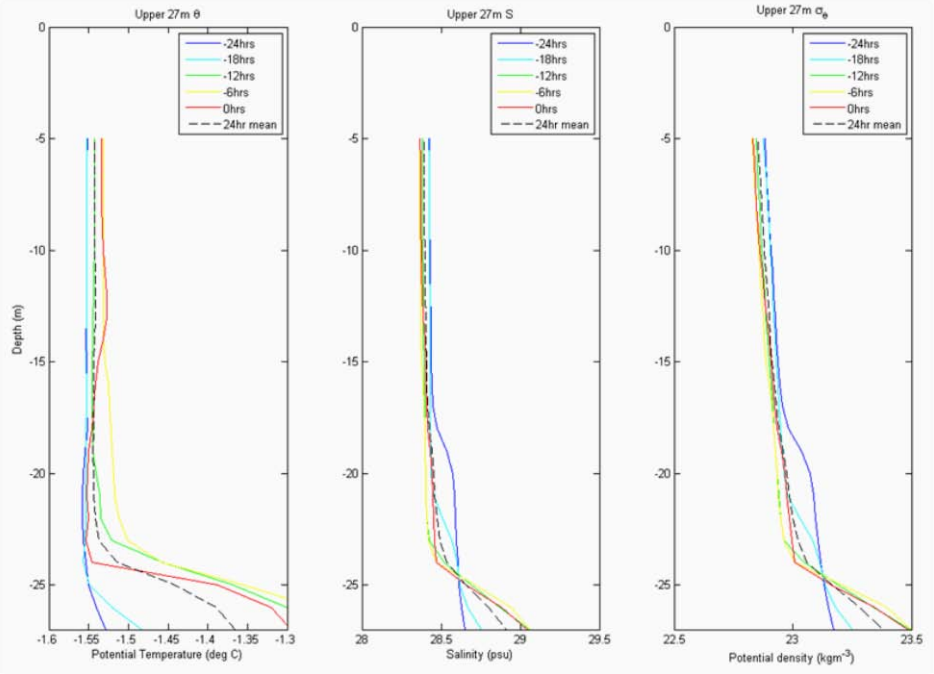

Figure 60. ITP3 upper 27m potential temperature (left), salinity (middle) and potential density (right) for profiles made 24 hours leading up to entrainment. Profile 474 (19 December) is shown in red and 24 hour mean is shown as dashed black line.

In order to determine the consequences of the sub-surface warm eddy on the sea ice drifting above, potential bottom melt was estimated using three different approaches. First, near surface ocean-to-ice heat flux (at depth 5m) was determined from the ITP data (Figure 61). Monthly mean ocean heat fluxes estimated by this method indicate that near surface heat fluxes were largest during the summer months due to solar heating, reaching a maximum of ~30Wm^{-2} in August, and that the smallest heat fluxes occurred during the

winter months, with a December 2005 mean value of 0.34Wm^{-2}. Closer investigation of the ocean heat flux time series reveals that several peaks (of up to 2Wm^{-2}, or about six times the monthly mean) occurred around the time of the identified event. The integration of heat flux with respect to time for the period 16 to 19 December yields a heat content of 2.26x10^{5}Jm^{-2} at 5m depth. Using this value of heat content, bottom melt over this period of time is estimated at 0.08cm.

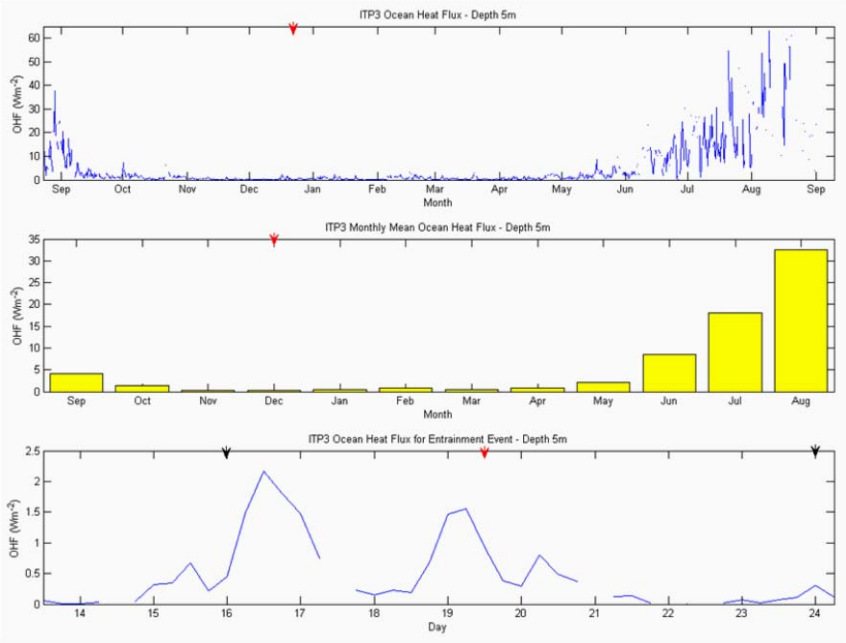

Figure 61. ITP3 ocean heat flux at depth 5m for entire time series (top), monthly mean ocean heat flux at depth 5m (middle) and ocean heat flux at depth 5m for period of focus during December (bottom). Red arrows show period of entrainment in December 2005.

The second method involves the determination of mixed layer heat content from the ITP3 data for the period of interest. Calculations of heat content per unit area over a depth of 27m show that heat content increased by 1.78x10^{6} Jm^{-2} between 16 December (before entrainment) and 19 December (during entrainment). This heat penetrated well above the base of the mixed layer, to a depth of at least 10m on the day of maximum entrainment, and persisted within the mixed layer for several days thereafter. Assuming that over time all of this heat reached the bottom of the ice and that no heat was lost to the atmosphere, 0.64cm of bottom melt would occur based on heat content calculated over

the depth of the mixed layer for profile 474 made during the identified event on 19 December. This estimate is eight times larger than the value previously obtained by calculating near surface ocean-to-ice heat fluxes.

Given that during entrainment, positive upward heat flux and subsequent small temperature increases may be partially 'cancelled' by downward mixing of water at freezing temperature from melting ice, estimates of potential bottom ice melt from heat content and especially from heat flux near the ice bottom may be quite conservative. More importantly, the integrated impact on sea ice by an eddy with a lifetime of several weeks to months might be better estimated by changes in mixed layer salinity as an indicator of total melt over the eddy lifetime and not just for the short drift time of the ITP passage through or along the perimeter of an eddy.

The third approach to estimating bottom ice melt therefore focused on salinity changes within the mixed layer following Toole et al. (2010). The mean salinity over the upper 27m for the entire ITP3 time series and for the December 2005 period of interest are shown in Figure 62. A simple calculation using the principle of conservation of volume indicates that over a depth of 27m, 0.33m of water would need to be replaced with melt water of 6psu in order to reduce salinity from the before (16 December) to the during (19 December) entrainment value of salinity. While it is possible that a local advection of freshwater could contribute to such changes, it is unlikely that such a horizontally-limited signal would be significant within the mixed layer during winter ice growth and resulting 'salinification' due to brine rejection processes. It is also worth noting that the salinity-based estimate of ice melt may still be conservative if the observed eddy persisted through mid-February, resulting in further freshening of the mixed layer (as discussed earlier and shown in Figures 51 and 55).

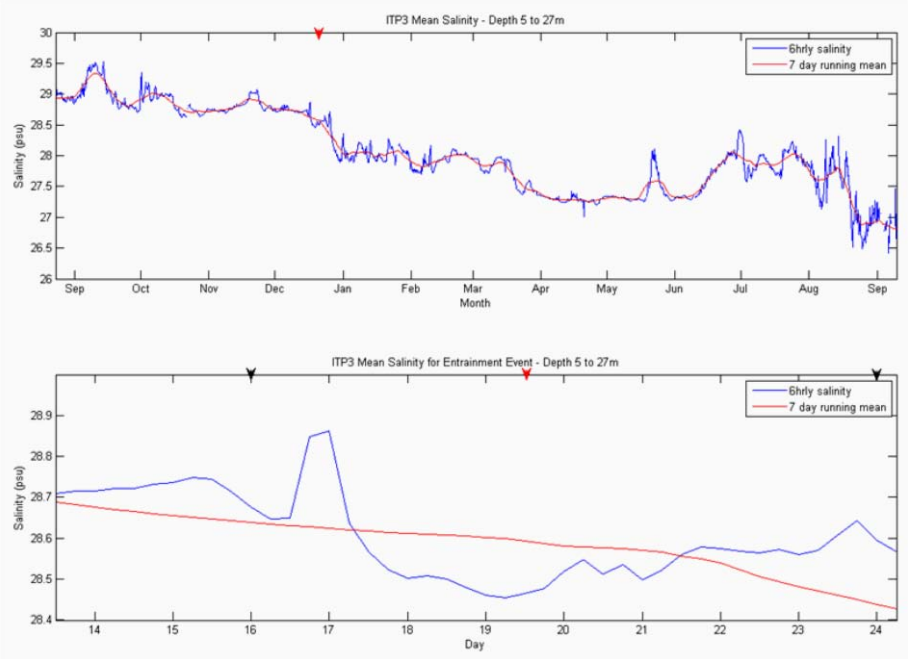

Figure 62. ITP3 upper 27m mean salinity for entire time series (top) and upper 27m mean salinity during period of interest in December 2005 (bottom). Red arrows show period of entrainment in December 2005.

IMB2005B was co-located with ITP3 and observations from this instrument are shown in Figures 63 to 65. Although this IMB survived a period of almost two years, there were some problems with the ice-ocean thermistors and with the snow depth sensor, resulting in some uncertainty and missing sections of data (seen in Figures 63 and 65) (B. Elder and D. Perovich, CRREL, personal communication). The jagged appearance of the temperature profiles (seen in Figure 65) is once again likely due to older buoy design, which produced an offset between the even and odd thermistors. Fluctuations in air pressure observations from December 2005 suggest that the IMB may have been influenced by a number of winter storm events. Air temperature remained well below freezing during the period corresponding to the ITP3 entrainment event, yet upper ocean temperatures measured by the IMB (in Figure 64) indicate an increase of ~0.03°C between 16 and 19 December 2005, which is similar to the increase in ocean temperature recorded by the ITP at 5m depth. Analysis of ice-ocean thermistor data shows that as in the previous cases the onset of winter ice growth did not occur until early December. Although ice bottom positions (Figure 65) suggest a total growth of ~8cm over the eight

day period corresponding to the ITP3 profiles, there are several significant fluctuations of order a few centimeters that occur throughout this time, which may be indicative of ice melt or reduced growth.

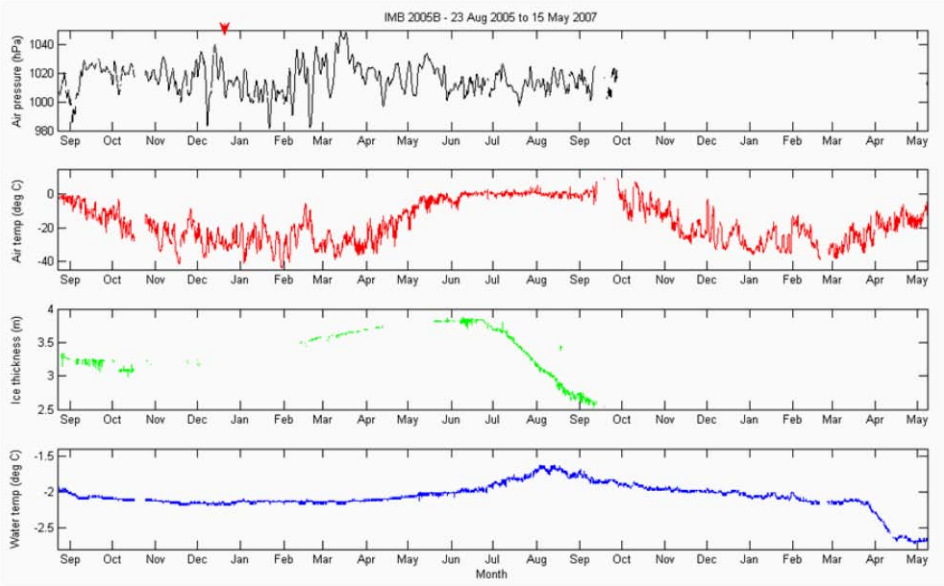

Figure 63. IMB2005B air pressure (black), air temperature (red), ice thickness (green) and water temperature (blue) for the period 23 August 2005 to 15 May 2007. Red arrow indicates position corresponding to ITP3 entrainment event in December 2005.

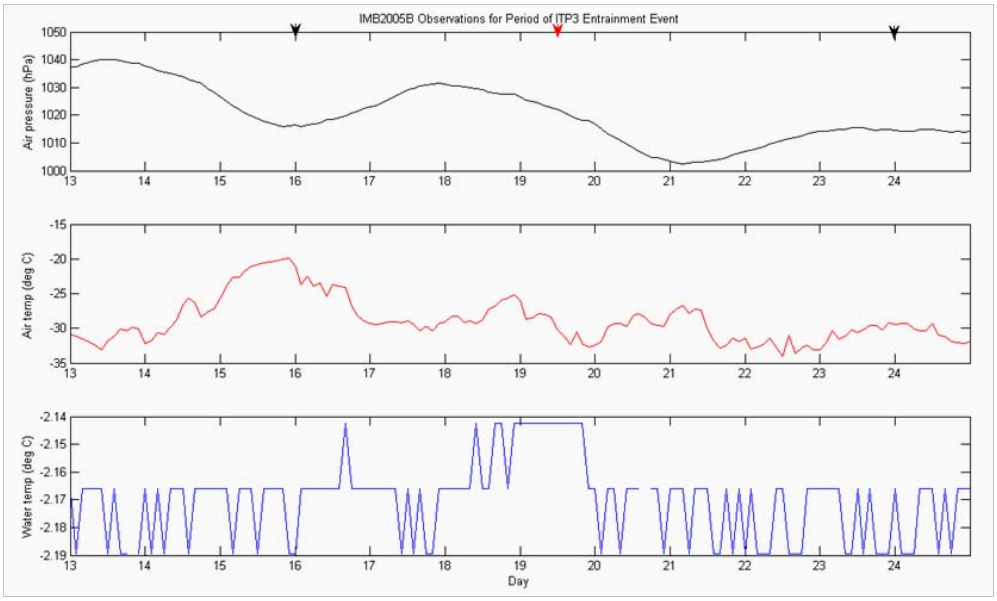

Figure 64. IMB2005B air pressure (black), air temperature (red) and water temperature (blue) for the period 13 to 25 December 2005. Arrows indicate positions corresponding to ITP3 profiles of interest before (16 December, profile 456 - black), during (19 December, profile 474 - red) and after (24 December, profile 490 - black) entrainment.

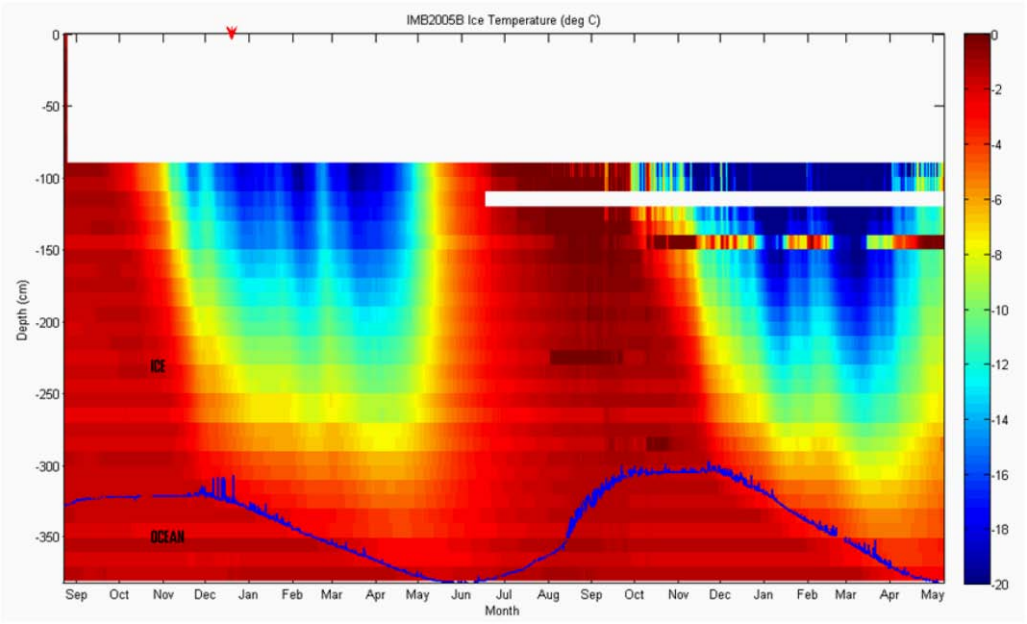

Figure 65. IMB2005B sea ice and upper ocean temperature. Blue line shows position of ice bottom and red arrow indicates position corresponding to ITP3 entrainment event in December 2005.

4. Case Study 2: Beaufort Sea Winter - ITP1 and IMB2005C

The second case study of an entrainment event in the Beaufort Sea in late winter 2005/06 focuses on oceanic data from ITP1 (16 August 2005 to 08 January 2007) and atmospheric data from co-located IMB2005C (16 August 2005 to 19 August 2006). Once again inspection of potential temperature, salinity and potential density measurements (Figures 66 and 67) indicate that a possible entrainment event, characterized by significant warming and freshening of the upper ~30m of the water column, occurred in mid to late May 2006 over a period of at least eight days. Satellite imagery from this time shows a sea ice concentration close to 100% in the vicinity of ITP1 during that time (Figure 68). Plots of ice floe speed, potential temperature and freezing point at 5m depth and temperature above freezing point are shown in Figure 69. The ice floe speed during the period of identified entrainment from 19 to 27 May was $<0.1 ms^{-1}$. Given the previously identified negative bias of approximately 0.02°C in the calculation of freezing point that appears to be a common feature of the ITP time series, it is likely that the temperature was just above freezing for the duration of the event. Investigation of the drift track for ITP1 at the time of entrainment (Figure 70) shows that the instrument encountered an anticyclonic mesoscale feature of about 10km diameter in mid to late May, which may have been a warm core eddy.

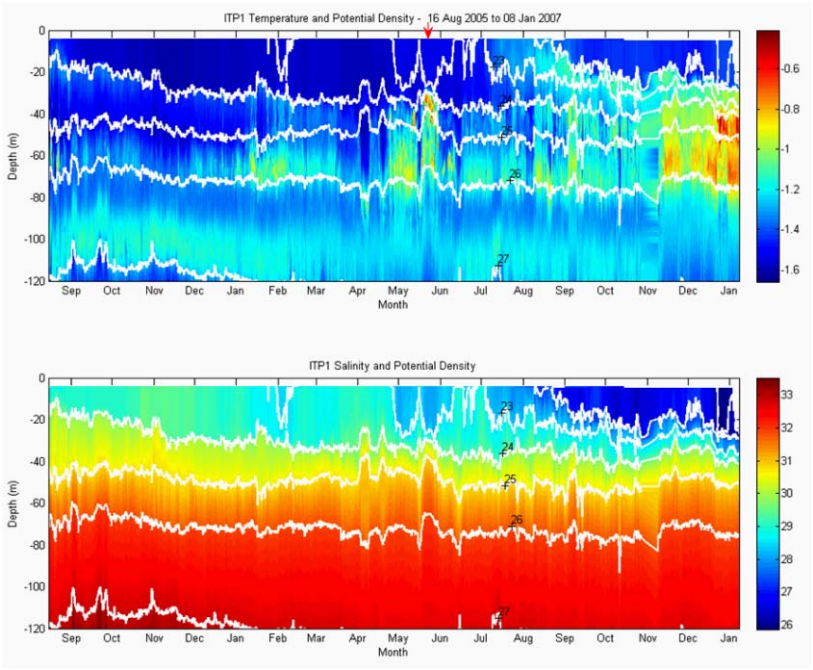

Figure 66. ITP1 potential temperature with potential density contours (shown in white, ranging from 23 to 27kgm^{-3} from top to bottom) (top) and salinity with potential density contours (bottom) for the period 16 August 2005 to 08 January 2007. Red arrow indicates entrainment event in mid to late May 2006.

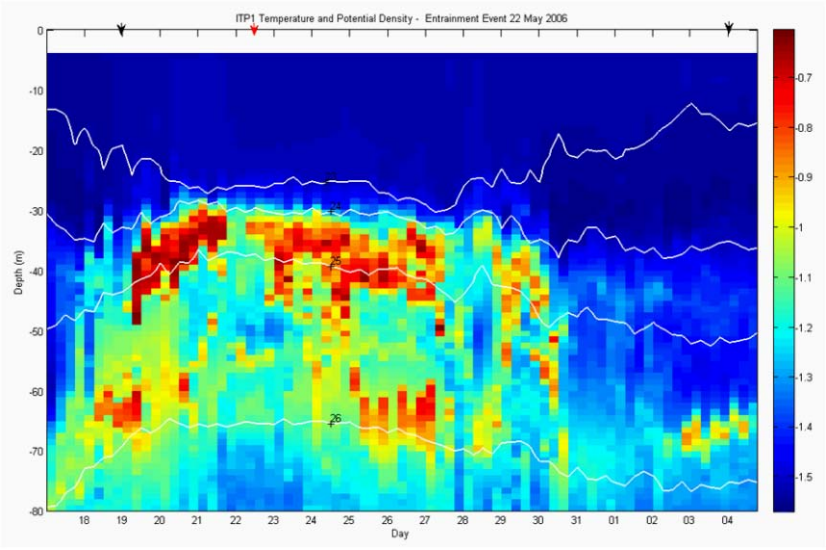

Figure 67. ITP1 potential temperature with potential density contours (shown in white, ranging from 23 to 26kgm^{-3} from top to bottom) for the period 18 May to 04 June 2006. Arrows indicate profiles of interest before (19 May, profile 1106 - black), during (22 May, profile 1118 - red) and after (04 June, profile 1168 - black) entrainment.

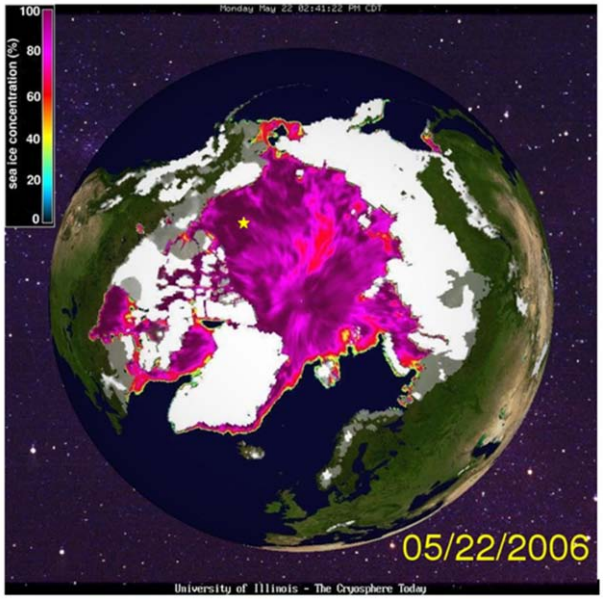

Figure 68. Sea ice concentration from satellite data on 22 May 2006. Yellow star shows ITP1 entrainment event position (from University of Illinois 2010).

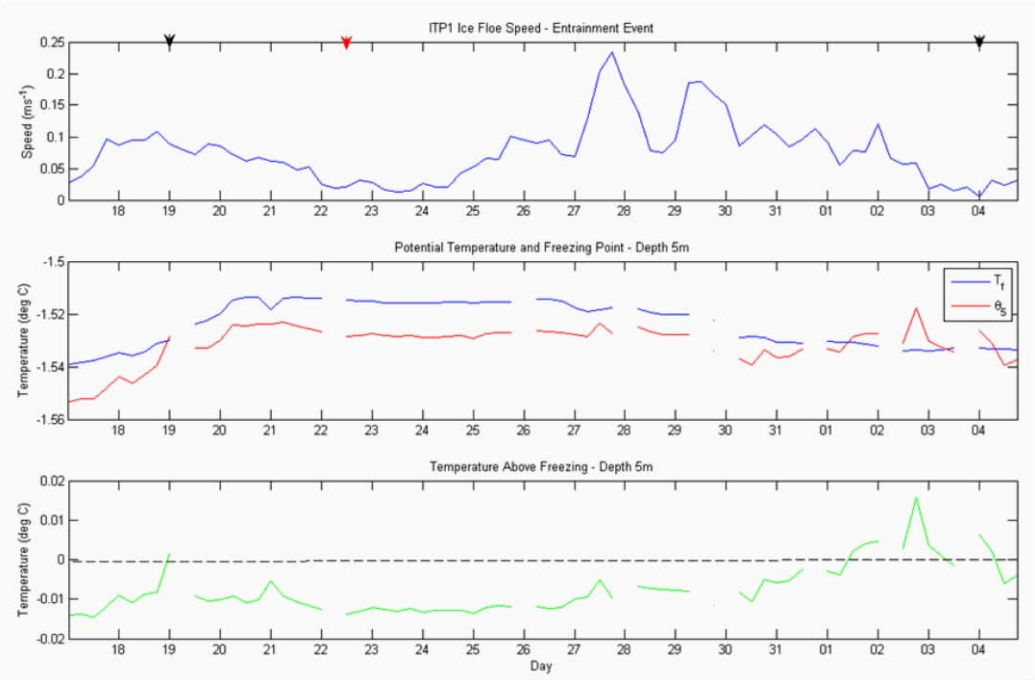

Figure 69. ITP1 ice floe speed (top), potential temperature and freezing point at depth 5m (middle) and temperature above freezing point at depth 5m, with black line showing reference point of zero (bottom) for the period 18 May to 04 June 2006. Arrows indicate profiles of interest before (19 May, profile 1106 - black), during (22 May, profile 1118 - red) and after (04 June, profile 1168 - black) entrainment.

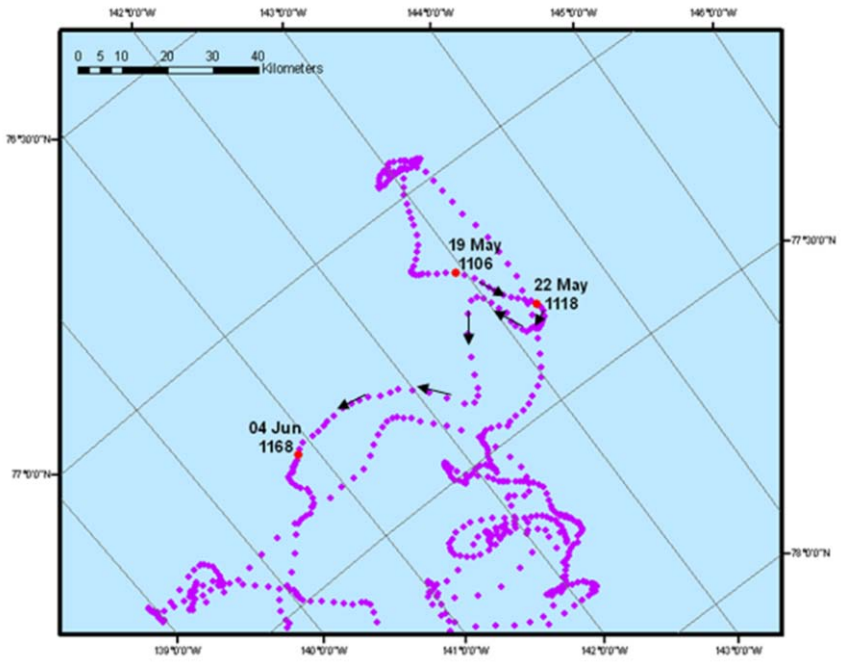

Figure 70. ITP1 drift track for period of focus. Purple dots indicate all profile positions and red dots show profiles of interest (date and profile number shown). Black arrows show actual direction of drift between profiles, including drift around an anticyclonic eddy-like feature in mid to late May.

Table 5 summarizes the characteristics of the upper water column to a depth of 26m (the depth of the shallowest mixed layer) based on the vertical profiles of potential temperature, salinity and potential density shown in Figure 71, taken before (19 May, profile 1106), during (22 May, profile 1118) and after (04 June, profile 1168) the event. The profile from 22 May shows a temperature maximum of -0.65°C at 33m (7m below the base of the mixed layer), which is 1°C above the freezing point at this depth. As for the previous case study, these profiles and the corresponding T-S scatter plot and plots of potential density (in Figures 72 and 73 respectively) show that the mixed layer became significantly warmer, fresher and less dense during entrainment in comparison to before and after. The mixed layer again became shallower during the time of entrainment. The magnitude of the changes to the upper 26m between the three profiles is more clearly shown in Figure 74 and in Table 6. During the three day period from 19 to 22 May, the mixed layer potential temperature increased by ~0.03°C, salinity decreased by 0.36psu and potential density also decreased by ~0.29kgm^{-3}. Profiles of potential temperature,

salinity and potential density over a 24 hour period leading up to the 22 May entrainment profile are shown in Figure 75. Analysis of these profiles reveals almost no temperature change over 24 hours, suggesting that the mixed layer was already warmer (as well as fresher and lighter) a day before the profile made on 22 May during the event. This points to difficulty in precisely identifying the date and time of an entrainment event with the available data as well as suggesting that heat entrainment into the mixed layer may occur in the form of pulses or small fluctuation on time scales of hours, rather than in the form of a continuous and steadily increasing heat source.

Profile Number	**Date**	**Mixed Layer Depth MLD (m)**	**Mean Potential Temp $\overline{\theta}$ (°C)**	**Mean Salinity $\overline{S}$ (psu)**	**Mean Potential Density $\overline{\sigma_\theta}$ (kgm^{-3})**	**Heat Content Q (Jm^{-2})**	**Ice Melt (cm)**	**Ice Floe Speed (ms^{-1})**
1106	19 May 2006	29	-1.5444	28.4471	22.9476	0	0	0.0948
1118	22 May 2006	26	-1.5159	28.0880	22.6566	477920	0.1700	0.0483
1168	04 Jun 2006	32	-1.5424	28.5816	23.0569	161590	0.0600	0.0170

Table 5. ITP1 summary of mixed layer characteristics for profiles of interest before (19 May, profile 1106), during (22 May, profile 1118) and after (04 June, profile 1168) entrainment.

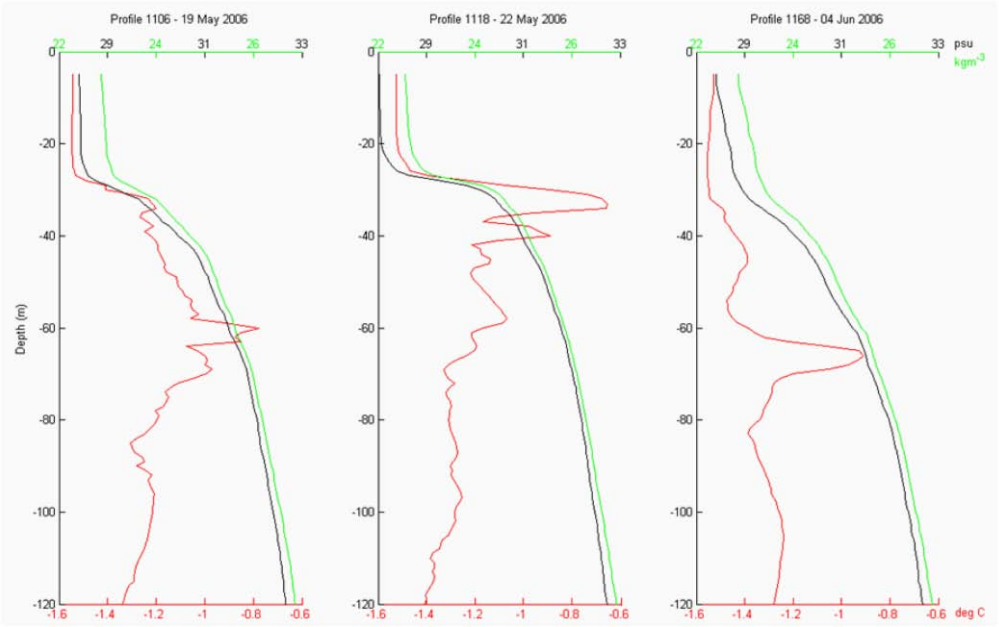

Figure 71. ITP1 vertical profiles of potential temperature (red), salinity (black) and potential density (green) for profiles of interest before (19 May, profile 1106 - left), during (22 May, profile 1118 - middle) and after (04 June, profile 1168 - right) entrainment.

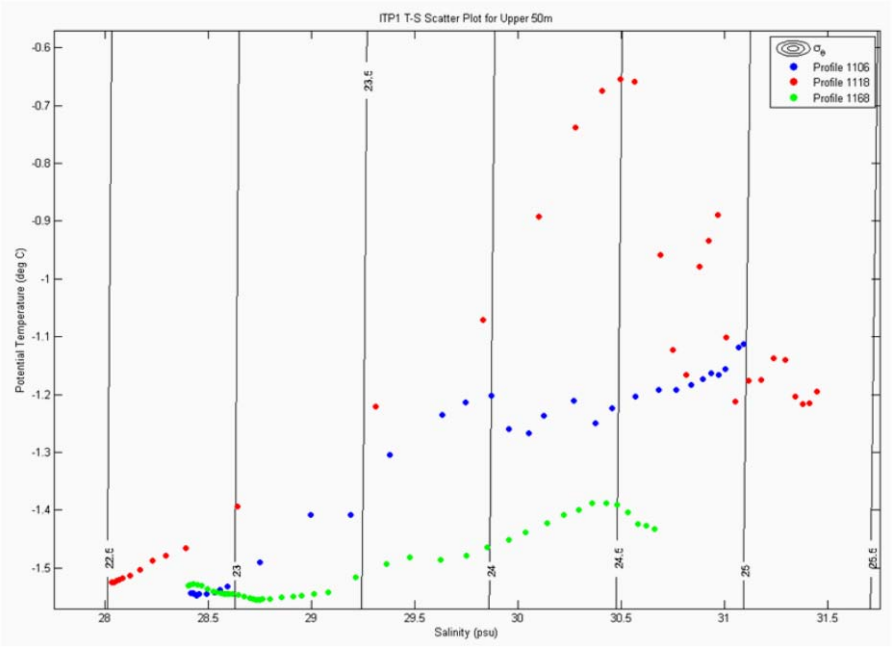

Figure 72. ITP1 scatter plot for upper 50m with contours of potential density for profiles of interest before (19 May, profile 1106 - blue), during (22 May, profile 1118 - red) and after (04 June, profile 1168 - green) entrainment.

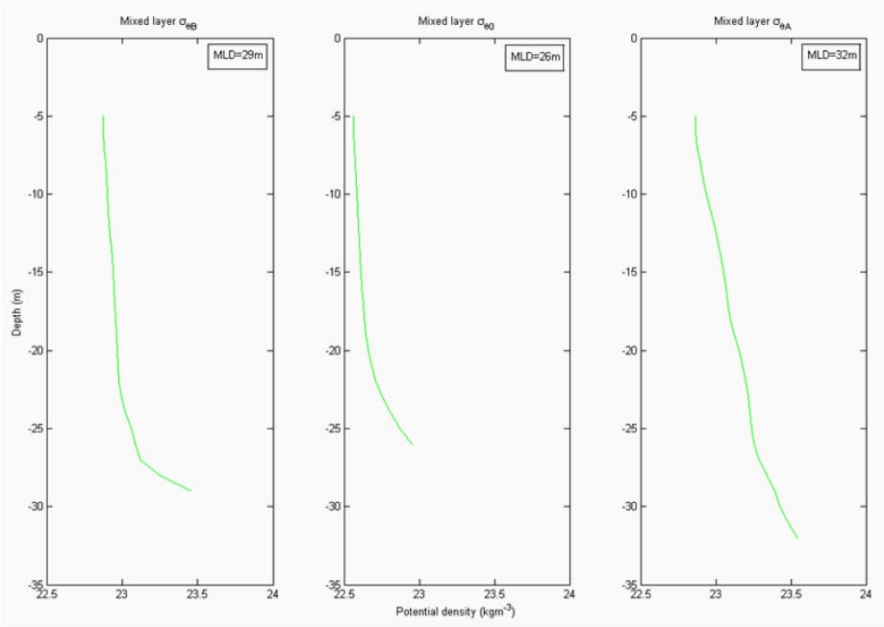

Figure 73. ITP1 mixed layer potential density for profiles of interest before (19 May, profile 1106 - left), during (22 May, profile 1118 - middle) and after (04 June, profile 1168 - right) entrainment.

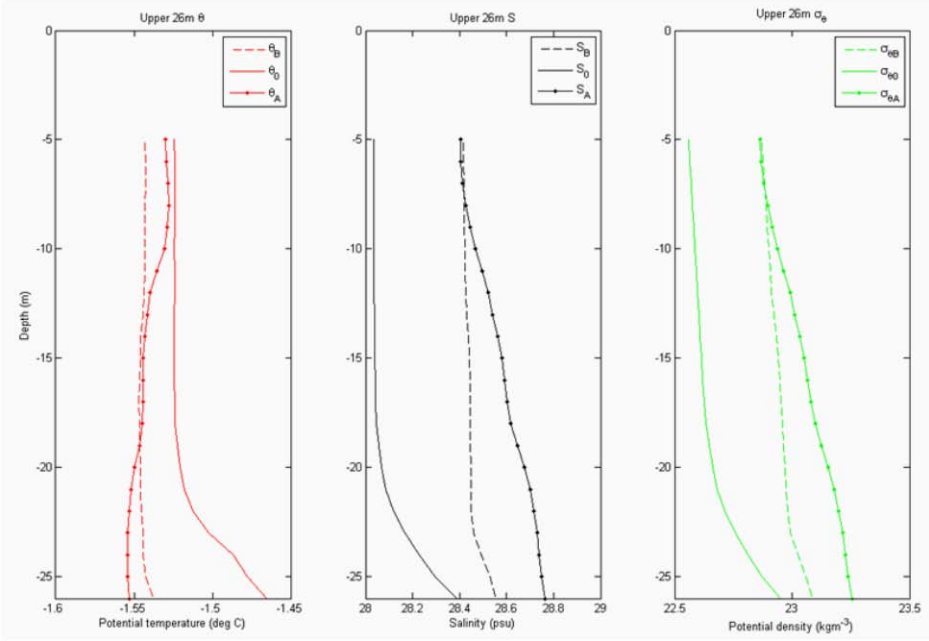

Figure 74. ITP1 upper 26m potential temperature (left), salinity (middle) and potential density (right) for profiles before (19 May, profile 1106 - subscript B), during (22 May, profile 1118 - subscript 0) and after (04 June, profile 1168 - subscript A) entrainment.

Parameter	During minus before entrainment (profile 1118-profile 1106)	After minus during entrainment (profile 1168-profile 1118)
Potential Temperature $\overline{\theta}$ (°C)	+0.0285	-0.0265
Salinity $\overline{S}$ (psu)	-0.3591	+0.4936
Potential Density $\overline{\sigma_\theta}$ (kgm^{-3})	-0.2910	+0.4003
Heat Content Q (Jm^{-2})	+477920	-316330

Table 6. ITP1 differences in upper 26m characteristics from profiles made before (19 May, profile 1106), during (22 May, profile 1118) and after (04 June, profile 1168) entrainment.

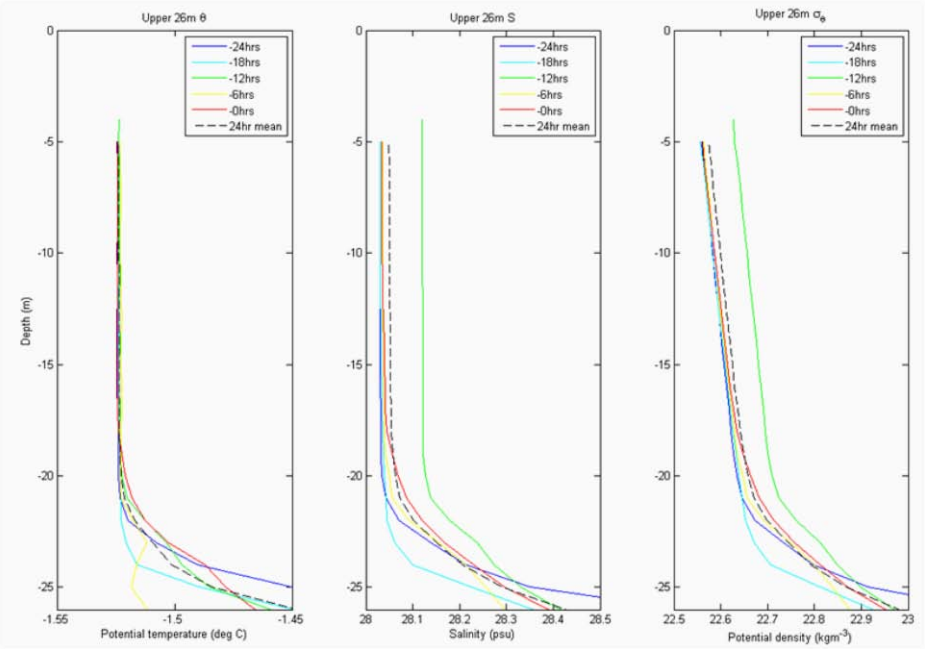

Figure 75. ITP1 upper 26m potential temperature (left), salinity (middle) and potential density (right) for profiles made 24 hours leading up to entrainment. Profile 1118 (22 May) is shown in red and 24 hour mean is shown as dashed black line.

In order to determine whether the identified entrainment event was significant enough to cause bottom melting, ocean heat flux and heat content was determined using the same methods as for the previous case study. Near surface ocean heat fluxes for ITP1 are shown in Figure 76. Maximum heat fluxes are once again seen in the summer months due to the effects of solar radiation, and much smaller heat fluxes correspond to the period of total darkness and maximum ice cover during winter. Analysis of the values of ocean heat flux during mid to late May indicate that several small peaks of up to

3.5Wm^{-2}, which is five times the May 2006 monthly mean of 0.7Wm^{-2}, occurred around the time of entrainment. The integration of heat flux with respect to time for the period 19 to 22 May results in an estimated near surface heat content of 4.27x10^{5}Jm^{-2} and a corresponding bottom melt of 0.16cm.

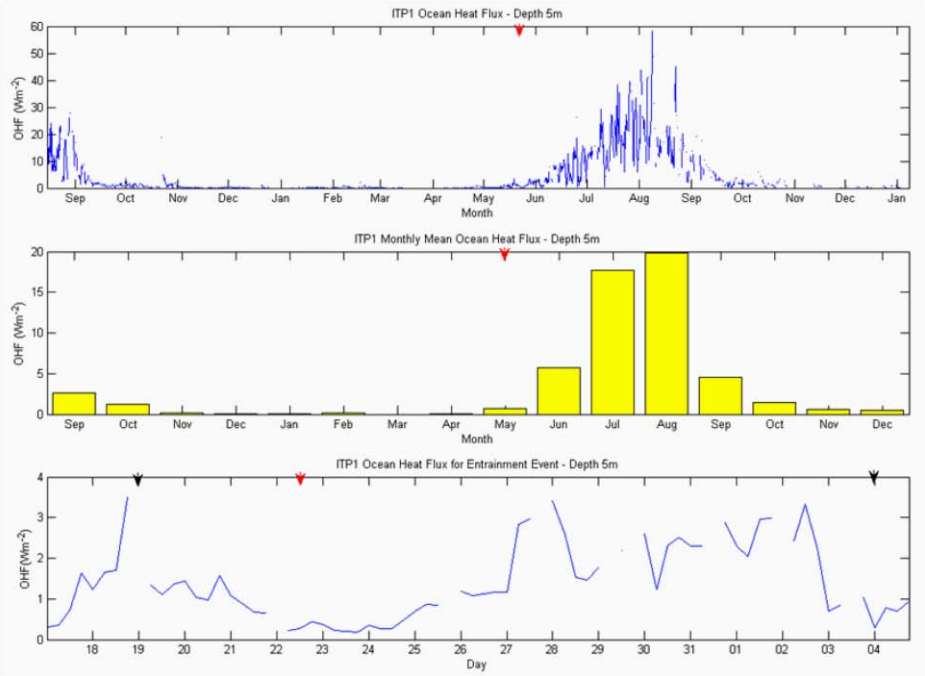

Figure 76. ITP1 ocean heat flux at depth 5m for entire time series (top), monthly mean ocean heat flux at depth 5m (middle) and ocean heat flux at depth 5m for period of focus during May/June (bottom). Red arrows show period of entrainment in for period of entrainment event (bottom). Red arrows show period of entrainment in May 2006.

From 19 May (before entrainment) to 22 May (during entrainment), heat content per unit area over the depth of the shallowest mixed layer increased by 4.78x10^{5}Jm^{-2}. Calculations of heat content over the same depth for profiles made at six hourly intervals over a period of several days either side of 19 May show that heat penetrated well above the base of the mixed layer and also confirm the presence of small fluctuations or pulses in magnitude and depth throughout this time. Based on the mixed layer heat content on 19 May, 0.17cm of bottom melt was estimated to occur at the time of the profile. In this

case the two methods of estimating bottom melt yield a very similar result in contrast to the previous case where the ice melt estimated with the first method was eight times lower than that using the second method. This suggests that mixing within the mixed layer might have been more efficient and therefore more heat reached the underside of the ice, and relatively less heat remained in the lower part of the mixed layer.

ITP1 mean salinity over the upper 26m is shown in Figure 77. Given that there was significant freshening of the mixed layer evident during entrainment, a salinity mass-balance calculation was once again made to determine the amount of water that would need to be replaced with melt water of 6psu to reduce salinity from the before entrainment value of 28.45psu to the during entrainment value of 28.09psu. This calculation yields a result of 0.63m, which is much greater than the amount of melt estimated using and heat flux and heat content values, and also twice the magnitude of the results obtained in the first case study.

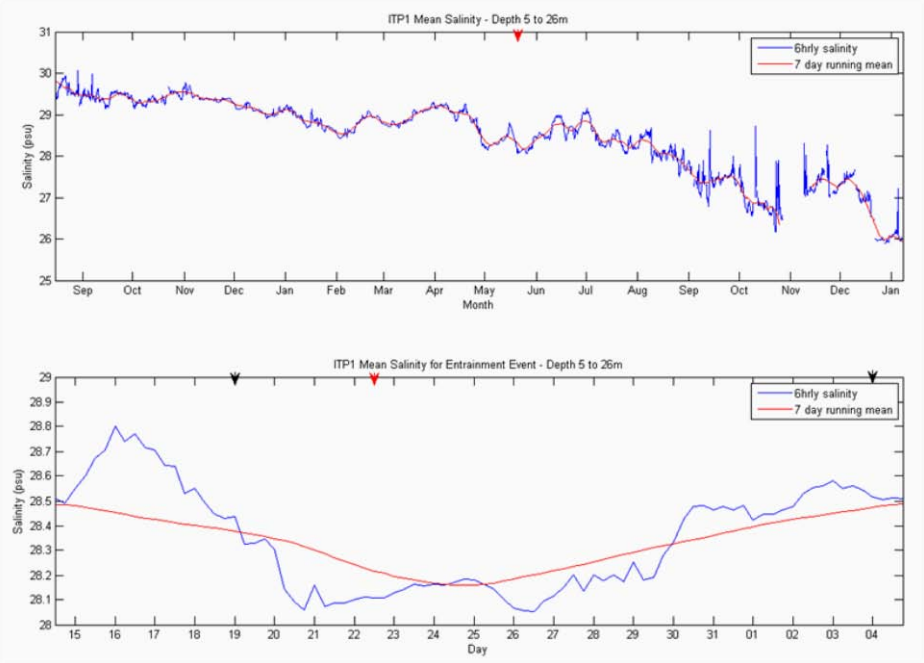

Figure 77. ITP1 upper 26m mean salinity for entire time series (top) and upper 26m mean salinity during period of interest in May/June 2006. Red arrows show period of entrainment in May 2006.

ITP1 was co-located with IMB2005C. Unfortunately most of the sensors on IMB2005C failed shortly after deployment, and the only data available from this instrument are atmospheric (D. Perovich, CRREL, personal communication, 2010). Given that air pressure and air temperature may provide some insight to the meteorological factors affecting the ice floe, these data are presented in Figure 78 for the period corresponding to the ITP1 entrainment event. Analysis of the mean sea level pressure time series for this period reveals that the ice floe was most likely under the influence of a high pressure system during the time of maximum entrainment, before being subjected to the passage of several storm systems in late May near the end of the event. Air temperature remained below freezing for most of the time, although these temperatures were much warmer than those observed during the December case study, which demonstrates the influence of solar heating near the onset of summer.

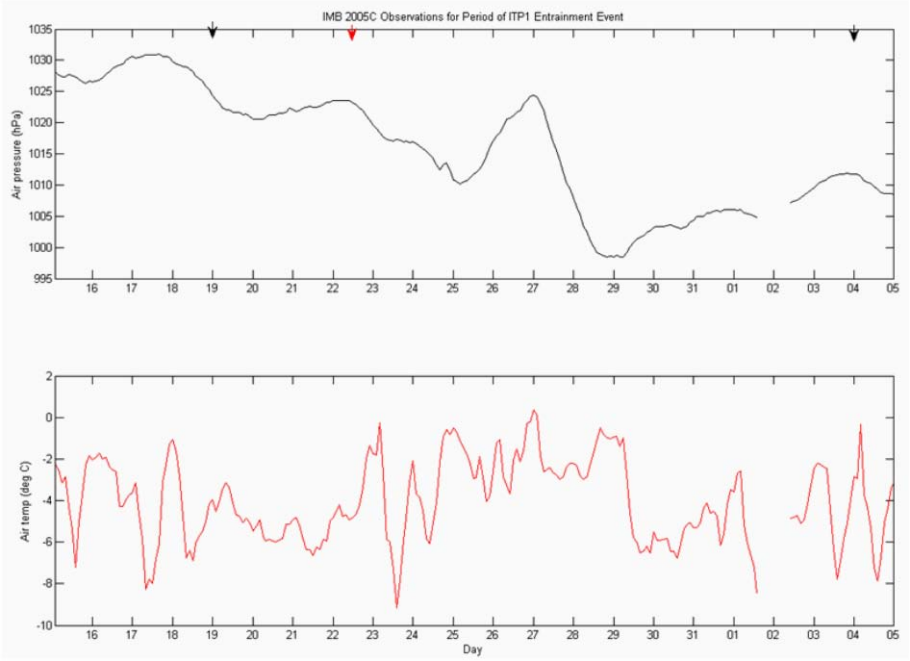

Figure 78. IMB2005C air pressure (black) and air temperature (red) for the period 15 May to 05 Jun 2006. Arrows indicate positions corresponding to ITP1 profiles of interest before (19 May, profile 1106 - black), during (22 May, profile 1118 -red) and after (04 June, profile 1168 - black) entrainment.

V. DISCUSSION OF RESULTS

Results and analyses of NPS model output and observations from co-located ITPs and IMBs in the central and western Arctic Ocean were presented in the previous chapters, with the primary purpose of determining whether the entrainment of heat from oceanic sources might locally contribute to sea ice melt, especially in winter. The following discussion attempts a synthesis of the numerical model and observational results, a comparison of the results of the current study to previous studies, and the identification of similarities to processes occurring in the Southern Ocean.

A. SYNTHESIS OF NPS MODEL AND OBSERVATIONAL RESULTS

Direct comparisons between the NPS model and observational results cannot be easily made due to the different methods used (i.e., Lagrangian data versus Eulerian model output) and the scales those results represent. Nor can the observations be used as a means of model verification, as the time periods of each available dataset do not overlap. The combination of these results does, however, allow a synthesis of small and large scale oceanic and sea ice processes that occur in the central and western Arctic Ocean.

Results from the 9km NPS model provide a good large scale overview of oceanic and sea ice conditions in the Arctic Ocean spanning a period of almost three decades. In comparison, observations from co-located ITPs and IMBs provide a higher resolution representation of important physical parameters over shorter time periods and smaller areas within the model domain. The analyses of annual variations in modeled winter monthly mean ice thickness, floe speed and upper ocean (averaged from 0 to 15m depth) salinity over a small region of the Arctic Ocean that corresponds to a similar area as that covered by the drifting instruments indicate a definite trend towards significantly decreased ice thickness, increased floe speed and slightly increased upper ocean salinity from 1993 to 2004.

Winter ice thickness observations from IMBs were sparse due to the frequent failure of the above ice acoustic sounder. However, assuming that ice draft constitutes 89% of total thickness (Rothrock and Wensnahan 2007), approximate thickness can be determined from IMB ice bottom measurements. Estimates of ice thickness from IMB observations for the winters of 2005/6, 2006/7 and 2007/8 (from IMBs 2005B and 2005C) suggest ice thickness of similar magnitude to that seen in the last few years of the model results in the western Arctic. For example, winter 2007/8 observations from IMB2006C (Figure 50) show that winter ice thickness reached a minimum winter mean of approximately 2m, and model results for the same region of the Beaufort Sea in winter 2002 (Figure 20) indicate a mean winter minimum ice thickness of similar magnitude. Observed ice thicknesses for 2005 to 2008 are therefore not suggestive of significantly thinner winter sea ice than seen in the numerical model results ending in 2004.

In addition, there is no evidence in the analyses of floe speed derived from western Arctic ITP positions (ITPs 1, 3 and 6) from 2005 to 2008 of the continuation of the trend towards higher winter floe speeds that are seen in the last decade of model results up until 2004 (Figure 21). The observed magnitudes of winter floe speed are once again comparable between the last few years of model results and those derived from the ITPs. Finally, winter time upper ocean salinities (average for 0 to 15m depth) determined from model results show a slight increasing trend in salinity up until 2004 (Figure 22), while ITP observations of salinity in the western Arctic (Figures 62 and 77) suggest that salinity decreased by up to 2psu from one winter to the next.

There are several possible reasons as to why the observations do not display a continuation of the trends shown in the last few years of model results. First of all, it may be unreasonable to expect to see similar trends in the model and observational results since the model results represent an Eulerian time series of ice drifting over a particular location in the Arctic, whilst the ITPs and IMBs are Lagrangian drifters that move with the thick multi-year floe to which they are tethered. Measurements of ice thickness and floe speed derived from ITP and IMB observations are biased due to the fact that the instruments are usually tethered to the thickest available ice floes in order to prolong their life and the period of observation. This bias towards thicker ice may also affect the

observed mixed layer salinity, which in winter strongly depends on the rate of ice formation and brine input. Thicker ice grows more slowly than thin ice in winter, therefore resulting in less brine rejection, which may explain the recent trend towards lower mixed layer salinities seen in the observations, as opposed to the increase seen in the later years of model results.

In order to assess the spatial and temporal distribution of mesoscale and small scale features such as eddies, which may facilitate the entrainment of heat into the mixed layer, EKE, currents and relative vorticity were analyzed from mean daily and monthly 9km and 2.3km model output for two days in winter 1983. Results from the 9km model suggest a relatively low energy upper ocean environment in December and May, whilst the 2.3km model was able to resolve much smaller scales (within the Rossby radius of deformation) and more numerous features, particularly over the Chukchi Cap, the Northwind Ridge and in the southern and central Beaufort Sea. The existence of many regions of negative relative vorticity at both resolutions at depths of 20 to 26m is suggestive of anticyclonic rotation and the potential for dynamical processes to facilitate the entrainment of warm water into the mixed layer.

Although the ITP and IMB winter case studies were for more recent years than the model results, closer analyses of their drift trajectories provide evidence for the existence of frequent anticyclonic meanders or eddies typically associated with some warming and freshening of the mixed layer. A more in-depth analysis of several of these features showed their potential to cause the bottom ablation of sea ice up to tens of cm during winter. Our hypothesis that the warming and freshening of the mixed layer and subsequent bottom melt caused by the physical process leading to the entrainment of warm water into the mixed layer by small or mesoscale features like those identified in the model results and in the observations has not been the focus of many previous studies, especially those using ITP and IMB observations. A possible explanation for this it that few observations from ice-tethered instruments are available for the areas of high eddy activity (such as the Chukchi Borderland and southern Beaufort Sea), as shown in the

model results. This once again may to be due to the fact that the sea ice has been generally thinner over these regions in recent times, which is not desirable for the deployment of ice-tethered instruments, as it can significantly reduce their lifetime.

B. COMPARISON TO PREVIOUS STUDIES

1. Model Results

The dramatic decline in sea ice thickness seen in the last decade in the 9km NPS model results supports the findings of several recent studies based on observations and numerical modeling (e.g., Kwok et al. 2009; Kwok and Rothrock 2009; Maslowski et al. 2007; Perovich et al. 2008). The recent decrease in sea ice thickness is difficult to attribute to any one particular factor in isolation, as it is likely due to a combination of atmospheric and oceanic feedback processes. The corresponding increase in the mean speed of the ice floe seen in the NPS model results from 1993 onwards is consistent with the results of Rampal et al. (2009), whose analyses of buoy data indicated that sea ice mean speed has substantially increased in recent decades. The increase in floe speed may be the result of sea ice kinematics, as thinner sea ice has decreased mechanical strength, thereby initiating a positive feedback loop of increased deformation, lead formation, open water and first year sea ice, which in turn results in further acceleration of sea ice (Rampal et al. 2009).

Any clear trends in western and central Arctic upper ocean salinity (averaged from 0 to 15m depth) are difficult to determine from the model results, possibly due to the fact that salinity over that depth range is influenced by mixed layer dynamics (vertical mixing, ice growth and melt, entrainment, etc.), changes to large scale circulation patterns, lateral transport processes, river runoff and precipitation rates. Similarly, other than the seasonal transition that was particularly apparent in areas of river runoff, model results for FWC over the upper 400m do not appear to correspond directly with changes in any of the other modeled parameters, or to the results of previous studies. For example, there is no clear evidence in the model results through 2004 of a shift towards the recent dramatic increase in FWC in the Beaufort Gyre reported by McPhee et al. (2009) and by Proshutinsky et al. (2009) based on observations.

The comparison of 9km and 18km ice-ocean models by Maslowski and Lipscomb (2003) showed that the higher resolution model improved the representation of sea ice features. Also, Maslowski et al. (2008) concluded that doubling the horizontal resolution increased the mean EKE by at least an order of magnitude in some pan-Arctic regions. Our study compares available output from the 9km and 2.3km NPS models for the first time. As noted in the aforementioned research, a significant increase in upper ocean EKE is evident in the eddy resolving model results, where much smaller scale and more numerous features are identified in the Beaufort Sea in comparison to the 9km model. These small scale oceanic features, many of which are associated with eddies, are prominent in the vicinity of the winter mixed layer depth. The fact that such features are not readily detectable at the surface in either EKE or SSHA may be due to the dominant effects of ice-ocean friction and atmospheric forcing. The potential existence of numerous eddies in the western Arctic has also been supported by other numerical modeling studies including those by Zhang et al. (1999), Timmermans et al. (2008) and Maslowski and Clement Kinney (2010). However, improved estimates of their quantitative impact on sea ice cover requires additional observations (e.g., of turbulent fluxes across the bottom of the mixed layer) and expanded spatial coverage to regions of high eddy activity as well as full eddy resolving, ice and ocean model output.

2. Observational Results

Observations from co-located instruments in the central Arctic (ITP10 and IMB2007H) and the western Arctic (ITP6 and IMB2006C) were analyzed to demonstrate the seasonal evolution of the mixed layer in these regions. The central Arctic case shows a classic seasonal polar ocean cycle, with evidence of near surface warming and a relatively shallow surface mixed layer in summer, followed by continuous cooling and deepening of the mixed layer throughout autumn and winter. In contrast, the western Arctic case shows much more variation in the upper ocean during the seasonal transition. In general, the seasonal variations in the mixed layer seen in ITP observations in the western Arctic, along with the annual cycle of sea ice growth and melt evident from IMB observations, are consistent with the findings of Toole et al. (2010). However, Toole et

al. (2010) did not investigate the possibility of warm water entrainment into the mixed layer by mesoscale eddies as a possible cause of the highly variable mixed layer depth observed in the winter ITP measurements.

The formation of the NSTM in summer and its subsequent deepening in autumn reported by Jackson et al. (2010) is also evident in the observations. At seasonal timescales, the limited observational results from the central Beaufort Sea suggest that oceanic processes may have little impact on sea ice. However, the general assertion that stratification barriers isolate surface waters, thereby inhibiting the entrainment of warm water into the mixed layer (Toole et al. 2010), is not necessarily true, especially in regions of higher eddy activity. Although strong stratification separates the mixed layer from the influence of relatively warm water masses below, smaller scale and highly energetic oceanic processes occurring on time scales of hours to months, such as eddies, have the potential to entrain heat into the mixed layer, causing bottom ablation or reducing sea ice growth.

The possibility of heat entrainment into the mixed layer by warm eddies was discussed in the winter case studies based on measurements from ITP3 and IMB2005B (December) and ITP1 and IMB2005C (May). The existence of anticyclonic eddies in the same ITP data was previously reported by Toole et al. (2006) and Timmermans et al. (2008). Their conclusion that the vast majority of these features were deeper and cold core, however, may be argued given that the results of this study show that anticyclonic drift patterns (i.e., implying eddy effects all the way to the surface) in many instances coincide with local temperature maxima at a depth range near the bottom of the mixed layer.

The analyses of winter time entrainment events identified from ITP and IMB observations to our knowledge have not been conducted previously. Close investigation of vertical profiles of temperature, salinity, and potential density clearly show that the mixed layer becomes shallower, warmer, fresher and less dense during the identified events of anticyclonic eddy activity. Since the regime of the Arctic Ocean during winter is typically associated with ice production, which results in brine rejection and increased mixed layer salinity, the most likely explanation for the observed localized freshening of

the mixed layer during the winter is ice melt (or reduction of growth) due to warm oceanic sources. Given that no sunlight is available in the Arctic during winter, coupled with the fact that IMB observations of air temperatures were well below freezing, rules out atmospheric forcing as a source of heat for either surface ice melt or for upper ocean warming. Additionally, satellite imagery shows that sea ice concentrations were very high over the regions of interest at the times of entrainment. The assertion of Perovich et al. (2008) that the primary mechanism for increasing oceanic heat and subsequently producing basal ice melt in summer is the ice-albedo feedback effect, is therefore not a high probability during winter. Furthermore, the near surface advection of radiatively heated water from ice-free Arctic areas (suggested by Toole et al. 2010) is also unlikely to be a source of bottom melt in winter as all the heat must be removed from the mixed layer to form sea ice. Both of these arguments are true during the summer melt season, when solar radiation is the dominant source of upper ocean heating and sea ice melt, but are not relevant during winter.

The potential of the identified warm core features to cause basal ice melting was further demonstrated through the analyses of upper ocean heat fluxes, heat content and salinity changes. The calculated winter heat fluxes at the ice-ocean interface from ITP Lagrangian data are relatively small, although at $2Wm^{-2}$ and $3.5Wm^{-2}$ (for ITPs 3 and 1 respectively) during times of entrainment, they are an order of magnitude larger than the winter average value of heat flux of $0.2Wm^{-2}$ estimated by Shaw et al. (2009) over the Canada Basin during SHEBA. The determination of heat content over the depth of the mixed layer based on individual profiles demonstrates that in many instances throughout the period of identified entrainment, heat penetrated well above the base of the mixed layer. However, the amount of ice melt estimated from heat content using two different methods (heat content calculated over the depth of the mixed layer and heat content found by integrating near surface heat flux over a period of several days) yielded very small magnitudes of sea ice melt. This may be attributed to the fact that the vertical profiles were made at six hourly intervals and therefore only give a ‘snapshot’ of the instantaneous heat content and melt occurring at a particular moment in time, making it difficult to estimate a true value of cumulative ice melt. Furthermore, in a scenario of ice

melt, positive upward heat flux and small temperature increases may be partially negated by the downward mixing of water at freezing temperature. Finally, significantly larger estimates (of order tens of cm) of basal melting were estimated using a volume mass-balance calculation similar to that of Toole et al. (2010). Given the aforementioned issues with estimating ice melt from heat fluxes and heat content, changes to mixed layer salinity may be a better indicator of the time-integrated ice melt caused by oceanic forcing in a regime of high eddy activity and heat sources stored below the mixed layer.

C. COMPARISON TO PROCESSES IN THE SOUTHERN OCEAN

A secondary aim of this study was to determine whether the current trajectory of sea ice decline being observed in the Arctic Ocean is partially the result of oceanic processes analogous to those occurring in the Southern Ocean. In a regime of persistently cold surface air temperatures and thick insulating snow cover, oceanic heat has long been recognized as the primary mechanism for melting sea ice in the Southern Ocean (Allison 1979; Gordon et al. 1984; McPhee et al. 1999), where sea ice is predominantly seasonal.

One of the most striking differences between the Arctic and Southern Oceans is the existence of the CHL in the Arctic Ocean, which inhibits the upward entrainment of warm water masses of Atlantic origin due to a strong stratification barrier. This feature in itself is evidence enough to suggest that the ability of deeper ocean heat to penetrate into the mixed layer and reach the underside of the ice on such large scales as those seen in the Southern Ocean is unlikely. However, the retreat of the CHL is possible, and there is evidence of this occurring in the eastern Arctic during the 1990s (Steele and Boyd 1998). It is likely that such a retreat had profound effects on the mass-balance of sea ice, at least on regional scales. Even in the absence of a retreat of the CHL, the results of this study show that oceanic features such as eddies in the Arctic Ocean can provide a mechanism for the entrainment of heat into the mixed layer as seen in the Southern Ocean (Gordon and Huber 1990; Murphy et al. 2010), but on smaller spatial scales. In a highly energetic eddying regime, such as the south-western Beaufort Sea and the Chukchi Borderland (Timmermans 2008; Maslowski and Clement Kinney 2010), the existence of numerous warm core features could result in significant cumulative effect of ice thickness reduction

on larger scales. As ocean temperatures and heat accumulation continue to increase under a regime of global warming and reduced summer sea ice cover, further evidence of bottom melting due to oceanic processes in the Arctic Ocean is expected.

Although it is an extreme example, the Southern Ocean's Weddell Polynya of the 1970s may have preconditioned the water column for the thinner ice cover that persisted for decades afterwards (McPhee 2003; Stanton and Shaw 2010). It is possible that as Arctic Ocean temperatures have increased during recent decades, the entrainment of heat into the mixed layer through eddies and other oceanic processes have also contributed to the ongoing regime of thinner ice cover that is now being observed. A positive ocean-ice feedback loop might thus be initiated, where relatively warm ocean water of increasing spatial coverage is entrained into the mixed layer via small and mesoscale processes such as eddies during winter, causing the growth reduction or bottom ablation of sea ice, which in turn results in thinner ice cover. This thinner ice is mechanically weaker, making it more vulnerable to deformation processes, and also moves faster, which may help further increase near surface heat fluxes, resulting in further thinning and thus closing the feedback loop. This ongoing positive feedback loop results in a cycle of continuously thinner sea ice cover in winter due to oceanic processes, which when subjected to the enhanced effects of summer solar heating and associated ice-albedo feedback, is likely to melt away completely, resulting in a regime of seasonal ice cover that is characteristic of the Southern Ocean.

THIS PAGE INTENTIONALLY LEFT BLANK

VI. CONCLUSIONS

The past six years have seen the six lowest Arctic Ocean summer sea ice extents since the beginning of the satellite era. Recent observations indicate a continuation of the dramatic decline, with Arctic sea ice reaching the third lowest extent in the satellite record in summer 2010. Although it is more difficult to quantify due to insufficient observations, it is thought that sea ice thickness and volume are declining at an even faster rate than ice extent, resulting in an alarming reduction in thick multi-year ice cover. The recent reduction in sea ice has seen a renewed interest in the Arctic region, and has raised environmental, economic, political and security concerns, in addition to claims for sovereignty and a scramble for territory. The development and implementation of new policies by Arctic nations is likely to see an increased military presence in the Arctic Ocean in the future.

There is unequivocal evidence that the earth is in a regime of global warming, which is being accelerated by anthropogenic influences. Natural cycles and modes of climate variability play a role in changing circulation patterns and sea ice cover, but the effects of increasing air and sea temperatures due to global warming cannot be ignored. Although sea ice is affected by a complex combination of contributing atmospheric and oceanic factors, the aim of this study was to better understand the role of oceanic forcing on sea ice variability. This was achieved through the analyses of numerical model output and observations from the western and central Arctic Ocean, and by making limited qualitative comparisons to processes occurring in the Southern Ocean. In order to determine the effect of oceanic processes affecting ice melt, we focused on the winter months, as atmospheric sources during this season can be excluded as a source of warming of the upper ocean and surface ice melt.

Results from the NPS coupled ice-ocean model show that a significant decline in western and central Arctic winter sea ice thickness occurred during the ten year period from 1994 to 2004, and that there was also an increase in ice floe speed throughout this time. Corresponding trends in upper ocean salinity and FWC were difficult to ascertain. The comparison of EKE from the eddy permitting (9km) and eddy resolving (2.3km)

models for winter 1983 indicate that the latter has the ability to resolve numerous small scale upper ocean features that are not evident in the former model results. The improvement in the representation of ocean eddies seen in the eddy resolving model results supports the hypothesis that such features may be quite common and they may contribute significant changes to the mass-balance of sea ice in the western Arctic.

The existence of warm oceanic features and their potential to entrain heat into the mixed layer was further quantified through the analyses of observations from co-located ITPs and IMBs. Warm eddies were identified as local temperature maxima in the upper ocean that coincided with anticyclonic meanders in the drift. The subsequent assessment of upper ocean heat fluxes, heat content and mixed layer salinity demonstrated the potential for the bottom ablation of sea ice (or reduction of growth) to occur during periods of entrainment of warm water into the mixed layer during winter.

The strong stratification of the Arctic Ocean's CHL means that the entrainment of warm water masses of Atlantic origin into the mixed layer continues to be limited. It is therefore unlikely that oceanic forcing in the Arctic Ocean will become the primary mechanism for sea ice melt as seen in the Southern Ocean unless there is a retreat of the CHL similar to that observed in the eastern Arctic in the 1990s (Steele and Boyd 1998). The results of this study do, however, suggest that shallow eddies may have significant impacts on mixing and the transfer of heat in the upper Arctic Ocean. They are potentially a mechanism for higher heat fluxes into the mixed layer, and can consequently result in the bottom ablation of sea ice similar to that seen in the Southern Ocean, just on smaller scales.

As Arctic sea ice continues to decline, a combination of several ongoing positive feedback loops make the ice increasingly vulnerable to further melt. During summer, the well documented ice-albedo feedback loop is the primary driver for sea ice melt. In contrast, during winter, sea ice concentrations are high and incoming solar radiation is significantly reduced to non-existent. It is during the winter months that oceanic processes may play a more prominent role in the ongoing cycle of melt or first-year ice growth reduction, due to a positive ocean-ice feedback loop. Through the combined effects of these atmospheric and oceanic processes, eventually a threshold will be reached

(if it has not been reached already), beyond which point the recovery of sea ice to the regime of thick multi-year ice seen in previous decades will become impossible. Even the presence of negative feedback loops (e.g., the tendency for thinner ice to grow faster, and the cloud-radiative feedback) are unlikely to be sufficient to counteract or reverse the effects of the positive feedback loops driving the continuing ice decline.

If the current trajectory of sea ice decline in the Arctic Ocean continues, seasonal ice cover similar to that seen in the Southern Ocean is therefore likely to become a reality in the near future. Despite the development of new oceanographic instruments and improvements in ice-ocean and climate modeling, the processes contributing to sea ice variability are not fully understood. A complex regime of environmental extremes, coupled with a sparse observing network in comparison to other world oceans make definitive predictions regarding the future of the world's ice-covered oceans difficult to achieve.

In 1915, Antarctic explorer Sir Ernest Shackleton and the crew of the *Endurance* became stranded in an ice-covered Weddell Sea. After spending six months crossing one of the most inhospitable and challenging continents on earth, Shackleton eventually led his entire crew of 28 men to safety. During this journey, he is famously quoted as saying 'Difficulties are just things to overcome, after all.' This sentiment remains true today, and only an ongoing commitment to the development and implementation of new technologies and a willingness to embrace new ideas will assist scientists to overcome the difficulties associated with making future predictions for the polar oceans and global climate, the fate of which remains uncertain at the present time.

THIS PAGE INTENTIONALLY LEFT BLANK

VII. RECOMMENDATIONS FOR FUTURE RESEARCH

A limiting factor in almost any field of research is the availability of data, and polar oceanography is no exception. With ongoing developments in in-situ instrumentation and data processing techniques as well as in numerical modeling, more observational data and improved model results will become available for the Arctic and Southern Oceans. These data will build on our current understanding of gaps and limitations and will provide further insights to the physical processes occurring in the polar regions. To that end, the following recommendations are made for future research.

A. NPS MODEL

The results of this study were limited by the availability of the NPS model output, which ceases at 2004 for the 9km model, and covers only the year 1983 for the 2.3km model thus far. The ongoing development of the model will result in more output becoming available, including recent years. Future studies should use the new model output to make direct comparisons to ITP and IMB observations, which in turn would provide a means of model verification. A more detailed comparison of the 9km and 2.3km model results spanning a longer period of time would also be useful in order to analyze and demonstrate gains in representation of seasonal, annual and decadal changes in both oceanic and sea ice processes. Additionally, further development of the model itself to include the ability to provide high resolution ocean and sea ice forecasts, rather than only hindcasts, would make it a much more useful operational tool for defense applications.

B. ITP AND IMB OBSERVATIONS

This research used only a portion of available ITP and IMB measurements, and concentrated on co-located pairs of instruments in the western and central Arctic. ITP data from completed missions and from active systems distributed throughout the Arctic Ocean are available, at various levels of post-processing. Future research could build on the results of this study by conducting further investigation into the oceanic processes affecting sea ice variability based on observations from stand-alone or co-located ITPs

and IMBs, possibly for different regions of the Arctic Ocean and for more recent periods. It would also be useful to compare the measurements from these instruments to observations from other in-situ instruments such as the Autonomous Ocean Flux Buoy (AOFB), which is used to directly measure turbulent fluxes in the upper ocean below the sea ice. Furthermore, the future development of instruments such as the AOFB to include the capability of measuring turbulent heat fluxes at the bottom of the mixed layer is needed to better quantify entrainment events, and would also aid in the improvement of ocean models.

C. SOUTHERN OCEAN MODELING AND OBSERVATIONS

The ability to make long term observations using instruments that are tethered to the ice floe in the Southern Ocean is hindered by the seasonality of the sea ice in this region. ITPs and IMBs have, however, been deployed for short periods in some of the regional seas surrounding Antarctica. The comparison of this limited available data with a high-resolution Southern Ocean numerical model would provide a quantitative measure of the importance of oceanic and sea ice processes and feedbacks analogous to those occurring in the Arctic Ocean.

APPENDIX A: ANALYSIS OF INERTIAL OSCILLATIONS FROM OBSERVATIONS

Inertial oscillations are often evident in the trajectories of ice floes under varying wind conditions (Wadhams 2002). In the Arctic Ocean they are characterized by anticyclonic meanders in drift that occur on relatively short inertial periods of ~12 hours near the pole. In order to determine whether inertial oscillations had significant influence on the drift trajectory (and therefore on other parameters such as ocean heat flux) of the ITPs and IMBs, high temporal resolution (1 to 3 hourly) positional data from these instruments were analyzed using methods summarized below. The results of this analysis from ITP1 and IMB2005B are presented below. In agreement with previous studies (e.g., Thorndike and Colony 1982), they show that during the winter months (December to May) inertial oscillations appear to play a negligible role in the drift trajectory of ice floes. This can partially be explained by high sea ice concentration during winter that may damp inertial motion.

A. ITP1 RESULTS

High resolution global positioning system (GPS) raw location data (Level 2 data) and six hourly profile data (Level 3 data) was obtained for ITP1 and interpolated onto a uniform two-hourly grid. A band pass filter was used to filter the horizontal components of velocity about the local coriolis parameter. The magnitude of the inertial oscillations and the difference in the horizontal velocity with and without the influence of these oscillations for the ITP1 time series are shown in Figure 79. Time series of two hourly horizontal velocities, inertial velocity and corresponding ocean heat fluxes for the May entrainment event discussed in Case Study 2 are shown in Figure 80. These results show that inertial oscillations are negligible during the winter months, and that they appear to have very little influence on estimated ocean heat fluxes.

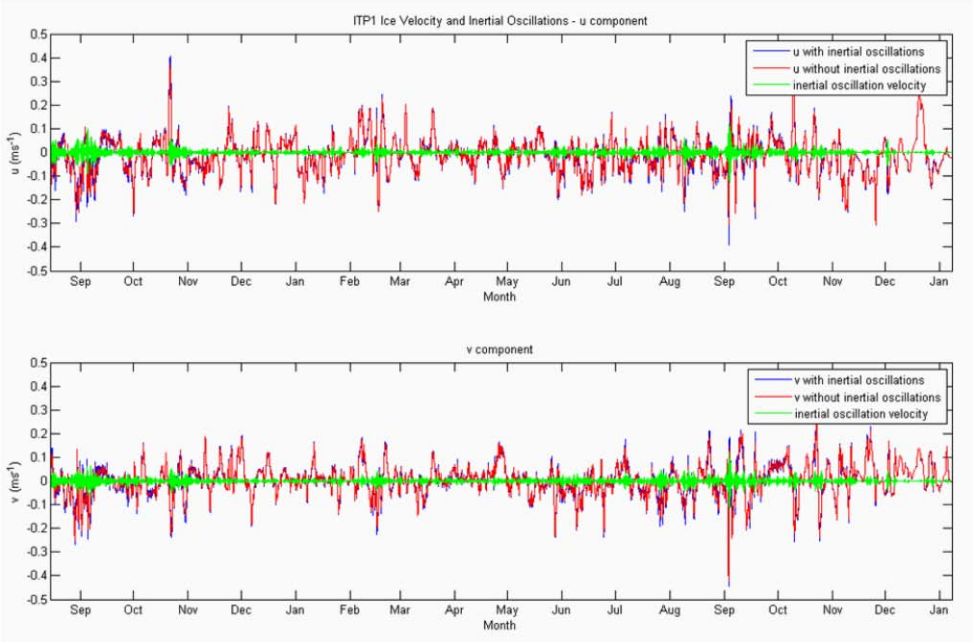

Figure 79. ITP1 two-hourly horizontal velocity and inertial oscillations for *u* component (top) and *v* component (bottom) for the period 16 August 2005 to 8 January 2007.

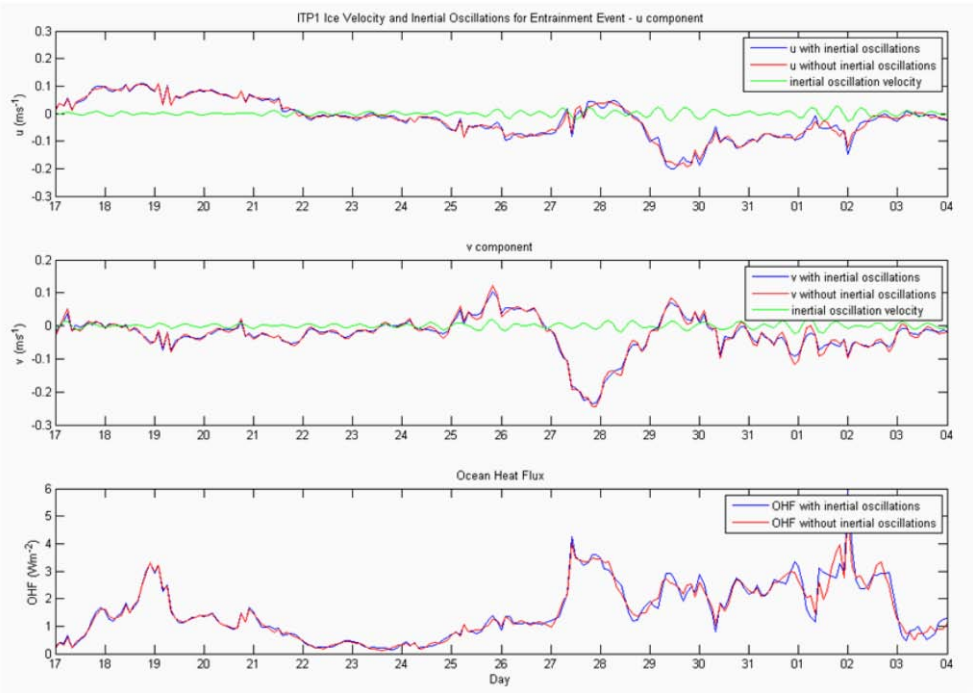

Figure 80. ITP1 two-hourly horizontal velocity and inertial oscillations for *u* component (top) and *v* component (middle) and corresponding ocean heat flux (bottom) for May 2006 entrainment period.

B. IMB2005B RESULTS

The following analysis of inertial oscillations using high resolution Argos position data from IMB2005B is based on methods described in Hutchings and Roberts (2010). Their buoy-track processing method was developed for drifters deployed as part of the Sea ice Experiment - Dynamic Nature of the Arctic (SEDNA) field campaign (see Hutchings et al. 2008). Initial hourly horizontal velocity components were determined by linearly interpolating between raw positional data. These velocities were then subjected to quality control by iteratively removing positions contributing to accelerations with a magnitude exceeding seven standard deviations outside the mean. New positions were then integrated from the resulting velocity set, filtered with a low-pass Butterworth filter to extract pulses with a period less than three hours, and a new velocity set was then interpolated from these positions. This iterative process was repeated until all outliers were removed from the dataset. The final velocity set was passed through a rotary wavelet filter to separate clockwise and anticlockwise motion in the semi-diurnal band (6 to 18 hour periods; Figures 81 and 82). This method negates the need to predetermine the frequency of motion as would be required using complex demodulation (e.g., Emery and Thomson 2004). Short period (~1/2 day) clockwise oscillations represent inertial oscillations. Other events (represented by high wavelet power) at longer time periods may represent storms or possibly ocean eddies. There is, however, no significant indication of high wavelet power at the time corresponding to the December 2005 entrainment event discussed in Case Study 1. Overall, these results once again show that inertial oscillations are significant during the summer months and negligible during winter relative to synoptic-scale sea ice drift.

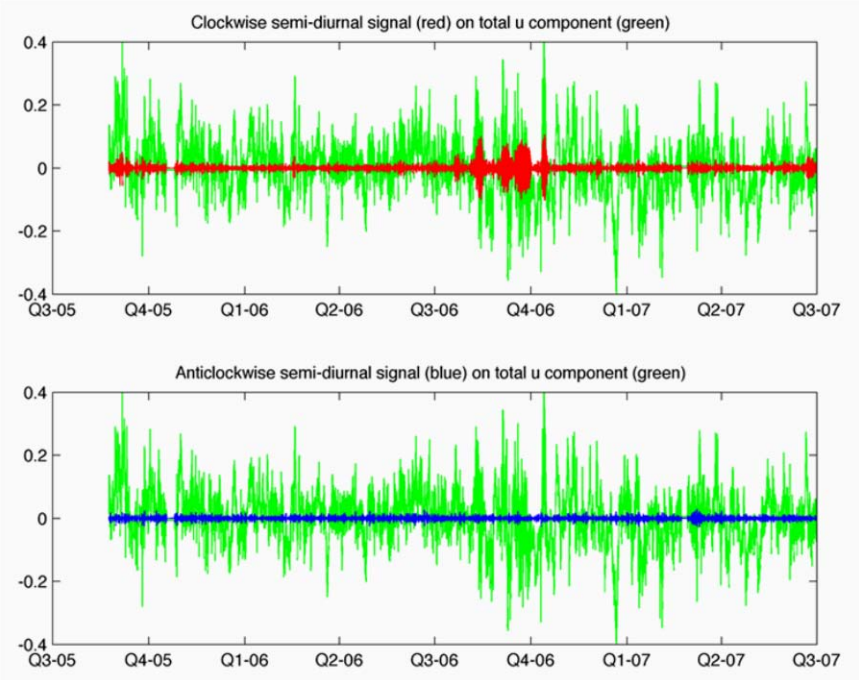

Figure 81. IMB2005B clockwise (top) and anticlockwise (bottom) semi-diurnal signal on total *u* component of horizontal velocity (ms^{-1}) for the period 23 August 2005 to 24 August 2007 (from methods described in Hutchings and Roberts 2010).

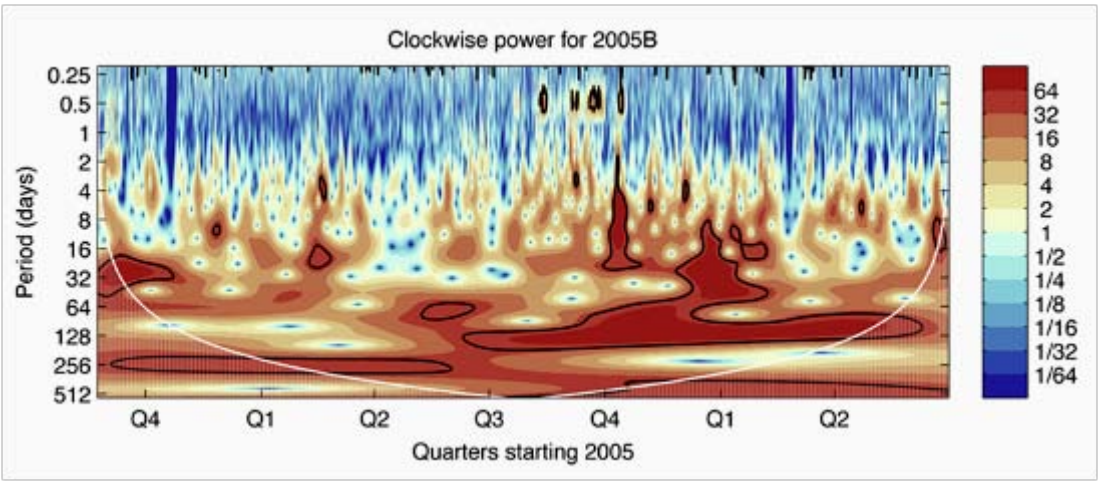

Figure 82. IMB2005B clockwise rotary wavelet power (m^2s^{-2}). Areas encircled by black contours are significant at the 95% confidence level above red noise and areas with white fill are influenced by edge effects (from methods described in Hutchings and Roberts 2010).

APPENDIX B: SUMMER (SEPTEMBER) MODEL RESULTS

Results from the 9km and 2.3km NPS models are presented for the summer month of September in order to provide a means of seasonal comparison to the winter results that are the main focus of this study.

A. DECADAL VARIATION IN SEA ICE AND OCEAN - SUMMER 9KM MODEL RESULTS

The decadal variation in summer sea ice thickness, upper ocean salinity and FWC from 9km monthly mean model results is shown for the western and central Arctic Ocean for September in Figures 83 to 85.

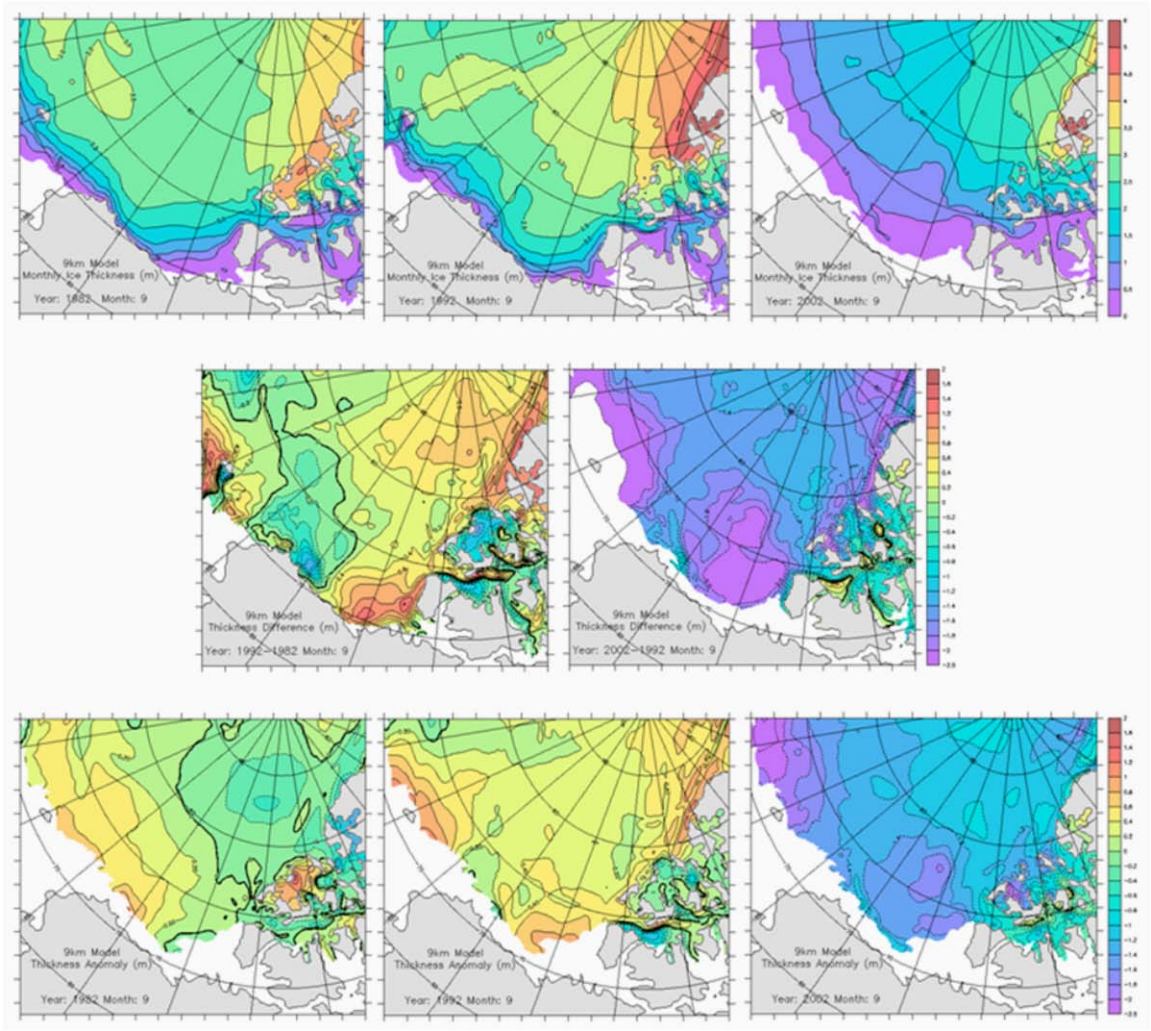

Figure 83. Decadal variation in monthly mean sea ice thickness for September for 9km model. Panels show mean ice thickness for September 1982 (top left), September 1992 (top center) and September 2002 (top right), thickness difference for September 1992 minus September 1982 (middle left) and for September 2002 minus September 1992 (middle right), and thickness anomaly (monthly mean minus 26 year September mean) for September 1982 (bottom left), September 1992 (bottom center) and September 2002 (bottom right).

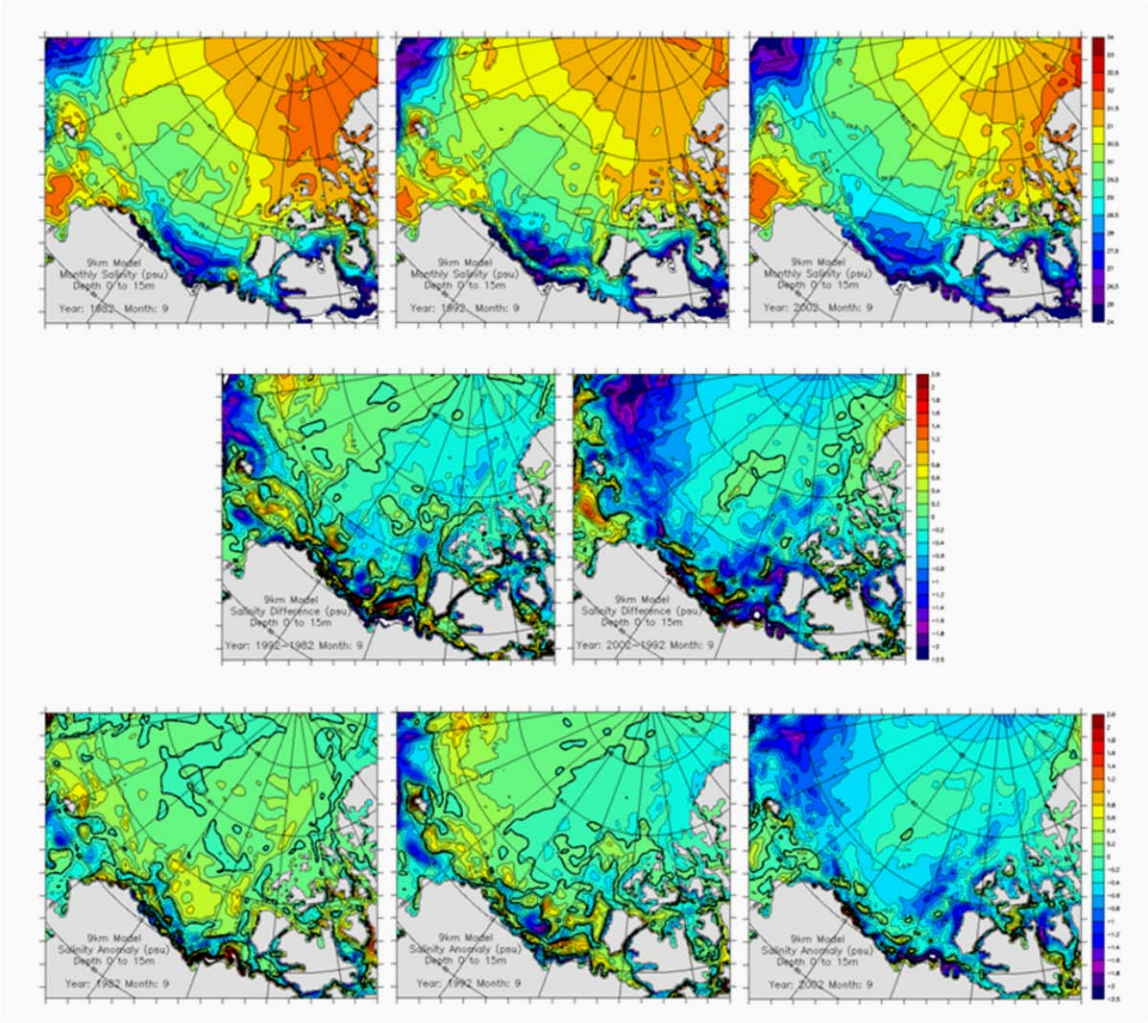

Figure 84. Decadal variation in monthly mean salinity (average 0 to 15m depth) for September for 9km model. Panels show mean salinity for September 1982 (top left), September 1992 (top center) and September 2002 (top right), salinity difference for September 1992 minus September 1982 (middle left) and for September 2002 minus September 1992 (middle right), and salinity anomaly (monthly mean minus 26 year September mean) for September 1982 (bottom left), September 1992 (bottom center) and September 2002 (bottom right).

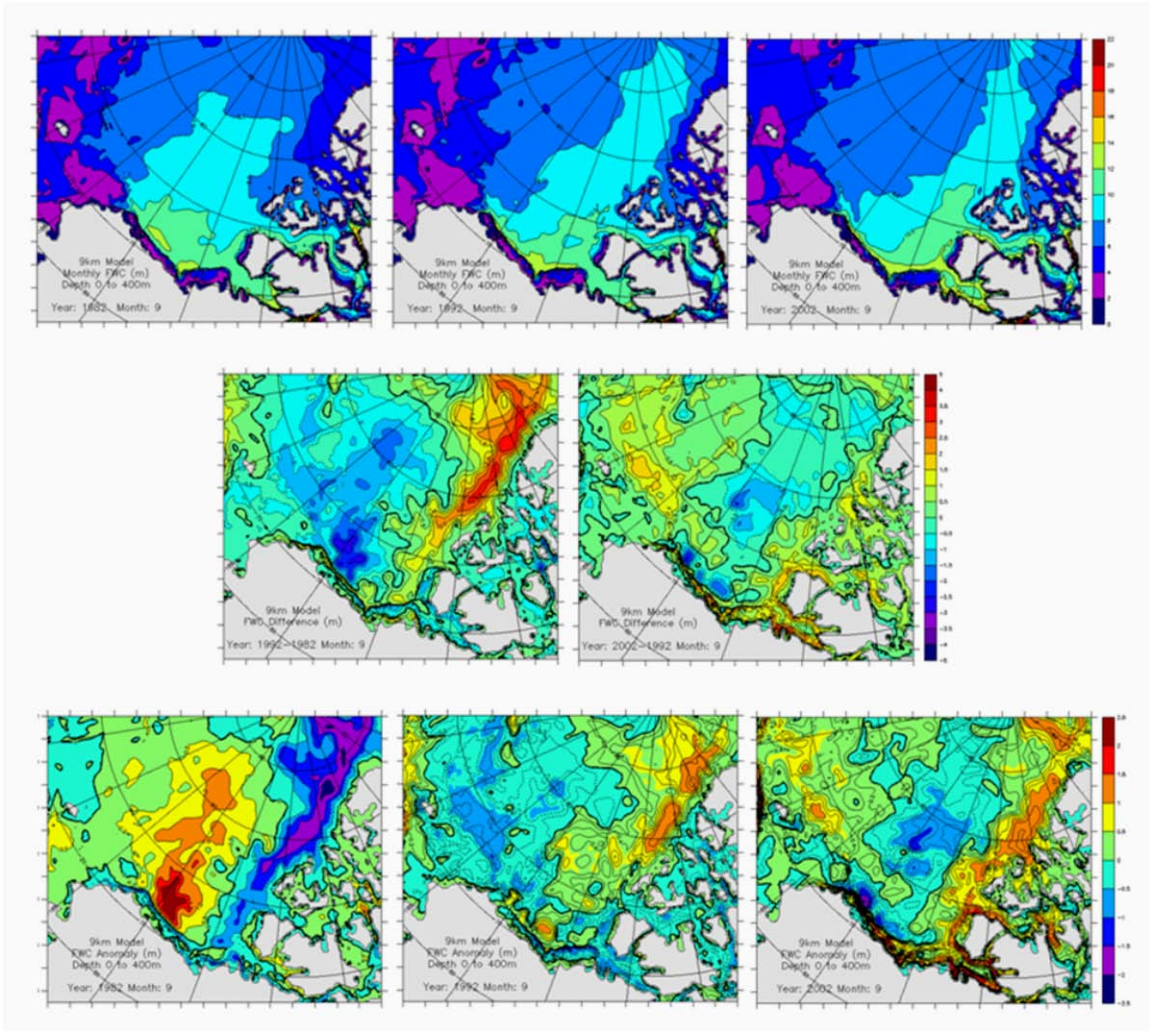

Figure 85. Decadal variation in monthly mean FWC (0 to 400m depth) for September for 9km model. Panels show mean FWC for September 1982 (top left), September 1992 (top center) and September 2002 (top right), FWC difference for September 1992 minus September 1982 (middle left) and for September 2002 minus September 1992 (middle right), and FWC anomaly (monthly mean minus 26 year September mean) for September 1982 (bottom left), September 1992 (bottom center) and September 2002 (bottom right).

B. SEPTEMBER 1983 - 9KM AND 2.3KM MODEL RESULTS

Daily mean modeled EKE for the 9km and 2.3km models for three depth ranges, and SSHA from the 9km model for 15 September 1983 is shown in Figure 86. Model results of EKE, currents and relative vorticity over a region of the Beaufort Sea for the same day are shown in Figures 87 and 88 for the 9km and 2.3km models respectively.

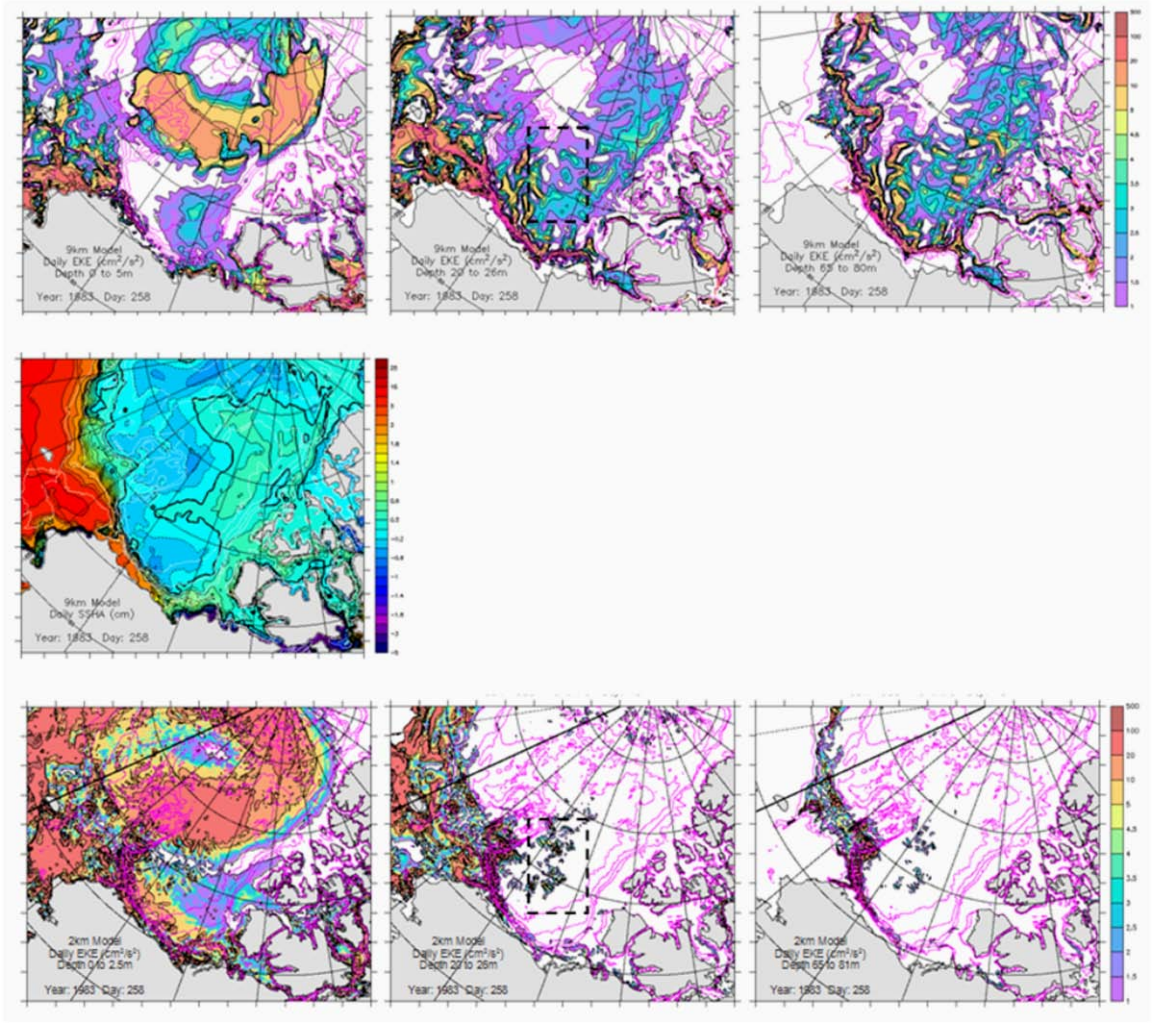

Figure 86. Daily mean model output for 15 September 1983 for 9km and 2.3 km models. Panels show 9km model results for EKE for depth 0 to 5m (top left), 20 to 26m (top center), 65 to 80m (top right) and SSHA (middle), and 2km model results for EKE for depth 0 to 2.5m (bottom left), 20 to 26m (bottom center) and 65 to 81m (bottom right). Dashed black box shows region of interest in the Beaufort Sea.

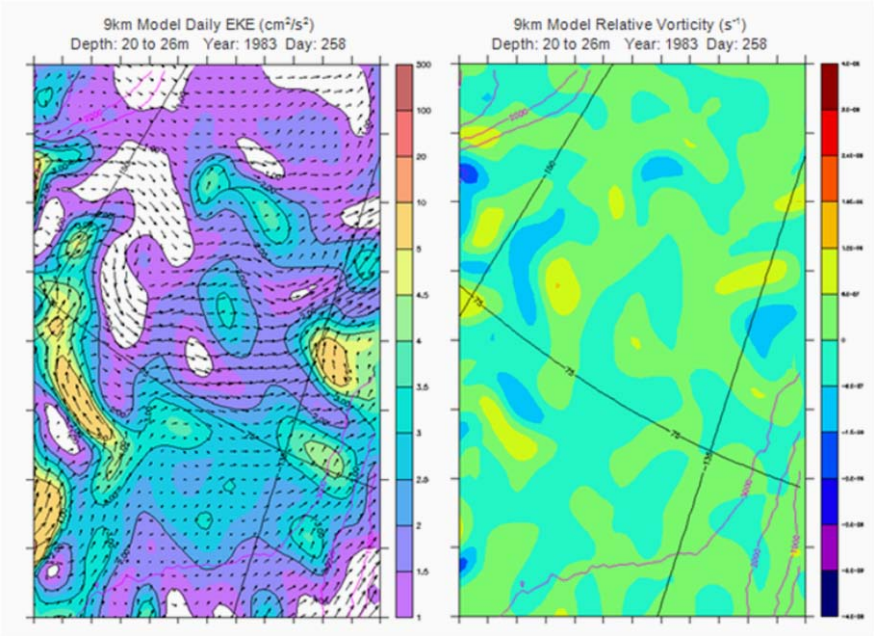

Figure 87. Daily mean model output for 15 September 1983 for the 9km model showing EKE with current vectors (left) and relative vorticity (right) at depth 20 to 26m for domain in Beaufort Sea shown by dashed black box in Figure 86.

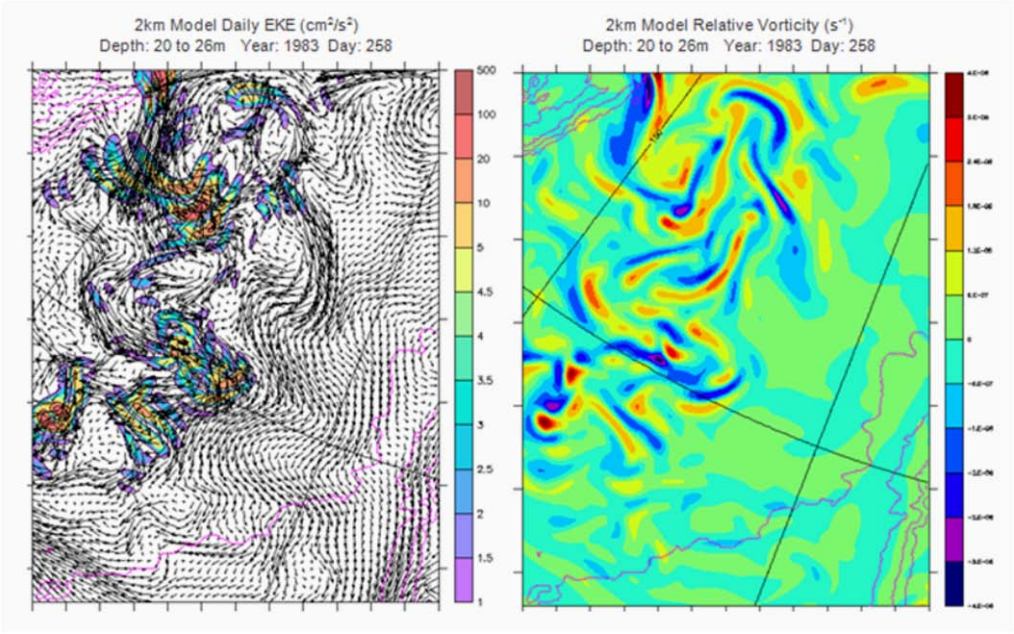

Figure 88. Daily mean model output for 15 September 1983 for the 2.3km model showing EKE with current vectors (left) and relative vorticity (right) at depth 20 to 26m for domain in Beaufort Sea shown by dashed black box in Figure 86.

LIST OF REFERENCES

Ackley, S., P. Wadhams, J.C. Comiso, and A.P. Worby, 2003: Decadal decrease of Antarctic sea ice extent inferred from whaling records revisited on the basis of historical and modern sea ice records. *Polar Research*, **22**, 1, 19–25.

Allison, I., 1979: Antarctic sea ice growth and oceanic heat flux. *Sea Level, Ice and Climatic Change (Proceedings of the Canberra Symposium, December 1979)*, IAHS Publ no. 131, 161–170.

Borgerson, S.G., 2008: Arctic meltdown: the economic and security implications of global warming. *Foreign Affairs*, **8**, 63–77.

Brandon, M.A., F.R. Cottier, and F. Nilsen, 2010: Sea Ice and Oceanography. *Sea Ice*, Second Edition, Eds. D.N. Thomas and G.S. Dieckmann, Wiley-Blackwell, 79–111.

Broecker, W.S., 1991: The Great Ocean Conveyor, *Oceanography*, **4**, 2, 79–89.

Cavalieri, D.J., and C.L. Parkinson, 2003: 30-year satellite record reveals contrasting Arctic and Antarctic decadal sea ice variability. *Geophysical Research Letters*, **30**, 18, doi:10.1029/2003GL018031.

CBC News, 2010: Huge iceberg breaks off Greenland Glacier, 10 August 2010. Retrieved from http://www.cbc.ca/canada/north/story/2010/08/10/greenland-petermann-iceberg.html (accessed 05 December 2010).

Comiso, J.C., 2010: Variability and trends of the global sea ice cover. *Sea Ice*, Second Edition, Eds. D.N. Thomas and G.S. Dieckmann, Wiley-Blackwell, 205–236.

Comiso, J.C., C.L. Parkinson, R. Gersten, and L. Stock, 2008: Accelerated decline in the Arctic sea ice cover. *Geophysical Research Letters*, **35**, L01703, doi:10.1029/2007GL031972.

D'Asaro, E., 1988. Observations of small eddies in the Beaufort Sea. *Journal of Geophysical Research*, **93**, C6, 6669–6684.

Deser, C., and H. Teng, 2008: Evolution of Arctic sea ice concentration trends and the role of atmospheric circulation forcing, 1979-2007. *Geophysical Research Letters*, **35**, L02504, doi:10.1029/2007GL032023.

Department of the Navy, 2009: Task Force Climate Change and the Arctic Roadmap. *Rhumb Lines*. Retrieved from https://www.navyreserve.navy.mil/Publications (accessed 05 August 2010).

Emery, W.J. and R.E. Thomson, 2004: *Data Analysis Methods in Physical Oceanography*. 2nd edition, Elsevier, 638pp.

Francis, J.A., and E. Hunter, 2006: New insight into disappearing Arctic sea ice. *Eos*, **87**, 46, 509–524.

Francis, J.A., and E. Hunter, 2007: Drivers of declining sea ice in the Arctic winter: a tale of two seas. *Geophysical Research Letters*, **34**, L17503, doi:10.1029/2007GL030995.

Francis, J.A., E. Hunter, J.R. Key, and X. Wang, 2005: Clues to variability in Arctic minimum sea ice extent. *Geophysical Research Letters*, **32**, L21501, doi:10.1029/2005GL024376.

Gascard, J.-C., J. Festy, H. Le Goff, M. Weber, B. Bruemmer, M. Offermann, M. Doble, P. Wadhams, R. Forsberg, S. Hanson, H. Skourup, S. Gerland, M. Nicolaus, J.-P. Metaxian, J. Grangeon, J. Haapala, E. Rinne, C. Haas, G. Heygster, E. Jakobson, T. Palo, J. Wilkinson, L. Kaleschke, K. Claffey, B. Elder, and J. Bottenheim, 2008: Exploring Arctic Transpolar Drift during dramatic sea ice retreat, *Eos*, **89**, 3, doi:10.1029/2008EO030001.

Goosse, H., and T. Fichefet, 1999: Importance of ice-ocean interactions for the global ocean circulation: a model study. *Journal of Geophysical Research*, **104**, C10, 23337–23355.

Gordon, A.L., C.T.A. Chen, and W.G. Metcalf, 1984: Winter mixed layer entrainment of Weddell Deep Water. *Journal of Geophysical Research*, **89**, C1, 637–640.

Gordon, A.L., and B.A. Huber, 1984: Thermohaline stratification below the Southern Ocean sea ice. *Journal of Geophysical Research*, **89**, C1, 641–648.

Gordon, A.L., and B.A. Huber, 1990: Southern Ocean winter mixed layer. *Journal of Geophysical Research*, **95**, C7, 11655–11672.

Gordon A.L., and B.A. Huber, 1995: Warm Weddell Deep Water west of Maud Rise. *Journal of Geophysical Research*, **100**, C7, 13747–13753.

Hutchings, J., C. Geiger, A. Roberts, J. Richter-Menge, R. Forsberg, K. Giles, C. Haas, S. Hendricks, C. Khambhamettu, S. Laxon, T. Martin, M. Pruis, M. Thomas, P. Wadhams, and J. Zwally, 2008: Role of ice dynamics in the sea ice mass balance. *Eos Transactions American Geophysical Union*, **89**, 50, 515.

Hutchings, J., and A. Roberts, 2010: Seasonality of tidal and inertial oscillations in the Arctic perennial ice pack. In preparation for the *Journal of Geophysical Research SEDNA Special Issue* (to be submitted 31 December 2010).

Intergovernmental Panel on Climate Change (IPCC), 2007: Climate Change 2007: Synthesis Report. Cambridge University Press, 52 pp.

Intergovernmental Panel on Climate Change (IPCC), 2007b: Summary for Policymakers. Climate Change 2007: The Physical Science Basis. *Contribution of Working Group I to the Fourth Assessment Report of the Intergovernmental Panal on Climate Change*, Eds. S. Solomon, D. Qin, M. Manning, Z. Chen, M. Marquis, K.B. Averyt, M. Tignor, and H.L. Millar, Cambridge University Press, 18 pp.

Jackson, J.M., E.C. Carmack, F.A. McLaughlin, S.E. Allen, and R.G. Ingram, 2010: Identification, characterization and change of the near-surface temperature maximum in the Canada Basin, 1993–2008. *Journal of Geophysical Research*, **115**, C05021, doi:10.1029/2009JC005265.

Johannessen, O.M., 2008: Decreasing Arctic sea ice mirrors increasing CO_2 on decadal time scale. *Atmospheric and Oceanic Science Letters*, **1**, 1, 51–56.

Krishfield, R., J. Toole, A. Proshutinsky, and M.-L. Timmermans, 2008: Automated ice-tethered profilers for seawater observations under pack ice in all seasons. *Journal of Atmospheric and Oceanic Technology*, **25**, 2091–2105.

Krishfield, R., J. Toole, and M.-L. Timmermans, 2008b: ITP data processing procedures. Unpublished manuscript available at http://www.whoi.edu/fileserver.do?id=35803&pt=2&p=41486.

Kwok, R., and J.C. Comiso, 2002: Southern Ocean climate and sea ice anomalies associated with the Southern Oscillation. *Journal of Climate*, **15**, 487–501.

Kwok, R., 2007: Near zero replenishment of the Arctic multiyear sea ice cover at the end of 2005 summer. *Geophysical Research Letters*, **34**, L05501, doi:10.1029/2006GL028737.

Kwok, R., and G.F. Cunningham, 2008: ICESat over Arctic sea ice: estimation of snow depth and ice thickness. *Journal of Geophysical Research*, **113**, C08010, doi:10.1029/2008JC004753.

Kwok, R., G.F. Cunningham, M. Wensnahan, I. Rigor, H.J. Zwally, and D. Yi, 2009: Thinning and volume loss of Arctic Ocean sea ice cover: 2003-2008. *Journal of Geophysical Research*, **114**, C07005, doi:10.1029/2009JC005312.

Kwok, R., E.C. Hunke, W. Maslowski, D. Menemenlis, and J. Zhang, 2008: Variability of sea ice simulations assessed with RGPS kinematics. *Journal of Geophysical Research*, **113**, C11012, doi:10.1029/2008JC004783.

Kwok, R., and D.A. Rothrock, 2009: Decline in Arctic sea ice thickness from submarine and ICESat records: 1958-2008. *Geophysical Research Letters*, **36**, L15501, doi:10.1029/2009GL039035.

Lindsay, R.W., and J. Zhang, 2005: The thinning of Arctic sea ice, 1988-2003: have we passed a tipping point? *Journal of Climate*, **18**, 4879–4894.

Liu, J., J.A. Curry, and D.G. Martinson, 2004: Interpretation of recent Antarctic sea ice variability. *Geophysical Research Letters*, **31**, L02205, doi:10.1029/2003GL018732.

Mahr, K., 2010: Is the Arctic headed for another Cold War? *TIME Ecocentric*, 12 October 2010. Retrieved from http://ecocentric.blogs.time.com/2010/10/12/is-the-arctic-headed-for-another-cold-war/ (accessed 24 November 2010).

Markus, T., J.C. Stroeve, and J. Miller, 2009: Recent changes in Arctic sea ice melt onset, freezeup and melt season length. *Journal of Geophysical Research*, **114**, C12024, doi:10.1029/2009JC005436.

Maslowski, W., 2010: Advances and limitations in understanding and predicting Arctic climate change. Presented at the State of the Arctic Conference, National Science Foundation. Retrieved from http://soa.arcus.org/abstracts/advancements-and-limitations-understanding-and-predicting-arctic-climate-change (accessed 24 November 2010).

Maslowski, W., J. Clement Kinney, and J. Jakacki, 2007: Toward prediction of environmental Arctic change. *Computing in Science and Engineering*, **9**, 6, 29–34.

Maslowski, W., and J. Clement Kinney, 2010: Influence of oceanic circulation, heat fluxes and eddies on recent warming in the western Arctic: results of a high-resolution ice-ocean model. Submitted to *Journal of Geophysical Research*.

Maslowski, W., J.L. Clement Kinney, D.C. Marble, and J. Jakacki, 2008: Towards eddy-resolving models of the Arctic Ocean. *Ocean Modeling in an Eddying Regime*, Eds. M.W. Hecht and H. Hasumi, American Geophysical Union, 241–264.

Maslowski, W., and W.H. Lipscomb, 2003: High resolution simulations of Arctic sea ice, 1979-1993. *Polar Research*, **22(I)**, 67–74.

Maslowski, W., D. Marble, W. Walczowski, U. Schauer, J.L. Clement, and A.J. Semtner, 2004: On climatological mass, heat, and salt transports through the Barents Sea and Fram Strait from a pan-Arctic coupled ice-ocean model simulation. *Journal of Geophysical Research*, **109**, C03032, doi:10.1029/2001JC001039.

Massom, R.A., H. Eicken, C. Haas, M.O. Jeffries, M.R. Drinkwater, M. Sturm, A.P. Worby, X. Wu, V.I. Lytle, S. Ushio, K. Morris, P.A. Reid, S.G. Warren, and I. Allison, 2001: Snow on Antarctic sea ice. *Reviews of Geophysics*, **39**, 3, 413–445.

McBean, G., G. Alekseev, D. Chen, E. Forland, J. Fyfe, P.Y. Groisman, R. King, H. Melling, R. Vose, and P.H. Whitfield, 2005: Arctic Climate: Past and Present. *Arctic Climate Impact Assessement: Scientific Report*, Eds. Arctic Council, Cambridge University Press, 21–60.

McNamara, T., 2006. Determination of changes in the state of the Arctic ice pack using the NPS pan-Arctic coupled ice-ocean model. Advisor: W. Maslowski. Retrieved from http://edocs.nps.edu/npspubs/scholarly/theses/2006/Mar/06Mar_McNamara.pdf (accessed 24 August 2010).

McPhee, M.G., 2003: Is thermobaricity a major factor in Southern Ocean ventilation? *Antarctic Science*, **15**, 1, 153–160.

McPhee, M.G., S.F. Ackley, P. Guest, B.A. Huber, D.G. Martinson, J.H. Morison, R.D. Muench, L. Padman, and T.P. Stanton, 1996: The Antarctic Zone Flux Experiment. *Bulletin of the American Meteorological Society*, **77**, 6, 1221–1232.

McPhee, M.G., T. Kikuchi, J.H. Morison, and T.P. Stanton, 2003: Ocean-to-ice heat flux at the North Pole environmental observatory. *Geophysical Research Letters*, **30**, 24, 2274, doi:10.1029/2003GL018580.

McPhee, M.G., C. Kottmeier, and J.H. Morison, 1999: Ocean heat flux in the central Weddell Sea during winter. *Journal of Physical Oceanography*, **29**, 1166–1179.

McPhee, M.G., A. Proshutinsky, J.H. Morison, M. Steele, and M.B. Alkire, 2009: Rapid change in freshwater content of the Arctic Ocean. *Geophysical Research Letters*, **36**, L10602, doi:10.1029/2009GL037525.

Murphy, E.A., S.F. Ackley, and H. Xie, 2010: Oceanic heat flux under pack ice in the Bellingshausen Sea and fast ice in the Amundsen Sea from autonomous ice mass balance buoys. Submitted to *Deep-Sea Research.*

National Sea and Ice Data Center, 2007: Arctic sea ice shatters all previous record lows. Retrieved from http://nsidc.org/news/press/2007_seaiceminimum/20071001_pressrelease.html (accessed 24 November 2010).

Overland, J., J. Turner, J. Francis, N. Gillet, G. Marshall, and M. Tjernstrom, 2008: The Arctic and Antarctic: two faces of climate change. *Eos*, **89**, 19, 177–184.

Overpeck, J.T., M. Sturm, J.A. Francis, D.K. Perovich, M.C. Serreze, R. Benner, E.C. Carmack, F.S. Chaplin, S.C. Gerlach, L.C. Hamilton, L.D. Hinzman, M. Holland, H.P. Huntington, J.R. Key, A.H. Lloyd, G.M. MacDonald, J. McFadden, D. Noone, T.D. Prowse, P. Schlosser, and C. Vorosmarty, 2005: Arctic system on trajectory to a new, seasonally ice-free state, *Eos*, **86**, 34, 309–316.

Parkinson, C.L., 1990: Search for the Little Ice Age in Southern Ocean sea-ice records. *Annals of Glaciology*, **14**, 221–225.

Perovich, D.K., J.A. Richter-Menge, K.F. Jones, and B. Light, 2008: Sunlight, water and ice: extreme Arctic sea ice melt during the summer of 2007. *Geophysical Research Letters*, **35**, L11501, doi:10.1029/2008GL034007.

Perovich, D.K., J.A. Richter-Menge, B. Elder, K. Claffey, and C. Polashenski, 2009: Observing and understanding climate change: monitoring the mass balance, motion and thickness of Arctic sea ice, http://IMB.crrel.usace.army.mil.

Proshutinsky, A., R. Krishfield, M.-L. Timmermans, J. Toole, E. Carmack, F. McLaughlin, W.J. Williams, S. Zimmerman, M. Itoh, and K. Shimada, 2009: Beaufort Gyre freshwater reservoir: state and variability from observations. *Journal of Geophysical Research*, **114**, C00A10, doi:1029/2008JC005104.

Rampal, P., J. Weiss, and D. Marsan, 2009: Positive trend in the mean speed and deformation rate of Arctic sea ice, 1979-2007. *Journal of Geophysical Research*, **114**, C05013, doi:10.1029/2008JC005066.

Reid, T., 2007: Arctic military bases signal new Cold War. *The Times*, 11 August 2007. Retrieved from http://www.timesonline.co.uk/tol/news/world/us_and_americas/article2238243 (accessed 24 November 2010).

Richter-Menge, J.A., D.K. Perovich, B.C. Elder, K. Claffey, I. Rigor, and M. Ortmeyer, 2006: Ice mass-balance buoys: a tool for measuring and attributing changes in the thickness of the Arctic sea-ice cover. *Annals of Glaciology*, **44**, 205–210.

Rigor, I.G., and J.M. Wallace, 2004: Variations in the age of Arctic sea-ice and summer sea-ice extent. *Geophysical Research Letters*, **31**, L09401, doi:10.1029/2004GL019492.

Rintoul, S.R., C. Hughes, and D. Olbers, 2001: The Antarctic Circumpolar Current system. *Ocean Circulation and Climate*, Eds. G. Siedler, J. Church, and J. Gould, Alfred-Wegener Institute for Polar and Marine Research, 271–302.

Roberts, A., A. Hinzman, J.E. Walsh, M. Holland, J. Cassano, R. Doscher, H. Mitsudera, and A. Sumi, 2010: A science plan for regional Arctic system modeling: a report by the Arctic research community for the National Science Foundation Office of Polar Programs. Retrieved from http://www.iarc.uaf.edu/publications/reports/IARCTP10-0001.pdf (accessed 05 August 2010).

Rothrock, D.A., D.B. Percival, and M. Wensnahan, 2008: The decline in Arctic sea-ice thickness: separating the spatial, annual, and interannual variability in a quarter of a century of submarine data. *Journal of Geophysical Research*, **113**, C05003, doi:10.1029/2007JC004252.

Rothrock, D.A. and M. Wensnahan, 2007: The accuracy of sea ice drafts measured from U.S. Navy submarines. *Journal of Atmospheric and Oceanic Technology*, **24**, 1936–1949.

Rothrock, D.A., Y. Yu, and G.A. Maykut, 1999: Thinning of Arctic sea-ice cover. *Geophysical Research Letters*, **26**, 23, 3469–3472.

SCICEX Science Advisory Committee, 2010: SCICEX Phase II Science Plan, Part I: Technical Guidance for Planning Science Accommodation Missions. US Arctic Research Commission, Arlington, VA, 76pp.

Sea Power Centre - Australia, 2006: RAN Activities in the Southern Ocean, *Semaphore*, **18**. Retrieved from http://www.navy.gov.au/w/images/Semaphore_2006_18.pdf (accessed 05 August 2010).

Serreze, M.C., M.M. Holland and J. Stroeve, 2007: Perspectives on the Arctic's shrinking sea-ice cover. *Science*, **315**, 1533–1536.

Shaw, W.J., T.P. Stanton, M.G. McPhee, J.H. Morison, and D.G. Martinson, 2009: Role of the upper ocean in the energy budget of Arctic sea ice during SHEBA. *Journal of Geophysical Research*, **114**, C06012, doi:10.1029/2008JC004991.

Shimada, K., T. Komoshida, M. Itoh, S. Nishino, E. Carmack, F. McLaughlin, S. Zimmerman and A. Proshutinsky, 2006: Pacific Ocean inflow: influence on catastrophic reduction of sea ice cover in the Arctic Ocean. *Geophysical Research Letters*, **33**, L08605, doi:10.1029/2005GL025624.

Simmonds, I., 2003: Modes of atmospheric variability over the Southern Ocean. *Journal of Geophysical Research*, **108**, C4, 8078, doi:10.1029/2000JC000542.

Stanton, T.P., and W.J. Shaw, 2010: NSF Proposal.

Steele, M., and T. Boyd, 1998: Retreat of the cold halocline layer in the Arctic Ocean. *Journal of Geophysical Research*, **108**, C5, 10419–10435.

Stroeve, J., M.M. Holland, W. Meier, T. Scambos, and M. Serreze, 2007: Arctic sea ice decline: faster than forecast. *Geophysical Research Letters*, **34**, L09501, doi:10.1029/2007GL029703.

Stroeve, J., and W. Maslowski, 2007: Arctic sea ice variability during the last half century. *Climate Variability and Extremes During the Past 100 Years*, **33**, 2, 143–154.

Thorndike, A.S., and R. Colony, 1982: Sea ice motion in response to geostrophic winds. *Journal of Geophysical Research*, **87**, C8, 5845–5852.

Thorndike, A.S., D.A. Rothrock, G.A. Maykut, and R. Colony, 1975: The thickness distribution of sea ice. *Journal of Geophysical Research*, **80**, 33, 4501–4513.

Timmermans, M.-L., J. Toole, A. Proshutinsky, R. Krishfield, and A. Plueddemann, 2008: Eddies in the Canada Basin, Arctic Ocean, observed from ice-tethered profilers. *Journal of Physical Oceanography*, **38**, 133–145.

Titley, D.W., and C.C. St. John, 2010: Arctic security considerations and the U.S. Navy's Roadmap for the Arctic. *Naval War College Review*, **63**, 35–48.

Toole, J.M., R. Krishfield, A. Proshutinsky, C. Ashjian, K. Doherty, D. Frye, T. Hammar, J. Kemp, D. Peters, M.-L. Timmermans. K. von der Heydt, G. Packard, and T. Shanahan, 2006: Ice-tethered profilers sample the upper Arctic Ocean. *Eos*, **87**, 41, 434–438.

Toole, J.M., M.-L. Timmermans, D.K. Perovich, R.A. Krishfield, A. Proshutinsky, and J.A. Richter-Menge, 2010: Influences of the ocean surface mixed layer and thermohaline stratification on Arctic sea ice in the central Canada Basin. *Journal of Geophysical Research*, **115**, C10018, doi:10.1029/2009JC005660.

Tseng, H-L.R., 2010: Toward quantifying the impact of atmospheric forcing on Arctic sea ice variability using the NPS 1/12 degree pan-Arctic coupled ice-ocean model. Advisor: W. Maslowski. Retrieved from http://edocs.nps.edu/npspubs/scholarly/theses/2010/Mar/10Mar_Tseng.pdf (accessed 01 August 2010).

Uttal, T., J.A. Curry, M.G. McPhee, D.K. Perovich, R.E. Moritz, J.A. Maslanik, P.S. Guest, H.L. Stern, J.A. Moore, R. Turenne, A. Heiberg, M.C. Serreze, D.P. Wylie, O.G. Persson, C.A. Paulson, C. Halle, J.H. Morison, P.A. Wheeler, A. Makshtas, H. Welch, M.D. Shupe, J.M. Intrieri, K. Stamnes, R.W. Lindsey, R. Pinkel, W.S. Pegau, T.P. Stanton and T.C. Grenfeld, 2002: Surface Heat Budget of the Arctic Ocean. *Bulletin of the American Meteorological Society*, **83**, 255–275.

Wadhams, P., 2002: *Ice in the Ocean*, Gordon and Breach Science Publishers, 351pp.

Wadhams, P., M.A. Lange, and S.F. Ackley, 1987: The ice thickness distribution across the Atlantic sector of the Antarctic Ocean in midwinter. *Journal of Geophysical Research*, **92**, C13, 14535–14552.

Wang, M., and J.E. Overland, 2009: A sea ice free summer in the Arctic within 30 years? *Geophysical Research Letters*, **36**. L07502, doi:10.1029/2009GL037820.

Whelan, J., 2007: Understanding recent variability in the Arctic sea ice cover – synthesis of model results and observations. Advisor: W. Maslowski. Retrieved from http://edocs.nps.edu/npspubs/scholarly/theses/2007/Sep/07Sep_Whelan.pdf (accessed 24 August 2010).

Whelan, J., W. Maslowski, J.L. Clement Kinney, and J. Jakacki, 2007: Understanding recent variability in the Arctic sea ice cover – synthesis of model results and observations, *Eos Trans.*, AGU 88, 52, Fall Meeting Supplement, Abstract C22A-06.

White, W.B. and R.G. Peterson, 1996: An Antarctic circumpolar wave in surface pressure, wind, temperature and sea-ice extent. *Nature*, **380**, 699–702.

Woods Hole Oceanographic Institution (WHOI), 2008: Ice-tethered profiler. http://www.whoi.edu/itp.

Worby, A.P. and J.C. Comiso, 2004: Studies of the Antarctic sea ice edge and ice extent from satellite and ship observations. *Remote Sensing of the Environment*, **92**, 98–111.

Worby, A.P., M.O. Jeffries, W.F. Weeks, and K. Morris, 1996: The thickness distribution of sea ice and snow cover during late winter in the Bellingshausen and Amundsen Seas, Antarctica. *Journal of Geophysical Research*, **101**, C12, 28441–28455.

Worby, A.P., C.A. Geiger, M.J. Paget, M.L. Van Woert, S.F. Ackley, and T.L. DeLiberty, 2008: Thickness distribution of Antarctic sea ice. *Journal of Geophysical Research*, **113**, C05S92, doi:10.1029/2007JC004254.

Zhang, J., 2007: Increasing Antarctic sea ice under warming atmospheric and oceanic conditions. *Journal of Climate*, **20**, 2515–2529.

Zhang, X. and J.E. Walsh, 2006: Towards a seasonally ice-covered Arctic Ocean: scenarios from the IPCC AR4 model simulations. *Journal of Climate*, **19**, 1730–1747.

Zhang, Y., W. Maslowski, and A.J. Semtner, 1999: Impact of mesoscale ocean currents on sea ice in high-resolution Arctic ice and ocean simulations. *Journal of Geophysical Research*, **104**, 18, 409–418.

THIS PAGE INTENTIONALLY LEFT BLANK

INITIAL DISTRIBUTION LIST

1. Defense Technical Information Center
   Ft. Belvoir, Virginia

2. Dudley Knox Library
   Naval Postgraduate School
   Monterey, California

3. Dr. Wieslaw Maslowski
   Naval Postgraduate School
   Monterey, California

4. Dr. William Shaw
   Naval Postgraduate School
   Monterey, California

5. Dr. Andrew Roberts
   Naval Postgraduate School
   Monterey, California

6. Jaclyn Clement Kinney
   Naval Postgraduate School
   Monterey, California

7. Dr. Donald Perovich
   Cold Regions Research and Engineering Laboratory
   Hanover, New Hampshire

8. Dr. Robert Osinski
   Institute of Oceanology Polish Academy of Sciences
   Sopot, Poland

9. Dr. Jacqueline Grebmeier
   Chesapeake Biological Laboratory
   Solomons, Maryland

10. Dr. Anjuli Bamzai
    National Science Foundation
    Arlington, Virginia

11. Dr. Erica Key
    National Science Foundation
    Arlington, Virginia

12. Dr. Neil Swanberg
National Science Foundation
Arlington, Virginia

13. Dr. William Wiseman
National Science Foundation
Arlington, Virginia

14. Dr. Dorothy Koch
United States Department of Energy
Washington DC

15. Dr. Renu Joseph
United States Department of Energy
Washington DC

16. Dr. Scott Harper
Office of Naval Research
Arlington, Virginia

17. RADM David Titley, USN
Oceanographer and Navigator of the Navy
Washington DC

18. CAPT Timothy Gallaudet, USN
Task Force Climate Change
Washington DC

19. CDRE Rod Nairn, RAN
Hydrographer of Australia
Wollongong, New South Wales, Australia

20. CMDR Robert Woodham, RAN
Directorate of Oceanography and Meteorology
Sydney, New South Wales, Australia

21. LEUT Joanne Haynes, RAN
Directorate of Oceanography and Meteorology
Sydney, New South Wales, Australia